Imperial College London

# Quantumness in Optomechanics

**Ludovico Latmiral**

Department of Physics

Imperial College London

Thesis submitted in partial fulfilment of the

requirements for the degree of

*Doctor of Philosophy in Physics*

July 2017

Supervised by Dr. Florian Mintert

I hereby declare that the content of this thesis is the result of my own work. Any information extracted from published and unpublished work of others has been appropriately acknowledged in the references.

Ludovico Latmiral

London, July 2017

# Acknowledgements

It is great pleasure for me to take this little opportunity to formally express my gratitude to all those people who have supported me in the past three years of my doctorate. Actually, I had the chance to work alongside with many people who have all contributed to my personal and academic growth.

First of all, I should thank Florian Mintert who has supervised me in the second part of my PhD and who revealed to be an extremely precise and dedicated tutor, willing to get his hands dirty with calculations and paper drafting. Our relationship has extended also outside academia with memorable lunches and cycling tours, the latter being really hard to forget.

I should then remember my first supervisor, Myungshik Kim, who introduced me to the world of quantum optics and taught me to never forget a deeper, ontological and philosophical approach when dealing with Physics. Visiting Korea together with him is something I will always remember.

Further, I would like to thank Nicoló Spagnolo and Fabio Sciarrino at University La Sapienza in Rome, with whom I have maintained a fruitful scientific collaboration.

I would also like to demonstrate my gratitude to Costantino Budroni at University of Siegen, who was eager to seize the opportunity to begin a project together and was kind to invite me to visit his group in Germany.

A special acknowledgement goes to Federico Armata, the PhD student at Imperial College with whom I have collaborated in several projects and papers. Federico shared many of his notions on optomechanics with me: it has been a pleasure for me to learn new things and grow as physicists and as people together. I am sure the companionship we shared over these years will be the base of a solid and lasting friendship.

As Italians tend to gather together like bosons tend to do, I was also lucky to have Luca Rigovacca as my desk neighbour. Beyond his help to dispel any doubt I had on Gaussian states, I will remember the pre-holidays days we spent alone in the office and I trust we have also strengthened a friendship that will make our roads crossing again in the future.

Eventually, a huge thanks is devoted to my parents, who continuously supported me practically and emotionally throughout my PhD.

# Abstract

Cavity optomechanics has become an established and equally promising branch in quantum optics. Thanks to the interaction between matter and electromagnetic radiation, it has proved to be an optimal platform for a range of scopes, from weak force sensing to the study of non-classicality of mechanical motion. Besides, the capability to isolate genuine quantum features of the interaction represents a test ground to address many important questions regarding decoherence, quantum-to-classical transitions and the interface between quantum mechanics and gravity.

The first part of the research embedded in this thesis is addressed towards the clear identification and characterisation of quantum features in optomechanics. The main model we will refer to is a deformable Fabry-Pérot cavity where one of the two mirrors moves under the radiation pressure of light. After having properly assessed the quantum peculiarities of the system, and also having revised some intakes from past literature, we will focus on the study of mechanical non-linearities, as they have been proved to be a key resource to bring out and enhance quantum properties. These investigations provide the basis to eventually propose a method to deterministically prepare and measure macroscopic quantum superposition states of the movable mirror. Such massive quantum states play a key role to inspect the foundations of physics, e.g. to test the collapse of the wave function and phenomenological models of quantum gravity, as well as to develop new enhanced quantum technologies.

# Contents

# Introduction

Quantum theory is based on the superposition principle, asserting that any two (or more) quantum states can be added together – superposed – and result in another valid quantum state. Conversely, every quantum state can be represented as the sum of two or more distinct states. The most popular example is Schrödinger cat, which is closed in a box together with a poison vial and remains alive and dead at the same time, until an observer opens the box and looks whether the vial broke or not, making the cat *collapse* in either one of its two possibile states – alive or dead. This picture contradicts our classical intuition, which is trained by daily experience where objects of macroscopic size or mass follow classical laws, while quantum nature is observed at small scales and energies of atoms and subatomic particles. At the same time, the emergence of classicality from quantum mechanical microcosmos has equally been a puzzle since the discovery of quantum mechanics.
In this direction, preparing a large object in a quantum state would be a powerful resource and trigger ground-breaking investigations on foundations of physics, ranging from the quantum-to-classical transition and collapse models to the interface between quantum mechanics and gravity. One of the challenges is to isolate genuine quantum features that are accessible in experiments, as several proposals to test the limits of quantum theory rely on specific quantum control sequences.

However, the preparation of non-classical quantum states has been so far largely limited by the stochastic nature that is common to quantum systems. Indeed, given an object to be prepared in a specific quantum state via the interaction with a subsidiary controlled system, correlations between the target and the bus arise such that the state of the former probabilistically depends on the measurement of the latter. Moreover, the larger the object is, the easier it correlates with its environment

and the more difficult it is to isolate it in a well defined quantum superposition state. With the exception of proof of principle examples with nanoscopic structures, there was no known protocol to deterministically prepare a massive object in a quantum state.

Optomechanical experiments in which a mesoscopic mechanical resonator interacts with light open the possibility to investigate quantum states on the border between quantum and classical worlds. The simplest framework consists of a cavity composed by two mirrors, one of which is modelled as a harmonic oscillator, where a light field is pumped from the outside and non-linearly interacts with the movable mirror via radiation pressure. The arbitrary choice of the initial input state of the light together with the cubic light-matter interaction allow the creation of a range of quantum superpositions and entangled states between the cavity and the mirror. In addition, the possibility to perform very precise interference measurements on the field escaping from the cavity, *e.g.* homodyne and heterodyne detection, naturally provides a precise readout of the system dynamics.

In this perspective, the first part of this thesis will be devoted to the study of non-classical features arising from the motion of the mechanical oscillator. The comparison with classical and semi-classical models will allow us to identify signatures of quantum nature that could be used in a variety of different applications.

We will further our studies with the analysis of non-linearities other than the light-matter interaction, such as mechanical anharmonicities, which are supposed to play a fundamental role to bring out and enhance quantum properties. The protocol that we present consists in displacing the mirror with a series of light pulses alongside a loop in phase space and coincides with the scheme that has been suggested to test more exotic topics, such as to measure deformations in commutation relations predicted by quantum gravity. Within this same line of research, we are currently working at exploiting the algebra of displacements in phase space (which is similar to the one that characterises Pauli matrices) to present a gedanken experiment to test contextuality with massive objects.

After these preliminary works where we investigate the quantum peculiarities of the system and learn how to assess the non-classicality of the dynamics, we propose

a scheme to create macroscopic quantum superposition states. By controlling the optomechanical resonator through easy-to-achieve suitably shaped light fields pumped with an external laser, we describe how to deterministically drive the mirror towards a set of highly non-classical mechanical quantum states. For our purposes, we will refer to *quantumness* as to the potential that an object driven in a superposition state has to manifest quantum interference between the distinct component states. In this context, we prove the achievement of maximum quantumness via a quantitative estimator that could be practically used to keep track of the mechanical decoherence of the mirror and to test the emergence of classicality and many other foundational topics.
In terms of future perspectives, the ability to reliably prepare massive mechanical states is not only a significant theoretical advance, but it opens up an avenue to a series of opto-mechanical experiments both of fundamental and technological nature. For example, the massive mirror could serve as continuous variable quantum memory, or as the base brick to build new enhanced quantum technologies, for which deterministic state preparation and measurement are an essential requirement and which are expected to outperform the efficiency of todays classical architectures.

It is worth emphasising that while in this thesis we will always refer to the practical case of an optomechanical resonator, the analysis and studies that we conduct are not restricted to the mirror-cavity setup. Similar considerations and conceptually similar control driving patterns can be successfully applied to a variety of systems that share similar non-linear Hamiltonians such as atomic spin ensembles, trapped atoms or levitated nanoparticles.

### *Boson Sampling and Integrated Circuits*

Since the beginning of my PhD I have dedicated part of my studies to another branch of research, providing theoretical support to experimentalists working with integrated photonic circuits. Even though *Boson Sampling and integrated circuits* are not going to be object of this thesis, it is worth to briefly summarise hereafter the problems that I have addressed in the field so far.

Quantum information science holds the promise of new technologies that can overcome their corresponding classical implementations, with applications in communication, sensing and computing. In particular, *quantum supremacy*, *i.e.* the condition where a quantum device outperforms its classical counterpart, represents a fundamental milestone to show the potential of quantum mechanics. In this context, S. Aaronson and A. Arkhipov introduced Boson Sampling (BS) as a candidate to reach the quantum supremacy regime for a specific computational problem. BS was initially conceived as a quantum generalisation of Galton's quinconce, which consists of a vertical board with interleaved rows of pins. Balls are dropped from the top and bounce either left or right as they hit the pins, being eventually collected into one-ball-wide bins at the bottom. Instead of a single ball at a time, BS contemplates a variety of possible inputs and replaces pins with a complex interference network where bosons evolve through before being eventually sampled. The interest in the problem arises since the final sampling can not be efficiently simulated by a modern computer, though it retrieves fundamental properties and information on the evolution of the particles.

Our contribution to the field has been oriented towards the theoretical enlargement of the domain of interest and applicability of BS through two different approaches. On the one hand, we studied the generalisation of the problem to an exponentially larger set of multiple random initial (input) states and introduced various sources of boson losses in the model. These techniques have paved the way to a quantum speedup of the problem complexity, and at the same time they have resolved the issue of taking into account some unavoidable sources of experimental errors such as erroneous preparation of the initial state or incorrect measurements and losses during the evolution. On the other hand, we have studied the efficiency and validation of various experimental approaches (optical networks, integrated circuits, quantum dot sources, superconducting qubits and microwave photons), and we provided for the first time a quantitative threshold that bounds the quantum supremacy regime.

Not only a thorough estimation of quantum supremacy is a pivot point for the study of complexity classes and algorithmic efficiency, but it is also crucial because in that regime classical control and correction systems are no longer reliable. Indeed,

the certification of a BS machine is believed to be a computationally hard task itself. Some effective ways that we provided to address this validation issue have enlightened special features attributable to the bosonic nature and could lead to generalisations for the solution of inverse problems. Up to date, BS has been demonstrated to have applications in the solution of searching problems (e.g. search an item in an unordered list) and in the efficient computation of molecular vibronic spectra. For instance, spectroscopy is a key tool to probe molecular properties such as the performance as solar cells or as dyes and to detect damage of deoxyribonucleic acid molecules, leading to significant chemical and medical applications. Eventually, very recent proposals to extend the BS problem to Gaussian states offer a formalism that responds well to a large range of noise sources, which can be easily modelled as Gaussian operations, and pave the way to further extensions of the problem.

Always looking at the potentialities of photonic systems, we also investigated the advantages of mapping the transmission of information within Spin-chain models to their bosonic counterparts. In particular, we have showed how to exploit the higher dimensionality of the Hilbert space of the chain elements, that could be encoded in qutrits and qudits in terms of Fock states, for the transmission of a larger amount of information.

A summary of the topics discussed in the various chapters is presented below.

- The *first chapter* is a review of the state-of-the-art in optomechanics. We present the general scheme of a Fabrit-Pérot cavity with a movable boundary and introduce the most studied regimes, as well as a seminal proposal to probe massive quantum superposition states.

- The *second chapter* is dedicated to the assessment of quantumness in optomechanical experiments via the readout of the phase shift of the outcoming light-field. The adoption of visibility in light interference fringes as a witness of the creation of a quantum superposition state is challenged, and a new explanation for the appearance of such losses and revivals of the visibility is presented.

- In the *third chapter* we investigate mechanical anharmonicities and present a scheme that allows very precise measurements of the final state of the field. The analysis is performed also in a fully classical picture to understand how mechanical non-linearities affect the quantum-classical correspondence. We conclude with a topological remark to link anharmonicity to a non-canonical transformation of the Hilbert space.

- The *fourth chapter* is devoted to presenting a protocol for the deterministic preparation of quantum states of the mirror through the engineering of suitably designed driving patters. We show how to create squeezed as well as highly non-classical massive superposition states. We provide evidence of the resilience of the scheme to a series of possible experimental errors.

- The *fifth chapter* contains the final remarks as well as perspectives and proposals for future investigations.

# List of Publications

Much of this thesis is based on the following publications and pre-prints, although material has been expanded and reworked throughout:

- F. Armata, L. Latmiral, I. Pikovski, M. R. Vanner, C. Brukner, and M. S. Kim, Quantum and classical phases in optomechanics, Physical Review A, **93**, 063862 (2016)
- L. Latmiral, F. Armata, M. G. Genoni, I. Pikovski, and M. S. Kim, Probing anharmonicity of a quantum oscillator in an optomechanical cavity, Physical Review A, **93**, 052306 (2016)
- L.Latmiral and F. Mintert, Deterministic preparation of highly non-classical quantum states of massive oscillators, arXiv: 1705.10334 (2017)

Other published works not included in the thesis are

- L. Latmiral, F. Armata, A.D.K. Plato, and M. S. Kim, Quantum Limits to Gravity Estimation with Optomechanics, Physical Review A **96**, 043824 (2017)
- L. Latmiral, N. Spagnolo, and F. Sciarrino, Towards Quantum Supremacy with Lossy Scattershot Boson Sampling, New Journal of Physics, **18**, 113008 (2016)
- L. Latmiral, C. Di Franco, P. L. Mennea, and M. S. Kim, State-transfer simulation in integrated waveguide circuits, Physical Review A, **92**, 022350 (2015)
- M. Bentivegna, N. Spagnolo, C. Vitelli, F. Flamini, N. Viggianiello, L. Latmiral, P. Mataloni, D. J. Brod, E. F. Galvao, A. Crespi, R. Ramponi, R. Osellame, and F. Sciarrino, Experimental scattershot boson sampling, Sciences Advances, **1**, e1400255 (2015)

An updated list of publications can be found on arXiv at the following link.

# Chapter 1

# State of the art

## 1.1 Introduction

We devote this first chapter to reviewing the basis of quantum optomechanics, specifically providing the state of the art on which we have grafted the research presented in this thesis.

From suspended membranes and micro-mirrors to micro-rods and cold atoms, many experimental groups have been working on a variety of approaches to couple mechanical objects to an optical field [1]. However, despite the range of different implementation proposals, they all rely on the same conceptual scheme. We will start by introducing such general model, composed of a macroscopic mechanical oscillator with a reflective surface and a light field which is incident on it, to further focus on the latest experimental proposals to prepare the system in a range of interesting states. We will review the so called *pulsed dynamics*, which has been introduced in different variations to create quantum superpositions of massive bodies [2], perform tests of deformed commutation relations [3] and probe decoherence of macroscopic objects [4, 5].

This first chapter serves as a starting point to address the novel research that has been conducted in the field, which is presented in the second part of the thesis. There, we will provide a detailed comparison between the study of optomechanics from a classical and a quantum perspective, also revising some of the formerly adopted

indicators of quantumness. We will then analyse the role of mechanical non-linearities in the dynamics and eventually propose a deterministic scheme to create and measure highly non-classical macroscopic superposition states of a massive object.

## 1.2 The Model

An optomechanical cavity can be conceived as a Fabry-Pérot apparatus, consisting of two highly reflective mirrors facing each other, which serve as boundaries for the electromagnetic field inside the cavity. In particular, in this thesis we will refer to a widely adopted implementation where the larger mirror is fixed while the smaller is harmonically bounded to the longitudinal axis and moves under the effect of radiation pressure (see Fig.1.1). This model of a deformable optical resonator encloses a variety of experimental implementations and provides a well defined starting point for theoretical studies. The movable mirror is modelled as a harmonic oscillator with mass $m$ and frequency $\omega$. Its equilibrium position $x_m = 0$ defines the mean cavity length $L$, which in turn characterises the normal mode resonance frequencies $\omega_c(n) = \pi cn/L$, with $n \in \mathcal{N}$ the mode number.
More generally, in a deformable cavity the frequencies are function of the oscillator position and for small displacements can be approximated as

$$\omega_c(x_m, n) = \frac{\pi cn}{L + x_m} \simeq \frac{\pi cn}{L}\left(1 - \frac{x_m}{L}\right) \ . \tag{1.1}$$

Eq.(1.1) is a direct consequence of boundary conditions imposed by classical electrodynamics to a stationary optical field in a cavity. This equation witnesses the Kerr non-linearity induced by radiation pressure of the field on the mirror, which was first observed by Dorsel et al. [6]. The length of the cavity depends on the optical intensity and in turn the amount of radiation entering the cavity is a function of the displacement of the mirror. Thanks to the high fidelity of todays accessible monochromatic laser sources which are used to pump the cavity, we will assume in the following, as in the majority of optomechanical schemes, that only a single optical mode is excited.

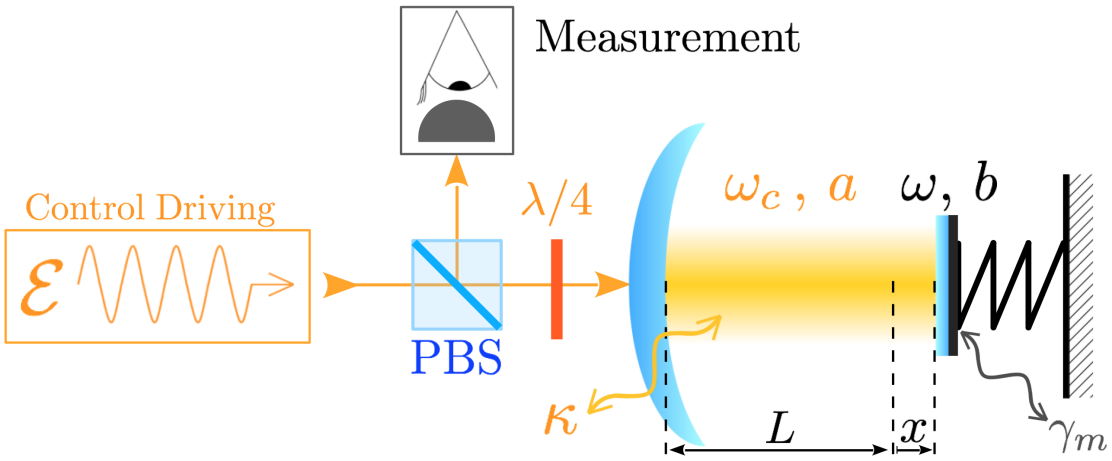


Figure 1.1: Conceptual scheme of the archetypical optomechanical setup. A control driving laser with amplitude $\mathcal{E}$ is adopted to pump a deformable Fabry-Pérot cavity whose resonance frequency at equilibrium is $\omega_c$ and whose movable mirror is modeled as a harmonic oscillator with mass $m$ and frequency $\omega$. When the light escapes the cavity it is rotated by a $\lambda/4$ wave-plate, reflected by a polarizing beam splitter (PBS) and measured interferometrically with respect to a reference beam.

Even though the relation between the resonance frequency and the position of the mirror in Eq.(1.1) was derived by resorting to classical physics, it already provides a good hint to obtain the quantised Hamiltonian of the system. It is not within the scope of this thesis to discuss the rigorous procedure adopted for this purpose by Law in Ref.[7]. Instead, we will naively proceed with an intuitive approach. We start by applying canonical quantisation to the position in Eq.(1.1) $x_m \to x_0(b + b^\dagger)$, where $b$ and $b^\dagger$ are the mechanical annihilation and creation operators satisfying $[b, b^\dagger] = 1$ and $x_0 = \sqrt{\hbar/(2mw)}$ is the standard deviation of the mechanical ground-state width. We then introduce the field operators $a$ and $a^\dagger$ and write the Hamiltonian of the system, which corresponds to two harmonic oscillators representing the electro-magnetic field and the mirror, where the frequency of the former depends on the position of the latter [1]

$$\frac{H}{\hbar} = \omega_c(x_m)a^\dagger a + \omega b^\dagger b = \langle\omega_c\rangle a^\dagger a + \omega b^\dagger b - g_0 a^\dagger a(b + b^\dagger), \tag{1.2}$$

with $a^\dagger a$ ($b^\dagger b$) the number operator of the cavity (mirror). Eq.(1.2) is obtained after having renormalized the zero point energy fluctuations of the optical field inside

[1] Hereafter we will always adopt $a^\dagger$ , $a$ ($b^\dagger$ , $b$) to refer to the field (mirror) creation and annihilation operators, choosing to drop the *hat* symbol " ˆ " for the sake of readability.

the cavity with the ones in free space (in absence of the boundary conditions). The difference between these two quantities is known as the Casimir force and will be assumed to be negligible for sufficiently large $L$. This is an important conceptual remark, as the outside field needs to be taken into account to maintain the consistency of the theory.

In the following, we will usually refer to $g_0 a^\dagger a(b + b^\dagger) = H_{int}$ as the interaction Hamiltonian ($H_{int}$) describing the non-linear light matter interaction. The quantity $g_0 = \langle\omega_c\rangle x_0/L$ is the coupling rate and has a key meaning in optomechanics. As we shall discuss in details, indeed, $H_{int}$ simultaneously induces a displacement of the mirror proportional to the number of photons in the cavity and a phase shift of the cavity optical field proportional to the mechanical displacement itself.

For a thorough understanding of the model presented so far we should now investigate how the quantum interaction is related with the classical radiation pressure and the standard parameters that define a Fabry-Pérot system. An important quantity that accounts for the leakage of photons from the cavity is the decay rate $\kappa$, defined as the inverse of photon lifetime $\tau = 1/\kappa = N_{\rm rt}\ 2L/c$, where $N_{\rm rt} = \mathcal{F}'/\pi$ is the average number of round trips that light performs in the cavity and $\mathcal{F}'$ is the coefficient of finesse, which depends on the reflectivity of the mirrors (e.g. $\mathcal{F}' = 4R/(1-R)^2$ in case of identical mirrors).[2] With these definitions at hand we can write the (average) force acting on the mechanical mirror as a result of the radiation pressure in more familiar terms

$$F = -\frac{\partial H}{\partial x} = \frac{2\hbar\omega_c \mathcal{F}' \langle a^\dagger a\rangle \kappa}{\pi c}\ , \tag{1.3}$$

where the cavity finesse linearly enhances the optical power transferred to the mirror.

In order to complete the picture of the general optomechanical framework, we should include in the model an external driving source to generate the electromagnetic field, *e.g.* a coherent laser entering through the fixed mirror (which is supposed to have a certain transmittivity) (see Fig.1.1). The driving amplitude is defined as

[2] We have chosen the label "$\mathcal{F}'$", instead of the widely adopted character "$F$", to avoid overlapping with the force acting on the oscillator, which will be denoted by "$F$". We recall here that the coefficient of finesse is strictly related to the finesse $\mathcal{F} = \pi\sqrt{R}/(1-R)$, which corresponds to the ratio between the free spectral range and the full-width half-maximum.

$\mathcal{E} = \sqrt{2P\kappa/\hbar\omega_0}$, where $P$ is the laser power input and $\omega_0$ the laser driving frequency, usually detuned from the cavity resonance. The Hamiltonian for a monochromatic driving will thus read (setting $\hbar = 1$)

$$H = \omega_c a^\dagger a + \omega b^\dagger b - g_0 a^\dagger a(b + b^\dagger) + i\mathcal{E}(a^\dagger e^{-i\omega_0 t} - a e^{i\omega_0 t}) \ . \tag{1.4}$$

This Hamiltonian fully characterises the unitary evolution of an optomechanical system, though it does not account any noise or dissipative effect induced by the environment. In particular, looking at the experimental state-of-the-art, we should acknowledge that promising results have already been obtained in terms of controlling the mechanical damping $\gamma_m$ to build high-quality resonators with quality factor $Q_m = \omega/\gamma_m \gg 1$. Conversely, many efforts are still dedicated to reducing optical losses and achieving the so called *resolved side-band regime*, which is defined by the condition $\kappa \ll \omega$.

The common approach to describe the open quantum system dynamics is to adopt a reference frame rotating at frequency $\omega_0$ and write the Langevin equations for the field and the mirror by using the input-output theory for quantum damping [8, 9]

$$\begin{aligned} \frac{da}{dt} &= -i\left[\omega_c - \omega_0 - g_0(b + b^\dagger)\right] a + \mathcal{E} - \frac{\kappa}{2} a + \sqrt{\kappa} a_{in} \ , \\ \frac{db}{dt} &= -i(\omega b - g_0 a^\dagger a) - \frac{\gamma_m}{2} b + \sqrt{\gamma_m} b_{in} \ , \end{aligned} \tag{1.5}$$

where $a_{in}$ and $b_{in}$ are noise operators associated with the input stochastic fluctuations. They are assumed to have zero mean, i.e. $\langle b(a)_{in}\rangle = \langle b^\dagger(a^\dagger)_{in}\rangle = 0$, and to be delta correlated, i.e. $\langle a_{in}(t) a^\dagger_{in}(t')\rangle = \delta(t - t')$, with zero optical thermal occupation, and $\langle b_{in}(t) b^\dagger_{in}(t')\rangle = (\bar{n}+1)\delta(t-t')$, with $\bar{n} = (\exp[\hbar\omega/k_B T]-1)^{-1}$ the average occupation defined by Bose statistics for a resonator at thermal equilibrium with the environment at temperature $T$.

As we have already remarked through considerations arising from the classical picture, the system of coupled equations in Eq.(1.5) displays a Kerr non-linearity since the optical dynamics depends on the optical intensity rather than on the amplitude. Because of this cubic non-linearity, an exact analytic solution for the motion has

not been derived so far and a widely adopted approach has been instead to linearise the differential equations [10, 11]. The procedure is effective in presence of strong driving and consists in splitting the cavity field $a$ into a fluctuating term $\delta a$ and its average coherent amplitude $\langle a \rangle = \bar{\alpha} = \sqrt{\langle a^\dagger a \rangle}$. The interaction Hamiltonian could then be approximated as

$$H_{int} = -g_0 a^\dagger a (b + b^\dagger) \simeq -g_0 |\alpha|^2 (b + b^\dagger) - g_0 (\bar{\alpha}^* \delta a + \bar{\alpha} \delta a^\dagger)(b + b^\dagger) \ , \tag{1.6}$$

where the first term on the right hand side accounts for the average radiation pressure, with $|\alpha|^2$ the mean intensity of the light field. It induces a shift of the equilibrium position of the mirror by an amount $+g_0|\alpha|^2/\omega$ with respect to the empty scenario. Conversely, the second term, which is proportional to $\propto g_0 \sqrt{\langle a^\dagger a \rangle}(\delta a + \delta a^\dagger)(b + b^\dagger)$, represents the desired linearised interaction and can be solved analytically.
While the linearisation is sufficient to explain many facets of the light-matter interaction (see Ref.[1] and references therein), e.g. entanglement generation, state transfer, mechanical ground state cooling and squeezing, it fails to explain any non-Gaussian evolution of the system. Besides, the main target of this thesis is to shed light on the quantum (or deemed so) peculiarities of cavity optomechanics, which are achieved precisely through the exploitation of the non-linear cubic interaction. We shall broadly discuss how this requires the analysis of the quantum nature of the optical light field entering the cavity and interacting with the mirror. Such exploitation of the granular effects of the photon stream can be achieved in an experimental regime characterized by a decay rate smaller than both the coupling and the mechanical eigenfrequency, $\kappa < g_0$ and $\kappa \ll \omega$ [12].

## 1.3 The measurement scheme

In the previous section we discussed the groundwork of the interaction between an electromagnetic field and a reflective movable mirror in an optomechanical cavity, suggesting that this would be at the core of the preparation and manipulation of

quantum states of mechanical motion. We should now explain how to apply tools from quantum optics to properly assess the distinctive features attributable to those quantum states.

The measurement of a quantum state is a complex issue in quantum mechanics and the collapse of the wavefunction as a result of a given measurement lies at the basis of the theory. Quantum State Reconstruction (QSR) of individual systems, i.e. the tomography of a quantum state, is a cornerstone of modern experimental quantum optics and a considerable benefit in optomechanics consists in attaining QSR of the mechanical motion by reading out the light leaking from the cavity. This is possible thanks to the peculiar interaction that generates correlated states of the field inside the cavity and the mirror. Indeed, since the cavity field and the mirror are in a correlated state, performing a measurement on the former when it escapes the cavity results in the probabilistic preparation of well defined mechanical states. This technique has been defined as *conditioning technique* [13, 14], and it has already been applied to achieve strong cooling via the well known *Zeno effect* [15]. Conversely, if at any point in time the system is in a separable state, then field and

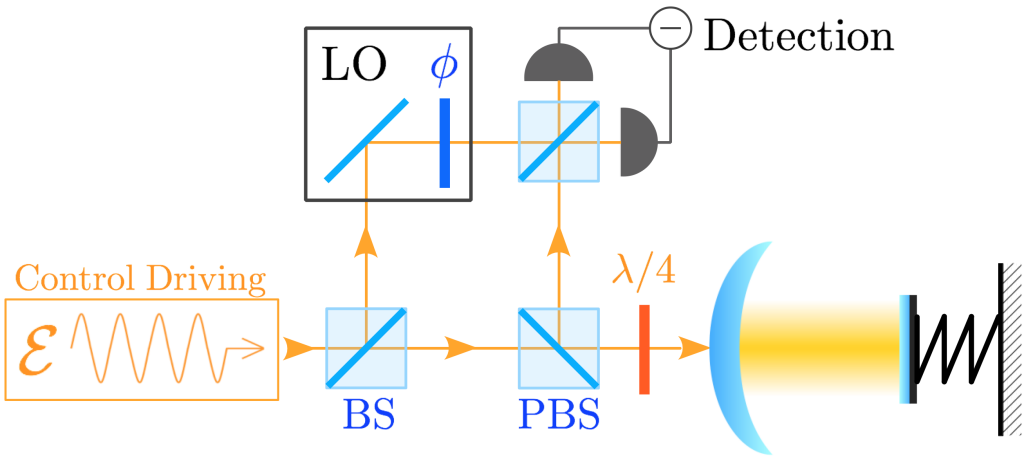


Figure 1.2: Conceptual scheme of the archetypical homodyne measurement setup for the light leaking from an optomechanical cavity. The coherent beam in input is divided by a beam splitter BS: one arm is used to pump the cavity and the other serves as a reference beam (LO) to perform interference measurements. Fringes are extracted from the difference between photo-current intensities in the final detectors. A polarising beam (PBS) and a $\lambda/4$ wave-plate are adopted to ensure that when light escapes the cavity it is conveyed towards the measurement apparatus.

mirror are uncorrelated and the latter is deterministically displaced in a given state. In order to characterise this state, a protocol has been proposed where the cavity is driven with a probe laser with frequency $\omega_0' = \omega_c - \omega$, the so called *red detuned* driving, such that the mechanical state is swapped from the mirror to the light field [11, 10]. A tomography of the original state of the mirror is eventually carried out reconstructing the Wigner function of the radiation that escapes the cavity through homodyne measurement [16]. This is a quasi-probability distribution that works as a quantum moment-generating functional, and thus encodes all quantum expectation values in phase space. From a mathematical perspective, the Wigner function of a quantum state $\rho$ is defined as the Fourier transform of its characteristic function: $W(\alpha) = \pi^{-2} \int d^2\beta \ \chi(\beta) e^{-2i(\alpha_r \beta_i - \alpha_i \beta_r)}$, with $\chi(\beta) = \mathrm{Tr}[\rho \ e^{\beta a^\dagger - \beta^* a}]$ and the subscript $_{r,(i)}$ is used to indicate the real (imaginary) part of the object it is referred to.

Let us then briefly introduce homodyne detection, as it is a standard technique consisting in measuring the probability distribution of the quadrature-field amplitudes. Its convenience lies in the fact that it directly provides a complete characterisation of the quantum state, which is achieved by reconstructing the Wigner distribution and its density matrix [17, 18]. The procedure is based on Michelson interferometry where the reference radiation, *i.e.* the local oscillator (LO), and the signal are derived from the same source: this arrangement has the advantage of being insensitive to fluctuations in the laser frequency (see Fig.1.2). The scattered light under scrutiny is eventually mixed with the local oscillator on a beam splitter BS and the interference fringes are measured subtracting the photo-current intensities on the final detectors. This difference, renormalised by the sum of the intensities, is defined as the *visibility* of the fringes and it is an important figure of merit, which will generally be a function varying with time and depending on a set of experimental parameters. The phase of the local oscillator $\phi$ is used to maximise the visibility. It can be shown (as we will do in Chap.2) that this scheme mathematically corresponds to a projection on light quadrature operators eigenstates, $X_\phi |x\rangle_\phi = x|x\rangle_\phi$, where $X_\phi = x_c \cos\phi + p_c \sin\phi$, the pair of operators $(x_c, p_c)$ denote respectively the *position* and *momentum* operators for the cavity field and $\phi$ is the phase relative to the local oscillator.

## 1.4 The quantum pulsed model

In the next two chapters we will consider the case where the continuous optical driving is turned off right after it has generated a defined light wave-packet within a very short time frame, *i.e.* a pulse. The system is then described by the time independent Hamiltonian presented in Eq.(1.2) (with $\hbar = 1$): $H = \omega_c a^\dagger a + \omega b^\dagger b - g a^\dagger a X$, where for convenience we have introduced the new symbol for the coupling $g = \sqrt{2} g_0$ and $X = (b^\dagger + b)/\sqrt{2}$ is the quadrature operator of the mirror. As the photon number $n_c = a^\dagger a$ is conserved and commutes with the whole Hamiltonian $H$, it is a common procedure to choose a frame rotating at the cavity frequency $\omega_c$ and subsequently describe the system in the interaction picture without the free evolution of the cavity. Defining $H_0 = \omega_c a^\dagger a$ and $H' = \omega b^\dagger b - g a^\dagger a X$, the states in the interaction picture can be written as $|\psi\rangle_I = e^{-iH_0 t} |\psi\rangle_s$, where $|\psi\rangle_s$ is expressed in the Schrödinger picture, and the evolution is induced by

$$H'_{int} = e^{i\omega_c a^\dagger a t} H' e^{-i\omega_c a^\dagger a t} = H' \ , \tag{1.7}$$

where we exploited the commutativity between $H_0$ and $H'$. For the sake of simplicity, in the next two chapters when no time dependent driving is considered, we will always choose this interaction picture and drop the subscript to the Hamiltonian, relabelling $H' \to H$.

To further investigate the pulsed model, we present hereafter its application to two different experimental regimes: the *bad* and the *good cavity* regime. They are defined respectively by low and high reflectivity of the fixed mirror, which directly affects the interaction time a single pulse remains into the cavity.

### 1.4.1 Bad cavity regime

The bad cavity regime has been developed over the last few years and is characterised by a very high decay rate (or, equivalently, very low finesse $\kappa = \pi c/(2L\mathcal{F}')$), i.e. $\kappa \gg \omega$, so that the interaction lasts much less than a mechanical period and light quickly escapes the resonator prior to a significant change in the position of

the movable mirror [19, 20]. In this case, the optimal input shape-resilient driving has proven to have a Lorentzian spectrum, which in the time domain assumes the form $\alpha_{in}(t) = \sqrt{\kappa}e^{-|\kappa|t}$. It is interesting to remark that from a quantum perspective the width of the light pulse $\delta\tau = \kappa^{-1}$ needs to satisfy the condition $\delta\tau \gg 2L/c$ to preserve the single mode approximation. Indeed, from Heisenberg uncertainty relation we know that the corresponding frequency bandwidth is $\delta\omega = \mathrm{K}(\delta\tau)^{-1}$ (with K a factor of order $O(10^{-1})$ depending on the shape of the pulse). Since from the resonance condition we have $\omega_c = (c/2L)n$, with $n$ the excited mode, we need $\delta\omega \ll (c/2L)$ to ensure that the adjacent modes to the resonance are not excited. Actually, interaction happens thanks to the fact that the bandwidth is larger than the length of the cavity, [3] while the pulsed condition $\kappa \gg \omega$ guarantees that the mechanical harmonic evolution can be neglected when solving the system dynamics. The interaction is thus determined via the unitary operator [20]

$$U_p = e^{i\lambda a^\dagger a X} \ , \tag{1.8}$$

with $\lambda = g/\kappa$ the rescaled coupling constant. We observe that this operator is a displacement of the mechanical oscillator along $P$ with amplitude $\lambda\langle n_c\rangle$, *i.e.* conditioned by the number of photons. We recall that the displacement operator is defined by its action on the vacuum state as $D(\beta)\,|0\rangle = |\beta\rangle$, where $|\beta\rangle$ is a coherent state, and reads

$$D(\beta) = e^{\beta b^\dagger - \beta^* b} = e^{i\sqrt{2}(\beta_i X - \beta_r P)}, \tag{1.9}$$

where $\beta_{r(i)}$ is the real (imaginary) part of $\beta$, corresponding to the amplitude by which the ground state is displaced along the $P$ $(-X)$ axis. The algebra of these objects derives from the commutation relation $[b, b^\dagger] = 1$ between $b$ and $b^\dagger$, and is specified in the identity

$$D(\beta)D(\gamma) = e^{i\ \mathrm{Im}\{\beta\gamma^*\}}D(\beta+\gamma) = e^{2i\ \mathrm{Im}\{\beta\gamma^*\}}D(\gamma)D(\beta) \ , \tag{1.10}$$

[3] As we are going to discuss, this is in contrast with the classical description of the phenomenon, where actually no interaction takes place, though light kicks the movable mirror and comes back and forth for $N_{\mathrm{rt}}$ times within a time interval $\tau$.

where $\mathrm{Im}\{\beta\gamma^*\} = \beta \cdot \gamma = |\beta|\ |\gamma| \sin\theta_{\beta,\gamma}$ corresponds to twice the area in phase space spanned by the pair of displacements and $\theta_{\beta,\gamma}$ is the angle between them.

It is clear at this point that a series of optical pulses inside the cavity, each of which are strongly interacting for a very short time, would result in a sequence of non commuting displacements of the mechanical oscillator with an additional extra phase term depending on the area enclosed in phase space. In particular, we will see that the angle between two subsequent displacements depends on the time elapsed between the two interactions. Opportunely tuning the time intervals among a series of pulses it is thus possible to drive the oscillator alongside predetermined polygons in phase space (either open or closed). To understand how this happens we should consider that as soon as light escapes the cavity, the harmonic oscillator evolves freely and $X$ and $P$ trade themselves under the action of $U_m(t) = e^{-ib^\dagger b\omega t}$

$$\begin{aligned} X(t) &= X(0)\cos\omega t + P(0)\sin\omega t\ , \\ P(t) &= P(0)\cos\omega t - X(0)\sin\omega t\ . \end{aligned} \tag{1.11}$$

The evolution in Eq.(1.11) corresponds a rotation in phase space by an amount $\omega t$, which will result in an angle of equal amplitude between two subsequent displacements separated by a time interval $t$. As an example, we present in Fig.1.3 a) the experimental scheme to draw a square by concatenating a series of four interactions and as many mechanical free evolutions, the former corresponding to the edges and the latter resulting in the (external) angle between two consecutive displacements. Let us then look closer at the analytical expression that describes this square evolution (see Fig.1.3b))

$$\begin{aligned} \xi_{square} &= U_p\ U_m^{\pi/\omega}\ U_p\ U_m^{\pi/\omega}\ U_p\ U_m^{\pi/\omega}\ U_p \\ &= U_p\ U_m^{3\pi/\omega}\ U_m^{-2\pi/\omega}\ U_p\ U_m^{2\pi/\omega}\ U_m^{-\pi/\omega}\ U_p\ U_m^{\pi/\omega}\ U_p\ , \end{aligned} \tag{1.12}$$

where for the sake of a compact expression we have $U_m(t) = U_m^t$. We also know that in general, given an unitary operator $\mathcal{T}$, we have that $\mathcal{T} f(\{Y_i\})\mathcal{T}^\dagger = f(\{\mathcal{T} Y_i \mathcal{T}^\dagger\})$ for any function $f$, unitary $\mathcal{T}$ and set of operators $\{Y_i\}$. It is then straightforward from Eq.(1.11) to verify that the operators $U_m^t$ rotate the mechanical quadrature in $U_p$ by

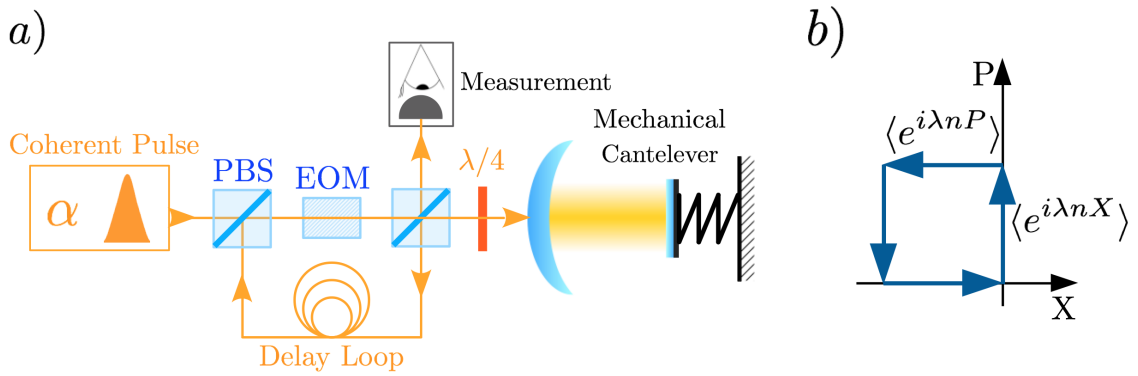


Figure 1.3: a) Schematic representation of the pulsed model. A sharp laser pulse horizontally polarised enters into an optomechanical cavity, interacts with the movable mirror and escapes remaining in a delay loop for an engineered time. The apparatus composed by the polarising beam splitters (PBSs), the $\lambda/4$ wave plate and the Electro-Optic Modulator (EOM) is used to rotate the polarisation before and after each pulse. After the last interaction the EOM does not rotate the polarisation and the pulse is measured interferometrically with respect to a reference field. b) Scheme of a four displacement operation in the phase space of the mechanical oscillator.

an angle $\omega t$, *e.g.* $U_m^{-\pi/\omega}\ e^{i\lambda a^\dagger a X}\ U_m^{\pi/\omega} = e^{i\lambda a^\dagger a P}$. Hence, we can rewrite Eq.(1.12) as (within a final rotation on the mechanics $U_m^{3\pi/\omega}$)

$$\xi_{square} = e^{-i\lambda a^\dagger a P} e^{-i\lambda a^\dagger a X} e^{i\lambda a^\dagger a P} e^{i\lambda a^\dagger a X} = e^{i\lambda^2 (a^\dagger a)^2}, \tag{1.13}$$

where we have used Baker-Campbell-Hausdorf (BCH) formula $e^A e^B = e^{A+B} e^{[A,B]/2}$ to compute the product of the exponentials (BCH would generally contain also all possible combinations of nested commutators, though in the present case they all happen to be zero). This expression *is strictly related to the commutation rules of mechanical quadrature operators* and as a whole it consists in a separable operator acting only on the optical field and leaving the mechanical state unchanged. This is a general property that applies to any evolution resulting in a closed polygon in phase space, which makes these transformations particularly significant since not only they leave the system in a separable state, but they are also noise resilient, being insensitive to the initial conditions of the mirror (*e.g.* mechanical thermal noise).

The separability of the system at the end of the evolution is the most significant

advantage of drawing closed loops in phase space, being an essential requirement to perform deterministic measurements on the mirror and to prevent losses of quantum coherence (which would be amplified by the presence of residual light-matter correlations). Indeed, as we have already mentioned, the correlations between the mirror and the optical field that arise during the interaction generally result in a mixed quantum state to be attributed to each system alone, preventing deterministic quantum preparation and measurement.

Eventually, let us anticipate a general property of $\xi_{loop}$, *i.e.* operators that describe closed loops: the phase acquired by a state undergoing the evolution in Eq.(1.13) always corresponds to the area drawn in the mechanical phase space when the system is initially assumed in its ground state. This holds for any initial state of mirror and is an important consequence of the Berry-like nature of the phase that we will discuss in details in the next chapter.

As we explained in Sec.1.3, an effective procedure to extract information on the operator in Eq.(1.13) is to perform an interference measurement between the light escaping the cavity after the fourth interaction and a reference field. This allows the reconstruction of the projection on light quadratures $\langle X_\phi\rangle = (\langle a^\dagger\rangle e^{i\phi} + \langle a\rangle e^{-i\phi})/2^{1/2}$ and finally perform QSR. From a theoretical perspective it is thus sufficient to compute the mean value of the optical field $\langle a\rangle$ after applying the displacement in (1.13) on the initial state of the system. As a first example, we take the field initially in a coherent state $|\alpha\rangle$, which can be decomposed in the basis of energy eigenstates $|j\rangle$ as $|\alpha\rangle = e^{-|\alpha|^2/2}\sum_j \alpha^j/\sqrt{j!}\,|j\rangle$, and the mirror in a generic, unspecified state. We obtain

$$\begin{aligned}\langle\alpha|\xi^\dagger_{square}\; a\; \xi_{square}|\alpha\rangle =& \langle\alpha|ae^{i\lambda^2(2a^\dagger a+1)}|\alpha\rangle \\ =& e^{-N_p}\;\alpha\sum_{j=0}^{\infty}\frac{N_p^j}{j!}e^{i\lambda^2(2j+1)} \\ =& \alpha\; e^{-N_p(1-\cos 2\lambda^2)}e^{i(\lambda^2+N_p\sin 2\lambda^2)}\;,\end{aligned} \tag{1.14}$$

where we have used the relation

$$e^{iSf[(a^\dagger a)^k]}ae^{-iSf[(a^\dagger a)^k]} = ae^{-iS(f[(a^\dagger a+1)^k]-f[(a^\dagger a)^k])} \tag{1.15}$$

and substituted $|\alpha|^2 = \langle n_c \rangle = N_p$. Eq.(1.14) shows that both the modulus and the phase of the field are affected by the non-linear interaction. On the one hand, the coherent amplitude $\alpha$ is exponentially suppressed by the number of photons, *i.e.* the intensity of the light field. This is directly attributable to the Kerr non-linear effect experienced by the field when entering into the cavity [21]; for small coupling the reduction can be estimated by expanding the cosine function with the factor $\sim e^{-2\lambda^4 N_p}$. On the other hand, the coherent field acquires a phase $\varphi_q = \lambda^2 + N_p \sin 2\lambda^2$, which scales linearly with the number of photons and the square of the rescaled coupling $\lambda$. In particular, as it emerges from Eq.(1.15), the offset term $\lambda^2$ comes exclusively from the commutation rules of the field. We anticipate here that both the visibility and the phase shift carry important information on the system.

### 1.4.2 Good cavity regime

The *good cavity* regime is defined by the condition $\kappa \ll \omega$, *i.e.* when the decay rate is smaller than the mechanical frequency. *red*Here a substantial amount of the input pulse remains in the cavity for a timescale that is comparable with the mechanical period thanks to the higher coefficient of finesse. The exact solution for the dynamics was firstly illustrated in Refs. [22, 2], where a detailed analysis is provided under the hypothesis to initially prepare the optical field in a given state and subsequently turn off the driving during the interaction. The assumption in this case is to operate in the so called *resolved side-band regime*, where optical damping and photon leakage from the cavity are negligible over an entire mechanical period and light and mirror continuously interact until the field escapes the cavity. A major theoretical advantage is that the time independent Hamiltonian $H = \omega b^\dagger b - g_0 a^\dagger a (b^\dagger + b)$ is diagonalisable and one can find the evolution operator $U(t) = \exp(-iHt)$ that fully describes the system.

Hereafter, we will go through the procedure presented in Refs.[22, 2] which starts by introducing the unitary operator

$$\mathcal{T} = e^{-\frac{g_0}{\omega} a^\dagger a (b^\dagger - b)} \tag{1.16}$$

to suitably transform $U(t)$. In particular, we should consider the transformations

$$\begin{aligned}
&\mathcal{T} b \mathcal{T}^\dagger = b + \frac{g_0}{\omega} a^\dagger a \ , \text{ and} \\
&\mathcal{T} a^\dagger a \mathcal{T}^\dagger = a^\dagger a \ , \text{ leading to} \\
&\mathcal{T} U(t) \mathcal{T}^\dagger = e^{-i b^\dagger b \ \omega t} e^{i \frac{g_0^2}{\omega^2} (a^\dagger a)^2 \ \omega t} \ .
\end{aligned} \tag{1.17}$$

Defining $k = g_0/\omega$ and multiplying the last expression on the left by $\mathcal{T}^\dagger$ and on the right by $\mathcal{T}$, so that to regain $U(t)$, we get

$$U(t) = e^{i(k a^\dagger a)^2 \omega t} e^{k a^\dagger a (b^\dagger - b)} e^{-i b^\dagger b \ \omega t} e^{-k a^\dagger a (b^\dagger - b)} \ . \tag{1.18}$$

Multiplying on the right by the identity $\mathbb{1} = e^{i b^\dagger b \ \omega t} e^{-i b^\dagger b \ \omega t}$, we swap the last two exponentials to move to the right the operators that act on the mirror. We obtain

$$U(t) = e^{i(k a^\dagger a)^2 \omega t} e^{k a^\dagger a (b^\dagger - b)} e^{-k a^\dagger a (b^\dagger e^{-i\omega t} - b e^{i\omega t})} e^{-i b^\dagger b \omega t} \ , \tag{1.19}$$

where we have used $e^{-i b^\dagger b \omega t} [a^\dagger a (b^\dagger - b)] e^{i b^\dagger b \omega t} = a^\dagger a (b^\dagger e^{-i\omega t} - b e^{i\omega t})$ (see Eq.(1.15)). Finally, by applying Baker-Campbell-Hausdorff formula we can combine the third and fourth exponentials and retrieve the compact form

$$U(t) = e^{i k^2 (a^\dagger a)^2 (\omega t - \sin \omega t)} e^{k a^\dagger a (\eta b^\dagger - \eta^* b)} e^{-i b^\dagger b \omega t}, \tag{1.20}$$

with $\eta = 1 - e^{-i\omega t}$. We could think of Eq.(1.20) as the sequential application of three operators. When $U(t)$ is applied to a product state of the cavity and the mirror, it first rotates the mechanical state by an angle $\omega t$, then (with the term in the middle) it displaces it by $k a^\dagger a \eta$, creating light-matter correlations, and finally it non-linearly acts on the cavity field alone.

Importantly, after a closed loop lasting a mechanical period the evolution is separable and results in $U(T) = \exp(2\pi i k^2 (a^\dagger a)^2)$, where we have neglected the term $\exp(-i 2\pi b^\dagger b)$ corresponding to the identity. As in Eq.(1.13), the expectation value of the final phase is related to the area drawn in the mechanical phase space assuming the mirror initially in the ground state, *i.e.* $2\pi k^2 \langle (a^\dagger a)^2 \rangle$. We will recover the same

result in the next chapter through a different approach.

Let us now look closer at the physics behind the continuous interaction and use the operator $U(t)$ in Eq.(1.18) to determine the evolution of an initial product state $|\Psi(0)\rangle = |\alpha\rangle_f \otimes |\gamma\rangle_m$, with $|\alpha\rangle_f$ and $|\gamma\rangle_m$ respectively a coherent state of the field and the oscillator. We obtain

$$|\Psi(t)\rangle = e^{-\frac{|\alpha|^2}{2}} \sum_{n=0}^{\infty} \frac{\alpha^n}{\sqrt{n!}} e^{ik^2n^2(\omega t - \sin\omega t)} e^{ikn[\gamma_R \sin\omega t + \gamma_I(1-\cos\omega t)]} |n\rangle_c \otimes |\Gamma_n(t)\rangle_m \ , \quad (1.21)$$

where $|n\rangle_c$ is a Fock state of the cavity field, $|\Gamma_n(t)\rangle_m = |\gamma e^{-i\omega t} + kn(1-e^{-i\omega t})\rangle_m$ a displaced coherent state of the mechanical oscillator, $\gamma_R$ and $\gamma_I$ respectively the real and imaginary part of $\gamma$.
Deriving the mean values of the oscillator position and momentum we reconstruct the path that the mirror draws in its phase space alongside the evolution. Computing the expectation values of mirror creation and annihilation operators

$$\langle \Psi(t)| \, b \, |\Psi(t)\rangle = \gamma e^{-i\omega t} + kN_p(1-e^{-i\omega t}) \ , \quad (1.22)$$

one gets the average values

$$\begin{aligned} \langle X(t)\rangle &= \sqrt{2}\gamma_R \cos\omega t + \sqrt{2}\gamma_I \sin\omega t + \sqrt{2}kN_p(1-\cos\omega t) \ , \\ \langle P(t)\rangle &= \sqrt{2}\gamma_I \cos\omega t - \sqrt{2}\gamma_R \sin\omega t + \sqrt{2}kN_p \sin\omega t \ . \end{aligned} \quad (1.23)$$

As shown in Fig.1.4, Eqs.(1.23) define a harmonic evolution in the quadrature phase space, *i.e.* a circle, shifted by $\sqrt{2}kN_p$ along $X$ and with initial conditions $\langle X(0)\rangle = \sqrt{2}\gamma_r$ and $\langle P(0)\rangle = \sqrt{2}\gamma_I$ and energy (amplitude) $E(t) = |\gamma|^2 + 2(kN_p)^2(1-\cos\omega t) + 2kN_p[\gamma_I \sin\omega t - \gamma_R(1-\cos\omega t)]$.

Second order moments also provide important information. We plot in Fig.1.4 the product $\Delta X^2(t)\Delta P^2(t)$ over a mechanical period as a quantifier of the quantum uncertainty associated with the mirror dynamics. While Heisenberg principle is always satisfied, the uncertainty oscillates and increases when mirror and light are correlated, and reaches the zero point level ($(\Delta X)^2 = (\Delta P)^2 = 1/2$) at every period, having a local minimum.

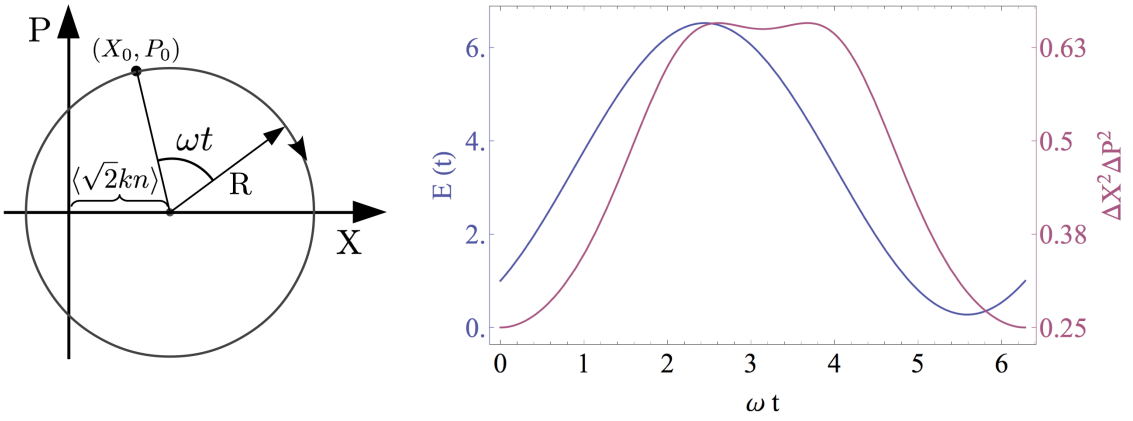


Figure 1.4: On the left: representation of the mirror dynamics ($\langle X(t)\rangle$,$\langle P(t)\rangle$) in the mechanical phase space with $\mathrm{R} = 2(|\gamma|^2 + N_p^2 + N_p(1 - 2\gamma_R k)$. On the right: energy of the mirror $E(t)$ (blue) and Heisenberg quantum uncertainty $\Delta X^2(t)\Delta P^2(t)$ (red) over an entire mechanical period (theoretical parameters are set as: $\gamma_R = \gamma_I = 0.5$, $k = 0.1$ and $N_p = 10$).

Eventually, we conclude the discussion computing the phase shift imparted to the light field after an interaction lasting a time $t$. In the case of a correlated state as the one represented by Eq.(1.21), we get the mean value of the optical field as $\langle\Psi(t)|\, a\, |\Psi(t)\rangle = \mathrm{Tr}[a\ \rho_c(t)]$, where $\rho_c(t) = \mathrm{Tr}_m\left[|\Psi(t)\rangle\langle\Psi(t)|\right]$ is the reduced density matrix of the cavity at time $t$, obtained after having traced out the mechanical degrees of freedom. The acquired phase shift reads

$$\varphi_q(\gamma, t) = 2k\left[\gamma_R \sin\omega t + \gamma_I(1 - \cos\omega t)\right] + P_Q(t) + N_p \sin\left[2P_Q(t)\right], \tag{1.24}$$

with $P_Q(t) = k^2(\omega t - \sin\omega t)$. As anticipated for the case of closed polygons, also in the continuous regime we recover the phase independence of the initial conditions when the loop in phase space is closed: $\varphi_q(\gamma, T) \equiv \varphi_q(T) = 2\pi k^2 + N_p \sin[4\pi k^2]$. This is a fundamental property that witnesses that any proposed experiment involving closed loops does not require specific initial mechanical state preparation (*e.g.* strong cooling). We will show in the next chapter how this plays a crucial role in the assessment of the quantum nature of the interaction.

## 1.5 Marshall et al. proposal

Prior to a thorough discussion on the features of the mechanical motion that can be deduced from the measurement of light phase shifts, we deem it appropriate to conclude this introductory review chapter by presenting the paper by William Marshall et al. "*Towards Quantum Superpositions of a Mirror*" [5]. Indeed, taking inspiration from the setup that was firstly proposed in Ref.[2], Marshall et al. argue that the visibility pattern associated with the interference measurement of light can be a tool to test the creation of superposition states of the mirror, and subsequently observe their decoherence.

The proposal adopts a Michelson interferometer conceptually similar to the one in Fig.1.2, that we represent in a slightly different version in Fig.1.5 for better clarity. Differently from the coherent pulses that we have used so far, the adoption of single photon sources is key to their *gedanken*-experiment, which also relies on a resolved

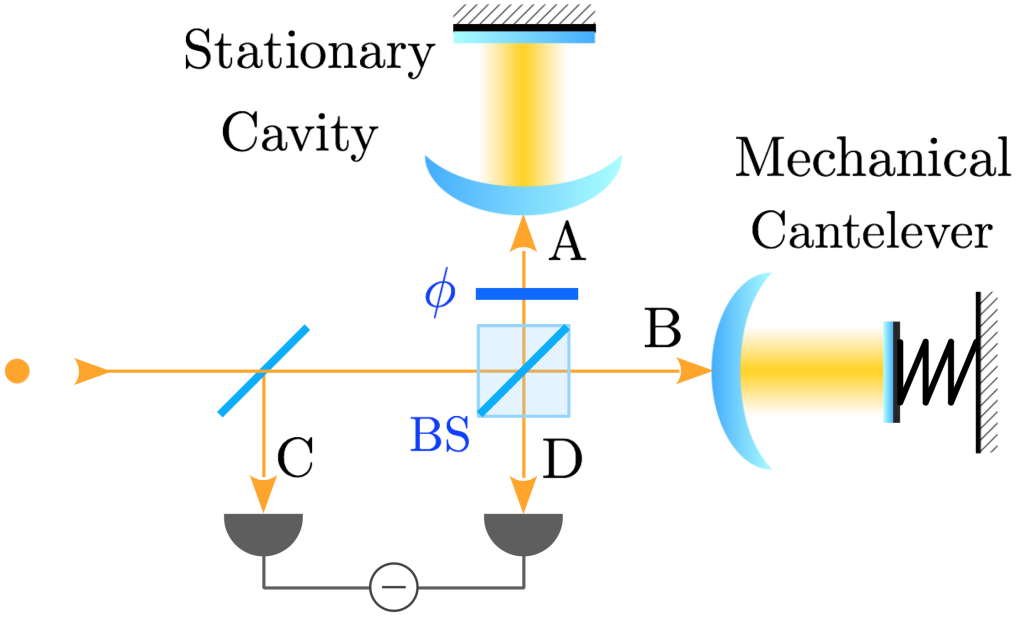


Figure 1.5: Proposed conceptual apparatus by Marshall et al. in Ref.[5]. A $|\psi^+\rangle$ Bell state is created impinging a single photon on a Beam Splitter (BS). The two outputs are sent respectively to a deformable cavity with a moving ending mirror (B) and a stationary one (A) with the same equilibrium length. When the single photon escapes the two resonators it interferes for a second time on the BS, whose outputs (C and D) are eventually interferometrically measured. The phase shift $\phi$ is part of the measuring scheme to maximise on the interference fringes.

sideband regime with very strong coupling $g/\omega \gtrsim 1$.

Let us then introduce the experimental apparatus, which is composed of two identical cavities arranged at the end of each arm of the interferometers. While cavity in arm $A$ has a fixed reflective boundary, the one in arm $B$ is supposed to have a movable ending mirror (which will be modelled as a harmonic oscillator). The latter is cooled down to its ground state and a single photon is injected in the interferometer so that an entangled state $|\Psi(0)\rangle = 2^{-1/2}(|0\rangle_A |1\rangle_B + |1\rangle_B |0\rangle_A) |0\rangle_m$ between the two arms is produced. After the interaction with the cavities, the photon exits the interferometer from outputs $C$ and $D$, and the whole system is in the superposition state

$$\begin{aligned} |\Psi(t)\rangle =& \frac{1}{2}\left[|1\rangle_C |0\rangle_D (|0\rangle_m + ie^{i(P_Q(t)-\Phi)} |\Gamma(t)\rangle_m)\right. \\ &\left. + |0\rangle_C |1\rangle_D (i|0\rangle_m + e^{i(P_Q(t)-\Phi)} |\Gamma(t)\rangle_m)\right] , \end{aligned} \tag{1.25}$$

where $P_Q(t) = k^2(\omega t - \sin\omega t)$ and $\Gamma(t) = k(1 - e^{-i\omega t})$. Repeating the experiment many times, we define with $I_{C(D)}$ the probability of detecting the photon in arm $C(D)$ (exploiting the similarity with the light intensity that is measured on the corresponding detector when Gaussian states are used). We then name $I = I_C - I_D$, such that the visibility for a single photon experiment can be expressed as the ratio $\nu_{sp} = (I_{max} - I_{min})/(I_{max} + I_{min})$, where $I$ is maximised and minimised by acting on the phase $\Phi$:

$$\nu_{sp} = e^{-\frac{|\Gamma(t)|^2}{2}} = e^{-k^2(1-\cos\omega t)}. \tag{1.26}$$

Eq.(1.26) clearly shows that the visibility of the interference fringes displays an oscillatory behaviour, being exponentially suppressed by the square of the coupling and exhibiting revivals at each mechanical period. This characteristic has led the authors in Ref.[5] to infer that "*the revival demonstrates the coherence of the superposition state that exists at intermediate times*". Conversely, "*if the environment of the mirror "remembers" that the mirror has moved, then, even after a full period, the photon will still be entangled with the mirror environment, and thus the revival will not be complete*". As a conclusion, the setup is eventually proposed as a tool to measure the decoherence of the mirror.

In the next chapter we will show that the preparation of the apparatus in a non-

classical state, *i.e.* ground state mechanical cooling and ultra-strong optomechanical coupling $g > \omega$, is an essential prerequisite to assess any form of decoherence. We present a very similar experimental proposal adopting classical coherent light in input. While no entanglement is generated in this way, still, we demonstrate that thanks to the particular optomechanical interaction, the mirror is projected in a superposition of coherent states with different amplitudes and the same figure for the visibility is recovered. On the other hand, we show that an initial thermal state of the mirror affects the visibility in a manner that can be fully explained from a classical perspective, so that loss and revivals are obtained without resorting to quantum mechanics.

# Chapter 2

# Probing the Quantumness in Cavity Optomechanics

## 2.1 Introduction

*The content of this chapter (with the exception of the last section) is part of a research that I conducted and shared in equal proportions together with a colleague at Imperial College, Federico Armata. More specifically, the topics covered in this chapter were the main object of a paper that has been published in Physical Review A with the title "Quantum and classical phases in optomechanics" [23].*

As a first step towards the study and manipulation of macroscopic quantum states, we review in this chapter the theoretical proposals and analyses presented in the *state of the art*, with the aim of identifying the truly quantum peculiarities of optomechanical cavities. The interest in the proper assessment of the quantumness in optomechanics stems from the fact that cavities are regarded as an optimal framework for comparisons between the predictions of classical theory [24] and their quantum counterparts [22, 2, 4], providing a thrilling arena to study the quantum-to-classical transition [25, 26, 27], collapse and decoherence models [28, 29, 30] and the interface between quantum mechanics and gravity [3, 31]. We will therefore devote the next two chapters respectively to the investigation of mechanical non-linearities and the deterministic creation of macroscopic quantum states.

We will see how the classical radiation pressure force due to the reflection of light on the mirror is able to explain the system dynamics under a wide range of achievable experimental conditions. Besides, we should also argue that such quantum-classical correspondence is not restricted to the specific optomechanical interaction proportional to $\propto g n_c X$. It is indeed a common feature of many two-body Hamiltonians where the displacement of one body (*e.g.* the mirror in our case) is conditioned by the state of the other (*e.g.* the cavity field) [32, 33, 34].
Deeper ongoing investigations consider this correspondence from a broader, topological perspective, looking at the link between the geometric origin of the quantum phase associated to the state of the system and the measurable classical optical phase shift of the light, *i.e.* the Hannay angle. The former derives from the non-commutativity of $X$ and $P$ [35], while the latter arises from the non-abelian character of the operations that are implemented, *e.g. displacements in phase space*. The phase acquired by a quantum state alongside its evolution is a topic of great interest, being an important carrier of information and exhibiting non-trivial behaviour [35]. It has been exploited in various contexts (see [36] and references therein) and has been considered as a candidate for quantum gate operations in quantum information processing [37, 38, 39, 40, 41, 42, 43].
As we have already shown, an important advantage in optomechanics is that the phase shift imparted to the light field during the interaction retrieves information on the quantum phase relative to the quantum superposition state that jointly describes the system of the cavity field and the mirror. As the optical phase can be easily read-out through interference measurements of the out-coming radiation, it has been reckoned as the ideal witness to measure quantumness in the motion of a mechanical oscillator [5, 3, 31].

We start this chapter by presenting a radically different description of the optomechanical system dynamics through classical mechanics and offering further insights on the transition from a *bad* to a *good* cavity regime. We then concentrate on the seminal work proposed by Marshall et al. [5] that was presented in Sec.1.5, where the authors suggested to study the creation and decoherence of superposition states of the mirror through visibility loss and revival of the field interference fringes. Key

to their proposal is the visibility recovery, which has always been of fundamental importance in physics, being explained by the *quantum recurrence theorem* which generalises Poincaré lemma[1] to quantum states [44, 45, 46]. Following this route, an intriguing problem is to clarify what can be predicted on the interaction of light fields and macroscopic objects by using only classical mechanics.
To this extent, we will show that the quantum and classical phases acquired by the field after the interaction with the mechanical oscillator coincide within today's widely used experimental parameters, with the exception of an offset, which we thus identify as the pure signature of quantumness. In addition, we find that both in the classical and in the quantum description the phase change becomes independent of the initial state of the oscillator at some interaction times where field and mirror are uncorrelated. As a direct consequence, the loss and revival of the visibility pattern can be recovered through a completely classical approach, which in turn implies that the visibility alone cannot be considered as a witness of quantum dynamics, *i.e.* as a proof of non-classical correlations between light and matter. Conversely, the classical analysis will allow us to attribute the visibility loss and revivals to an *ebb and flow* of information, which are related to a statistical uncertainty on the system initial condition.

## 2.2 The classical pulsed model

An optical field that reflects many times off a movable boundary gets a phase shift that is due to a doppler shift and a displacement of the mirror [47, 48]. More specifically, the phase associated with a single reflection of a field on a movable mirror is proportional to the product of the field wavevector $\mathrm{k}_f$ and the mirror position. Indeed, let us define with $\gamma = (c-v)/(c+v) \simeq 1 - 2v/c$ the Doppler coefficient for the reflection from a boundary moving with velocity $v \ll c$. The phase shift for a

[1] In Hamiltonian mechanics Poincaré lemma states that: *A system evolving in a bounded phase space will occupy a state arbitrarily close to its starting point after a sufficiently long time.*

planar wave can be written as

$$\frac{d\varphi_c}{dt} = -(1-\gamma)c\mathrm{k}_f \;\rightarrow\; \varphi_c(x) = 2\mathrm{k}_f \int v dt = 2\mathrm{k}_f \oint dx \;, \tag{2.1}$$

where the path-integral extends over all the positions occupied by the reflective mirror during the interaction.

In the bad cavity regime, the interaction described by $U_p$ in Eq.(1.8) can be classically depicted as a light kick transferring a momentum $\mathcal{I} = 2N_{rt}(E_0/c)$ to the mechanical oscillator, where $E_0$ is the energy of the input pulse. This could be naively explained if we consider that light remains inside the cavity for a time $\tau$, during which it performs $N_{rt} = c\tau/2L$ round trips, and at each reflection it transfers a momentum $2E_0/c$ [2].
Since in the bad cavity regime the interaction time is assumed to be much smaller than the mechanical timescale, $\tau \ll \omega^{-1}$, the mirror position is considered constant and a single reflection at position $\tilde{x}$ gives

$$\varphi_c(\tilde{x}) = 2\mathrm{k}_f \int_0^\tau \tilde{x} dt = 2\mathrm{k}_f N_{rt} \tilde{x} \;, \tag{2.2}$$

where time can be naively discretised by imposing the relation $dt = 2L/c$. The enhancement $N_{rt} = \mathcal{F}'/\pi$ arises if we consider that the interaction is composed of multiple reflections taking place within the short interval $\tau$.

Following Eq.(2.2), after a single kick the field picks up a global phase shift depending on the reference frame, which does not contain any extractable, frame independent information on the performed displacement. This is in agreement with the discussion in Sec.1.4.1 on the bad cavity regime, where a single displacement projected the system in a correlated state of mirror and light, without being measurable independently of the initial state. Conversely, it is interesting to extend this classical scheme to closed loops generated by multiple interactions. We use the 4 kicks case

[2] A rigorous solution of the dynamics induced by light reflection would also take into consideration the conservation of energy. The field frequency is in fact red-shifted after each *"kick"* and the momentum acquired by the mirror should be conveniently rescaled. However, the overall correction on $\mathcal{I}$ given by the exact solution scales as $\delta\mathcal{I}/\mathcal{I} = O(\mathcal{I}/(mc)) \sim 10^{-8}$ and can thus be neglected.

as specimen

$$\varphi_c = 2\mathrm{k}_f N_{rt} \sum_{j=0}^{3} x(t_j) \ , \tag{2.3}$$

where $x(t_j)$ are the classical positions of the mirror at times $t_j = j\pi/(2\omega)$, before the $(j+1)^{th}$ pulse enters the cavity. For a better understanding of the dynamics, we show in Fig.2.1 the evolution of the mirror in the classical phase space, together with the related quantum operators in the quadratures phase space. Each kick corresponds to an instantaneous variation of the mechanical momentum, i.e. to a vertical displacement in the classical phase space, while the harmonic evolutions are represented by blue circle arcs with amplitude $\pi/2$ (they are all supposed to last a quarter of period). Starting with the mirror at rest in a reference frame where $x(0) = 0$, the first kick transfers a momentum $\mathcal{I}$, such that after a time $t_1 = T/4$ it moves to $x(t_1) = \mathcal{I}/(m\omega)$ with instantaneous zero velocity $p(t_1) = 0$. A second kick comes in the cavity with the same momentum $\mathcal{I}$ and increases the energy of the oscillator, which is found at $t_2$ in the same position $x(t_2) = x(t_1)$, though with a

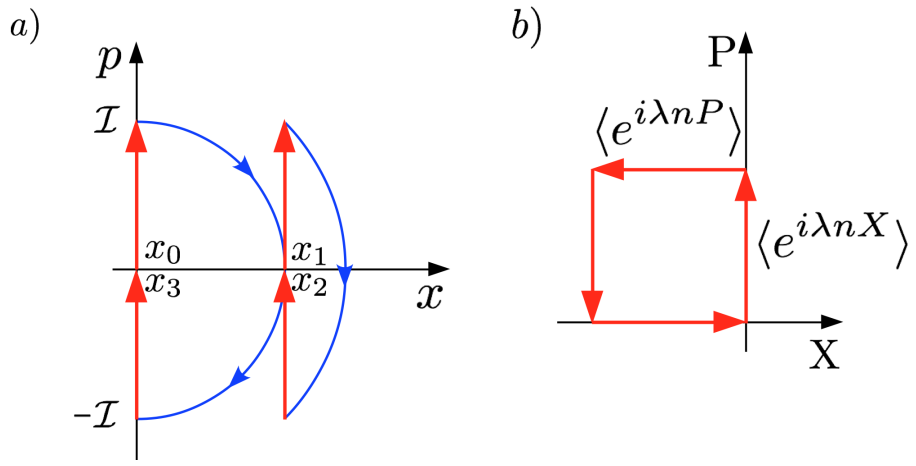


Figure 2.1: Four pulses cyclic evolution of the mirror. a) Motion in the classical phase space where the red arrows correspond to the instantaneous kicks each transferring a momentum $\mathcal{I}$ and the blue circle arcs the harmonic evolutions lasting a quarter of period. For the sake of a compact expansion we have $x_j = x(t_j)$, with $x_0 = x_3 = 0$ and $x_1 = x_2 = \mathcal{I}/(m\omega)$. b) Quadrature mechanical phase space: the displacements are represented by the same red arrows and the harmonic evolution within each interaction corresponds to the external angle. The two plots are related through the dimensional identity $\mathcal{I} = \sqrt{\hbar\omega m}\langle\lambda n\rangle$. (The figure has been readapted from Ref.[23].)

negative momentum $-\mathcal{I}$. The third kick instantaneously stops the mirror though the remaining energy makes it evolve harmonically for another quarter of period, when, in correspondence with the origin, it is definitely halted by a fourth kick. Substituting in Eq.(2.3) the positions at which the four reflections take place we obtain the classical phase

$$\varphi_c = 2\mathrm{k}_f N_{rt}\ 2\ x\left(\frac{\pi}{\omega}\right) = 4\mathrm{k}_f N_{rt}\frac{\mathcal{I}}{m\omega}\ , \tag{2.4}$$

where the linear scaling with respect to the light intensity is distinctive of a (classical) Kerr effect. This phase dependency on the intensity of the electromagnetic field, rather than its amplitude, plays a key role in the effectiveness of the classical description as well as in the quantum-classical parallelism. Hence, using Planck's law we express the transferred momentum in terms of the electromagnetic frequency and the number of incident photons to compare Eq.(2.4) to the quantum case. Substituting $E_0 \to N_p\hbar\omega_c$, we get $\varphi_c = 2\lambda^2 N_p$ which indicates how for today's state-of-the-art experimental parameters, *i.e.* small coupling and large number of photons [49, 1], we recover the classical limit of the quantum phase and $\varphi_q \to \varphi_c$. The discrepancy between the two pictures becomes instead substantial for large coupling and small $N_p$, when quantum features of the system are strongly enhanced [50, 51, 52]. It is worth noticing that the small coupling limit ($\varphi_q \to \lambda^2(2N_p+1)$) reveals quantum peculiarities due to the quantization of the field: *i.e.* the $+1$ term coming from field-bosonic commutation rules. Within such a feasible experimental regime, the main difference between $\varphi_q$ and $\varphi_c$ is an offset depending on $\lambda^2$. Since this offset can not be predicted with semi-classical descriptions where either the light or the mirror is quantised and the other is treated classically (see AppendixA for further details on semi-classical pictures), it represents the most accurate measurable signature of the quantum nature of the light-matter interaction. Indeed, one could engineer an experiment to measure the phase as a function of the photon number per pulse $N_p$ and fit the resultant data to obtain an estimate for $\lambda^2$. Counter-intuitively, a large optomechanical coupling is not strictly necessary for the purpose, as long as the phase is detected with high precision. Indeed, uncertainty is experimentally

mainly amenable to the quantum noise of the coherent state probe, which scales approximately as $\delta\varphi_q \sim 1/\sqrt{N_p N_r}$, where $N_r$ is the number of experimental runs. Current experiments that operate in the range $10^{-5} \lesssim \lambda \lesssim 10^{-1}$ and $N_p \sim 10^8$ [53, 54] would thus satisfy $\delta\varphi_q < \lambda^2$ and provide a good estimate for the quantum offset.

## 2.3 Multiple pulses: towards the continuous interaction

In the last section we have presented a parallelism between classical and quantum pictures when dealing with the pulsed driving of a bad cavity introduced in Sec.1.4.1. Aiming to derive an analogous equivalence for the good cavity regime, we now generalise the above argument and extend the correspondence between $\varphi_q$ and $\varphi_c$ to a generic number of kicks $\mathcal{N}$, drawing $\mathcal{N}$-sided polygons in phase space. This is achieved by reducing the waiting time between two consecutive pulses in Eqs.(1.11)-(1.12) and tuning it to $\Delta t = 2\pi/(\mathcal{N}\omega)$. We display in Fig.2.2 the evolution for six and eight kicks in phase space of the mechanical degree of freedom. Pulses correspond to straight displacements while harmonic evolution between two subsequent interactions

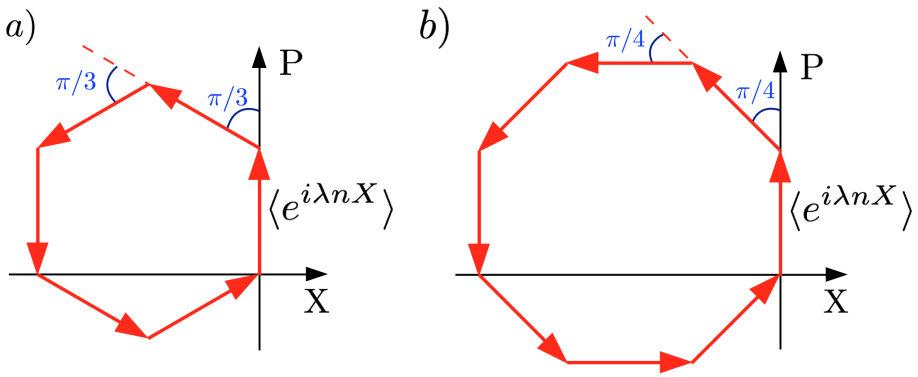


Figure 2.2: Quadrature phase space representation of a multiple pulse interaction with six (a) and eight (b) kicks. Red arrows depict the displacements induced by the short interaction with the strong light pulses. The length of the arrows is related to the intensity of the transferred momentum by $\mathcal{I} = \sqrt{\hbar\omega m}\langle\lambda n\rangle$. Mechanical harmonic evolutions within each interaction lasting $T/6$ (a) and $T/8$ (b) correspond to the external angles.

results in a rotation in phase space by $\theta = 2\pi/\mathcal{N}$.

*Quantum scheme.* For this scope it is useful to define the general displacement operator $\xi_{\mathcal{N}}$ which generalises Eq.(1.13) and corresponds to a closed trajectory in the phase space of the oscillator with the shape of a regular polygon of $\mathcal{N}$ sides of amplitude $\eta = \lambda n_c$

$$\xi_{\mathcal{N}} = \prod_{j=0}^{\mathcal{N}-1} e^{i\eta[X\cos(\theta j)+P\sin(\theta j)]} \ , \tag{2.5}$$

with $X\cos(\theta j) + P\sin(\theta j) = X(\theta j)$ from Eq.(1.11). This expression can be analytically calculated with a generalisation of first order Baker-Campbell-Hausdorff (BCH) formula to the product of $\mathcal{N}$ exponentials as

$$\prod_{k=0}^{\mathcal{N}-1} e^{A_k} = \exp\left[\sum_{k=0}^{\mathcal{N}-1} A_k + \frac{1}{2}\sum_{k>j}[A_k, A_j]\right] \ , \tag{2.6}$$

where the sum is extended over all the ordered combinations of couples of exponentials, and where we exploited the fact that since $[A_k, A_j]$ is a number, all other possible nested commutators in BCH expansion are zero. As expected in case of closed loops, the result does not contain any operators of the mechanical oscillator and can be written in a compact form as

$$\xi_{\mathcal{N}} = e^{i\Phi(\eta,\mathcal{N})}, \tag{2.7}$$

where $\langle\Phi(\eta,\mathcal{N})\rangle = \frac{1}{4}\langle\eta^2\rangle\mathcal{N}\cot(\pi/\mathcal{N})$ is the area mapped out by the sequence of displacements in phase space. We repeat the same algebraic steps performed in Eq.(1.14) to extract the phase and visibility of the outcoming field that is used to probe the mechanical dynamics. Assuming the incoming radiation initially in a coherent state $|\alpha\rangle_f$, we find the mean value of the optical field when the operator in Eq.(2.7) is applied

$$\langle a\rangle = \langle\psi_0|\xi_{\mathcal{N}}^{\dagger} a\ \xi_{\mathcal{N}}|\psi_0\rangle = \alpha\ e^{-N_p(1-\cos 2c)} e^{i(c+N_p\sin 2c)} \ , \tag{2.8}$$

with $c = (\lambda^2/4)\mathcal{N}\cot(\pi/\mathcal{N})$. The first exponential factor on the right hand side of Eq. (2.8) represents the amplitude of the outcoming radiation, while the second

characterises the phase shift that we rewrite for clarity

$$\varphi_q = \frac{\lambda^2}{4}\mathcal{N}\cot\left(\frac{\pi}{\mathcal{N}}\right) + N_p \sin\left[\frac{\lambda^2}{2}\mathcal{N}\cot\left(\frac{\pi}{\mathcal{N}}\right)\right] \ . \tag{2.9}$$

As for the pulsed and the continuous regimes discussed in Sec.1.4.1-1.4.2, Eqs.(2.7)-(2.8) are independent of the initial state of the mirror, being referred to an evolution lasting an entire mechanical period and performing a closed loop in phase space. We observe from Eq.(2.9) that the phase shift, as well as the quantity $\Phi(\eta, \mathcal{N})$ in Eq.(2.7), scales quadratically in the number of kicks, being $\mathcal{N}\cot(\pi/\mathcal{N}) \sim \mathcal{N}^2/\pi$ for large $\mathcal{N}$. This is consistent with the geometric representation in Fig.2.2, where the area enclosed in phase space scales quadratically in $\mathcal{N}$ if one keeps the side of the polygon constant and increases the number of sides. However, such regime does not have a meaningful physical interpretation, since for arbitrary $\mathcal{N}$ it would lead to arbitrarily large displacements and energies, outside the scope of applicability of the interaction Hamiltonian $H_{int}$ [7] and of the pulsed-bad cavity regime ($N_{\rm rt} > 1$).

Instead, one obtains feasible results by conveniently rescaling the transferred momentum while reducing the waiting time between two pulses, and thus increasing the number of pulses applied in one mechanical period. To understand the procedure, let us start from the end and take the limit $\mathcal{N} \to \infty$: the evolution naturally approaches the case of a continuous interaction given by the unitary operator in Eq.(1.20), i.e. when light remains in the cavity for the entire mechanical period. Interestingly, as we have already mentioned, this corresponds to a different regime, long-pulsed or continuous, characterised by optimal cavity reflectivity and negligible decay $\kappa \ll \omega$. The connection can be explored by modelling the continuous interaction as a series of kicks, each followed by a very short harmonic evolution. This is indeed the very general assumption at the basis of the Suzuki-Trotter expansion for a unitary

operator, which in our case reads

$$\begin{aligned} e^{-\frac{i}{\hbar}Ht} &= \lim_{\mathcal{N}\to\infty} (e^{-\frac{i}{\hbar}H_0 t/\mathcal{N}}\, e^{-\frac{i}{\hbar}H_{int} t/\mathcal{N}})^{\mathcal{N}} \\ &= \lim_{\mathcal{N}\to\infty} \prod_{j=0}^{\mathcal{N}-1} (e^{-\frac{i}{\hbar}H_0 tj/\mathcal{N}}\, e^{-\frac{i}{\hbar}H_{int} t/\mathcal{N}}\, e^{-\frac{i}{\hbar}H_0 tj/\mathcal{N}}) \\ &= \lim_{\mathcal{N}\to\infty} \prod_{j=0}^{\mathcal{N}-1} e^{ign_c[X\cos(\theta j)+P\sin(\theta j)]\frac{t}{\mathcal{N}}} \ . \end{aligned} \tag{2.10}$$

It is straightforward to notice that Eq.(2.10) corresponds to the limit $\mathcal{N} \to \infty$ in Eq. (2.5), with the rescaling $\eta \to \eta t/\mathcal{N}$. This is a counterintuitive identity between two opposite physical regimes. While the continuous dynamics is obtained in the good cavity regime, when the reflectivity of the mirror is very high and light remains in the cavity for a long time, applying the rescaling in Eq.(2.5) implies a very poor mirror reflectivity with a finesse inversely proportional to $\mathcal{N}$. Here, light interacts for a very short time $t/\mathcal{N} \gtrsim 2L/c$, escapes the resonator and is equally rapidly re-injected. This last assumption will prove to be essential to retrieve the good cavity regime. The mathematical limit for $\mathcal{N} \to \infty$ can be computed analytically and for $t = T = 2\pi/\omega$ gives

$$e^{-iH\frac{2\pi}{\omega}} = e^{i\frac{\pi g^2 n_c^2}{\omega^2}} \ , \tag{2.11}$$

which corresponds to the unitary operator in Eq.(1.20) evaluated after a mechanical period and describing a circle with radius $g\langle n_c\rangle/\omega$ in phase space.

*Classical scheme.* From a conceptual point of view, it is straightforward to extend the model that regulates the phase shift imparted to the light in Eq.(2.3) to a general number of light kicks $\mathcal{N}$ occurring at times $t_j = 2j\pi/(\mathcal{N}\omega)$

$$\varphi_c = 2\mathrm{k}_f N_{rt} \sum_{i=0}^{\mathcal{N}-1} x(t_i) \ . \tag{2.12}$$

During the time between two consecutive kicks the movable mirror freely evolves accordingly to the equations of motion of a harmonic oscillator $x(t) = x(t_j)\cos\omega(t -$

$t_j) + p(t_j)/(m\omega)\sin\omega(t-t_j)$ with $t \in [t_j, t_{j+1}]$. In this period of time a waiting loop should be engineered to delay the light pulse before it is re-injected in the cavity. The length of such loop should linearly decrease with $\mathcal{N}$, as the time window corresponds to the external angle between two subsequent displacements in phase space (*i.e.* two subsequent sides of the polygon).
The general idea is that for a large $\mathcal{N}$ we will progressively go towards a regime with a lower finesse and where the number of round trips $N_{\rm rt}$ that light performs in the cavity at each interaction decreases. This physically corresponds to a rescaling of the transferred momentum $\mathcal{I} \to \mathcal{I}/\mathcal{N}$ and mathematically matches the rescaling of the interaction in Eq.(2.10) $g\langle n_c\rangle\tau \to g\langle n_c\rangle\tau/\mathcal{N}$ that arises with Trotter expansion.

Without losing generality, we suppose the mirror initially at rest in ($x = 0$, $p = 0$)[3] and plot in Fig.2.3 a loop of six kicks in the phase space of the harmonic oscillator and compare it with the four kicks case. The solution of such discrete dynamics for a general number of kicks $\mathcal{N}$ is quite a pedantic arithmetic problem that requires a non-trivial parametrisation of the motion in phase space. We proceed through geometric considerations and swap to the polar coordinates $(R(t_j), \vartheta(t_j))$ to describe the state of the mirror at time $t_j$, just before the $(j+1)^{\rm th}$ kick (see Fig.2.3). At the first interaction we have $R(t_0) = 0$ and $\vartheta(t_0) = 0$ while, for the following kicks, i.e. $j = 1, ..., (\mathcal{N}-1)$, we have

$$\begin{aligned} R(t_j) &= \sqrt{\zeta^2 + 2R(t_{j-1})\zeta\cdot\cos\left(\vartheta(t_{j-1})\right) + R(t_{j-1})^2} \\ \vartheta(t_j) &= \frac{2\pi}{\mathcal{N}} + \arcsin\left[\frac{R(t_{j-1})}{R(t_j)}\cdot\sin\left(\vartheta(t_{j-1})\right)\right] , \end{aligned} \tag{2.13}$$

where $\zeta = \mathcal{I}/(m\omega)$ quantifies the classical displacement and the positions $x(t_j)$ are simply given by the projections $x(t_j) = R(t_j)\sin(\vartheta(t_j))$. The sum over all the $\mathcal{N}$ positions turns out to have a simple analytical expansion $\sum_{j=0}^{\mathcal{N}-1} x_j = \zeta\mathcal{N}\cot(\pi/\mathcal{N})/2$, which leads directly to the classical phase (substituting in Eq. (2.12))

$$\varphi_c = \mathrm{k}_f N_{rt}\frac{\mathcal{I}}{m\omega}\mathcal{N}\cot\left(\frac{\pi}{\mathcal{N}}\right) \to \frac{2\hbar\mathcal{F}'^2\mathrm{k}_f^2 N_p}{\pi^2 m\omega}\mathcal{N}\cot\left(\frac{\pi}{\mathcal{N}}\right) , \tag{2.14}$$

[3]The generalisation to different initial conditions is obtained by simply applying a translation in phase space.

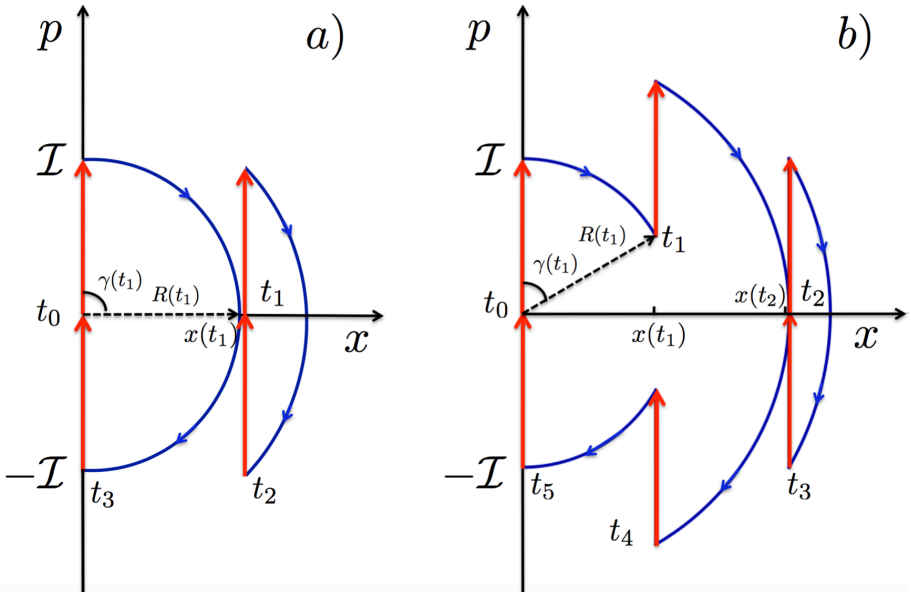


Figure 2.3: Phase space description of the mirror dynamics in a pulsed experiment in the classical picture. a) Four pulse interaction model: the oscillator is assumed at rest at the origin of the phase space. The oscillator gains a momentum $\mathcal{I}$ due to the interaction at $t = t_0$. Then it freely evolves to the maximum amplitude $x(t_1)$ when the second pulse happens, this causes another momentum gain of the oscillator at time $t_1$. At this time the oscillator evolves to $x(t_2) = x(t_1)$ where the third pulse interaction brings its momentum to zero. Now, it evolves to $x(t_3) = 0$ where its momentum becomes $-\mathcal{I}$. Finally, the oscillator is brought back to the origin of the phase space by the last pulse-oscillator interaction. b) A similar dynamics is plotted for the six pulse interaction.

where we have replaced the classical expressions for $\mathcal{I}$ and $E_0$.

The relation between the quantum and classical optical phases in Eqs. (2.14) and (2.9) is the same as for the pivotal case with four kicks. Eq.(2.9) holds also for strong coupling regimes where quantum features of the system are enhanced and the $+1$ term in Eq.(2.15) reveals quantum peculiarities due to the quantization of the field. Nevertheless, for the most common experimental conditions, i.e. small coupling ($\lambda \ll 1$) and strong laser sources ($N_p \gg 1$), quantum and classical phases coincide. Indeed, in the reasonable experimental limit of small coupling in Eq.(2.9) we have

$$\varphi_q \simeq \frac{\lambda^2}{4}\mathcal{N}\cot\left(\frac{\pi}{\mathcal{N}}\right)(1+2N_p) = \frac{\hbar\mathcal{F}^2\mathrm{k}_f^2}{\pi^2 m\omega}\mathcal{N}\cot\left(\frac{\pi}{\mathcal{N}}\right)(1+2N_p)\ . \tag{2.15}$$

## 2.4 The Classical Continuous interaction

We now approach the case of a continuous interaction in a good cavity regime from a classical perspective (with pulsed driving). As suggested by the past analysis with an asymptotically large number of pulses, we will retrieve the same correspondence between the two pictures. However, instead of taking the limit of the discrete regime for large $\mathcal{N}$, we prefer to directly write and solve the classical Hamiltonian of the system. This is a rather easy problem since the continuous interaction consists in a constant force during the whole evolution, whose strength is derived from the impulse-momentum theorem $F = \partial P/\partial t = 2E_0/(cdt) = E_0/L$, with $E_0$ the field energy. The classical Hamiltonian will then read

$$H_c = \frac{1}{2}m\omega^2 x^2 + \frac{1}{2m}p^2 - \frac{E_0}{L}x \ , \tag{2.16}$$

and gives rise to the solution

$$x(t) = x(0)\cos\omega t + \frac{p(0)}{m\omega}\sin\omega t + \frac{E_0}{m\omega^2 L}(1-\cos\omega t) \ . \tag{2.17}$$

Substituting the optomechanical parameters and bearing in mind that $E_0 = \hbar\omega_c N_p$ and that the initial displaced Gaussian quantum state $|\gamma\rangle_m$ corresponds to the classical boundary conditions $x(0) = \sqrt{2}\gamma_R\sqrt{\hbar/(m\omega)}$ and $p(0) = \sqrt{2}\gamma_I\sqrt{\hbar m\omega}$, we verify the correspondence with the quantum dynamics found in Eq.(1.23).

Furthermore, we derive the classical phase acquired during a continuous evolution by generalising Eq.(2.2) to the case in which the mirror position changes during the interaction

$$\begin{aligned}\varphi_c(x(0),p(0),t) &= 2\frac{\mathrm{k}_f}{d\tilde{\tau}}\int_0^t x(\tau)d\tau \\ &= \frac{\omega_c}{L\omega}\left[x(0)\sin\omega t + \frac{p(0)}{m\omega}(1-\cos\omega t)\right] + \frac{\omega_c}{\omega^3 m L^2}E_0(\omega t - \sin\omega t),\end{aligned} \tag{2.18}$$

with $d\tilde{\tau} = 2L/c$ the round trip time.

The limit $\varphi_q \to \varphi_c$ is satisfied for small coupling and large photon number and for a

closed loop we get a phase shift $\varphi_c(T) = 2\pi\omega_c E_0/(\omega^3 m L^2) = 4\pi k^2 N_p$ that is linearly dependent on the field intensity.

Again, the main difference between $\varphi_q$ and $\varphi_c$ is an offset depending on $k^2$ (it coincided with $\lambda^2$ for the four pulse case), whose measurement would certify the quantum nature of the light-matter interaction in an experiment.

## 2.5 Quantum vs classical visibilities

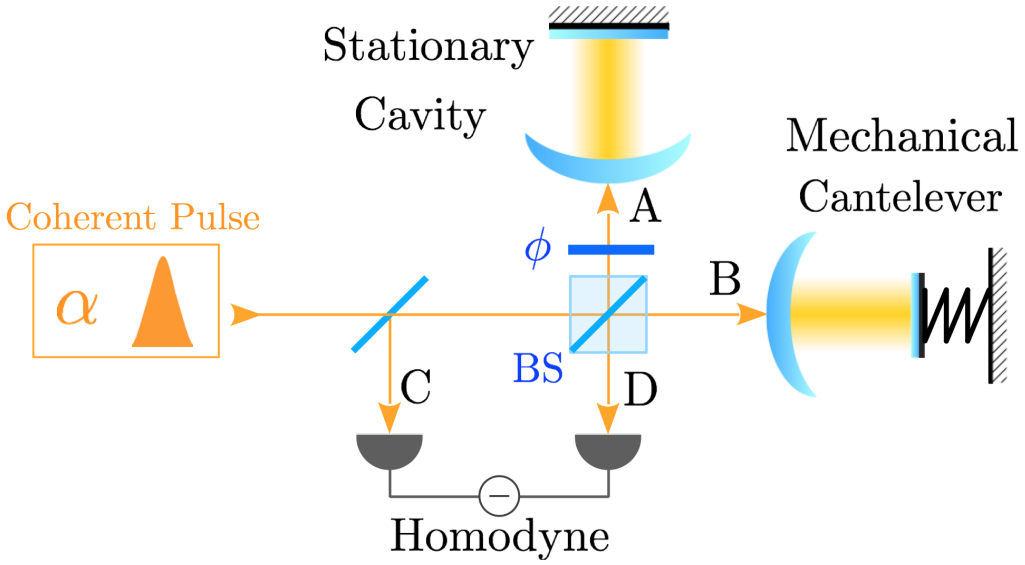


Figure 2.4: Michelson interferometer: a coherent field $|\alpha\rangle_f$ is split by a beam splitter (BS) in the two arms of the interferometer. Arm B ends with an optomechanical cavity with a movable oscillator, while arm A is composed of a phase shifter and a stationary cavity. Homodyne detection is performed subtracting the photo-currents in the detectors at the end of arms C and D.

In the following, we will see how the dependence of the light phase shift on the initial conditions is related to the creation of correlations between light and matter. This will have non-trivial implications on the quantum-classical correspondence. Let us refer to the Michelson interferometer that we presented in Sec.1.5 and reproduced in a slightly different version in Fig.2.4 for better clarity. Differently from previous proposals, we study the visibility of the interference pattern assuming the field initially in a coherent state $|\alpha\rangle$. The choice of such a Gaussian state, that has its classical counterpart in a monochromatic wave, allows us to perform a comparison

between the two pictures. Besides, coherent states are deterministically split into two equal components by $50:50$ beam splitters, and no (quantum) entanglement is created between the arms of the interferometer, as was the case in previous proposals [5, 55].

*Quantum Picture.* We assume the input field and the mirror initially in a separable state, the latter being in a mechanical thermal state $\rho_m(0)$ at equilibrium with the environment at temperature $T_e$

$$\rho(0) = \rho_c(0) \otimes \rho_m(0) = |\alpha\rangle_c \langle\alpha| \otimes \frac{1}{\pi\bar{n}} \int d^2\gamma e^{-\frac{|\gamma|^2}{\bar{n}}} |\gamma\rangle_m \langle\gamma| \ , \tag{2.19}$$

where $\bar{n} = 1/(e^{\beta\hbar\omega} - 1)$ is the average thermal occupation number and $\beta = (k_B T_e)^{-1}$, with $k_B$ the Boltzmann constant. By solving Liouville equation $\dot{\rho} = -i[\rho, H]$ for the system density matrix one obtains the evolution at time $t$

$$\rho(t) = e^{-|\alpha|^2} \sum_{m,n} \frac{\alpha^n \alpha^{*m}}{\sqrt{n!m!}} \times e^{iP_Q(t)(n^2-m^2)} D[kn\gamma]\rho_m(0)D[-km\gamma] |n\rangle_c \langle m| \ , \tag{2.20}$$

with $P_Q(t) = k^2(\omega t - \sin\omega t)$ and $D(\sigma) = \exp[\sigma b^\dagger - \sigma^* b]$. As the reader will know by now, we will eventually read out the mechanical motion through interference measurements of the field. Let us then calculate the field reduced density matrix tracing out the mechanical degrees of freedom. Remembering that the trace is invariant under cyclic permutations and that the product of two displacements satisfies $D(\varsigma)D(\sigma) = e^{i\mathrm{Im}[\varsigma\sigma^*]}D(\varsigma + \sigma)$, we get

$$\rho_c(t) = e^{-|\alpha|^2} \sum_{m,n} \frac{\alpha^n \alpha^{*m}}{\sqrt{n!m!}} \times e^{iP_Q(t)(n^2-m^2)} e^{-k^2(n-m)^2(1-\cos\omega t)(2\bar{n}+1)} |n\rangle_c \langle m| \ . \tag{2.21}$$

With the state of the cavity field at hand, the intensities on the output detectors $I_D^C(t)$ in Fig.1.5 read

$$\begin{aligned} I_D^C(t) = \frac{I_0}{2}\left(1 \pm \frac{\langle X_\phi\rangle}{\sqrt{2}}\right) = \frac{I_0}{2}\{1 \mp e^{-\left\{k^2[1-\cos\omega t](2\bar{n}+1)+N_p[1-\cos(2P_Q(t))]\right\}} \times \\ \times \cos[P_Q(t) - \phi - N_p \sin(2P_Q(t))]\} \ , \end{aligned} \tag{2.22}$$

where $I_0$ is the intensity measured on the detectors for the unperturbed initial

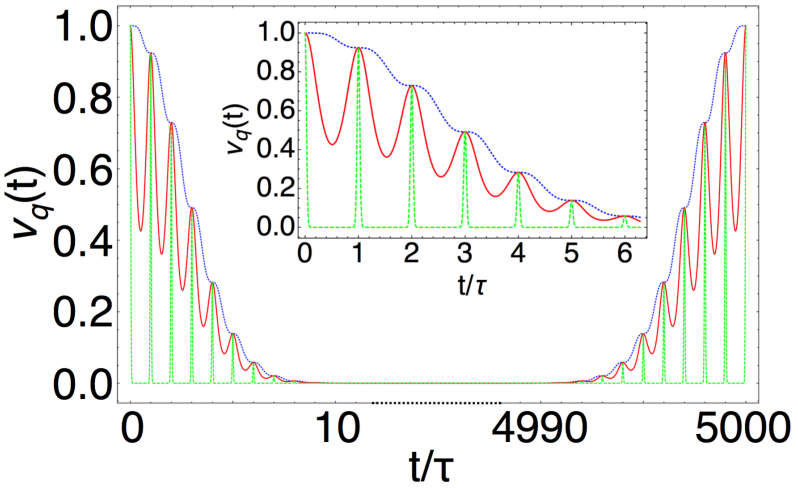


Figure 2.5: Quantum visibilities $\nu_q(t)$ in Eq.(2.23) for $T_e = 10^{-5}$k (blue dotted line), $T_e = 10^{-2}$k (red continuous line) and $T_e = 1$ k (green dashed line); optomechanical coupling $k = 10^{-2}$, number of photons $N_p = 10^5$ and period $T = 10^{-5}s$. For relatively high temperature the visibility is strongly suppressed within every single oscillating period. Instead, in the low temperature limit visibility is slightly lowered and the main effect is due to the Kerr non-linearity experienced by the field. (The figure has been taken from Ref.[23].)

coherent state. As we have already discussed, performing homodyne detection basically consists in operating on the local oscillator to vary the phase shift $\phi$ such that $\phi = P_Q(t) - N_p \sin(2P_Q(t))$ and the difference of the two induced photo-currents is maximised. The exponential in Eq.(2.22) then corresponds to the related quantum visibility $\nu_q(t)$ and can be conveniently expressed as the product of two components $\nu_q(t) = \nu_q^{cor}(t)\nu_q^{Kerr}(t)$

$$\begin{aligned} \nu_q^{cor}(t) &= e^{-k^2(1-\cos\omega t)(2\bar{n}+1)} \ , \text{ and} \\ \nu_q^{Kerr}(t) &= e^{-N_p[1-\cos(2k^2(\omega t-\sin\omega t))]} \ , \end{aligned} \tag{2.23}$$

which will later be linked to the light-matter correlations and the Kerr non-linearity. In Fig.2.5 we plot the visibility $\nu_q(t)$ over several mechanical periods and for different initial temperatures. The picture shows how the combination of two periodic functions with different frequencies in Eq.(2.23) gives rise to visibility drops and revivals over two time scales. The thermal noise in the initial state of the mechanical oscillator is responsible for the fastest oscillations $\nu_q^{cor}(t) = e^{-k^2(2\bar{n}+1)(1-\cos\omega t)}$, whose period

coincides with the mechanical period $T = 2\pi/\omega$, as expected from the fact that the mirror displaces closed loops in phase space. These oscillations act as a carrier wave for the modulation in the visibility pattern induced by $\nu_q^{Kerr}(t)$ that operates on a longer timescale $\tau' = 2\pi/(2k^2\omega) \to T/2k^2$. This behaviour had never been studied before and plays a crucial role for the visibility: for a complete understanding of the phenomenon it is essential to regard the two terms in comparison.
$\nu_q^{cor}(t)$ shows revivals of the visibility only due to the decoupling of field and mirror after an integer number of periods (i.e. for a closed loops in phase space) and witnesses light-matter correlations at intermediate times (see Fig.2.5). However, as we will verify in the next section, the $+1$ term in the exponent $-k^2(1-\cos\omega t)(2\bar{n}+1)$ is the only reliable marker of quantum correlations, corresponding to the result obtained in Eq.(1.26), where the creation of light-matter entangled states was proposed via a single photon experiment. Conversely, without initial ground state cooling, the predominant term depending on the average thermal population $\bar{n}$ causes a drop in the visibility that is due to the statistical uncertainty of the initial state of the mirror, on which the phase shift strongly depends (see Eq.(1.24)).
On the other hand, $\nu_q^{Kerr}(t)$ arises from the Kerr effect experienced by the field when entering into the cavity [21]. In particular, while the mirror returns to its original position in phase space after a mechanical period $T$, this does not apply to the field. The coherent state $|\alpha\rangle$ is not an eigenstate of the number operator $n_c$ in the interaction Hamiltonian $\propto n_c X$, and the field is transformed in a different coherent superposition of Fock states. In other words, from a quantum perspective a coherent field is not monochromatic, being actually defined by a precise, Poissonian, energy distribution: it is exactly this *uncertainty* of the energy of the state that causes the loss of visibility over a timescale $\tau'$. This explanation will become more clear in the next section, where we discuss the expected visibility pattern under a classical perspective. Most importantly, however, we are already able to induce a general rule: the loss of visibility is always associated with a source of uncertainty on the initial conditions.

*Classical Picture.* Let us now investigate the system with a fully classical approach and show under which conditions the visibility pattern with losses and revivals

can be recovered. We will conclude that correlations between light and matter predominantly have a classical nature and are due to the statistical uncertainty on the initial conditions.

We start by describing the Michelson interferometer in Fig.2.4 in a classical picture. After escaping the cavities the two fields have the form

$$\begin{aligned} \mathcal{E}_C &= \frac{i}{\sqrt{2}}\mathcal{E}_0 e^{i\varphi_c(t)} \ , \\ \mathcal{E}_D &= \frac{1}{\sqrt{2}}\mathcal{E}_0 e^{i\phi} \ , \end{aligned} \tag{2.24}$$

with $\mathcal{E}_0$ the input field amplitude and $\varphi_c(t)$ and $\phi$ the phases acquired in the deformable and fixed cavity respectively. The final intensity on the detectors results in

$$I_D^C(t) = \frac{I_0}{2}[1 \pm \cos(\varphi_c(t) - \phi)] \ , \tag{2.25}$$

where as usual $I_0 = |\mathcal{E}_0|^2$ is related to the energy $E_0$ carried by the field. We introduce thermal fluctuations on the mirror by expressing the initial state in terms of polar coordinates $\varrho$ and $\theta$ as

$$\begin{aligned} x(t=0,\ \theta, T_e) &= \sqrt{2/(m\omega^2)}\varrho(T_e)\cos\theta \ , \\ p(t=0,\ \theta, T_e) &= \sqrt{2m}\varrho(T_e)\sin\theta \ , \\ \varrho^2(T_e) &= \frac{m\omega^2}{2}x^2(0,\theta,T_e) + \frac{p^2(0,\theta,T_e)}{2m} \ , \end{aligned} \tag{2.26}$$

where $\varrho^2(T_e)$ is the initial thermal energy of the mirror defined by a Maxwell-Boltzmann distribution (see Fig.2.6a for the probability density function that characterises the distribution of $\varrho(T_e)$). Such classical thermal state is characterised by zero mean values of the oscillator position and momentum, $\bar{x} = 0$ and $\bar{p} = 0$, and average energy $\bar{\rho^2}(T_e) = \beta^{-1} = k_B T_e$. The phase shift associated with each possible evolution starting at various initial points in phase space is obtained by substituting Eqs.(2.26) as initial conditions in Eq. (2.18):

$$\varphi_c(\varrho,\theta,t) = \sqrt{2}\chi\varrho\left[\cos\theta\sin\omega t + \sin\theta(1-\cos\omega t)\right] + \frac{\omega}{\omega_c}E_0\chi^2(\omega t - \sin\omega t) \ , \tag{2.27}$$

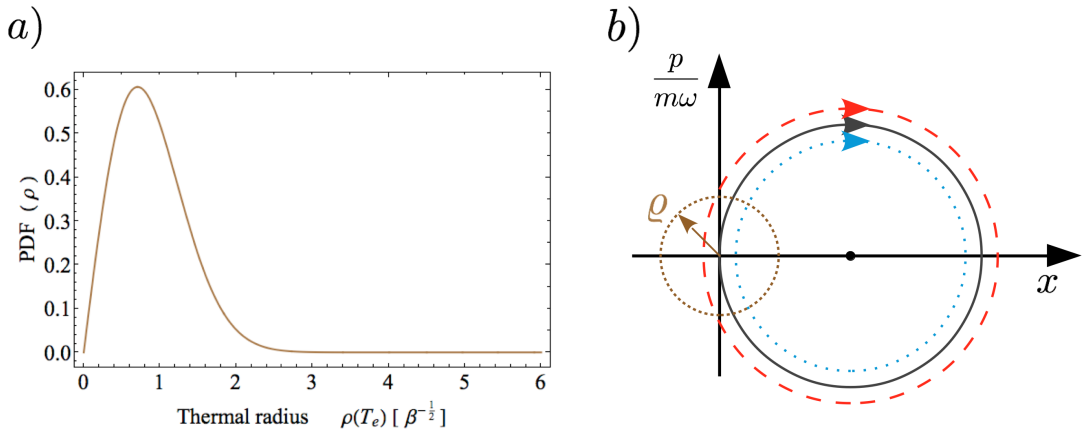


Figure 2.6: a) Maxwell-Boltzmann probability density function of the radius $\varrho(T)$, *i.e.* the square root of the energy, characterising the initial thermal state of the mirror. The mode of the distribution is $(\beta/2)^{-1/2}$, while the average is $\beta^{-1/2}$. b) Phase space representation of some paths in phase space: for $\varrho(T_e) = 0$ we have the ground state case (black circle), while for $\varrho(T_e) > 0$ depending on the initial point $(x(0), p(0))$ we may have longer (red dashed circle) or shorter (blue dotted circle) contributions. Interestingly, the path integral of $x(\tau)$ over a period $T$ is the same in all cases.

where $\chi = \omega_c/(\omega^2 L\sqrt{m})$. Fig.2.6b sketches a few examples of evolution paths: the total phase shift of the field will result from the contribution of all possible paths in phase space, weighted by the thermal distribution on the initial conditions $(\varrho(T_e), \theta)$. While dynamical fluctuations average to zero at any time $t$, and so does the first term in Eq.(2.27), this does not apply to the intensities in Eq.(2.25), which instead result in

$$\begin{aligned}\langle (I_C - I_D)(t)\rangle &= \frac{\beta}{\pi}\int_0^\infty \varrho\, d\varrho \int_0^{2\pi} d\theta\, (I_C - I_D)(\varrho,\theta,t)\, e^{-\beta\varrho^2} \\ &= I_0 e^{-\frac{\chi^2}{\beta}(1-\cos\omega t)} \cos\left[\frac{\omega}{\omega_c} E_0 \chi^2(\omega t - \sin\omega t) - \phi\right] .\end{aligned} \tag{2.28}$$

The argument of the cosine function corresponds to the average phase shift of the field that is measured by operating on the phase shifter ($\phi$) maximising the visibility. While when the initial conditions are known and fixed the exact shift can be observed and one obtains full visibility equal to one, the exponential pre-factor in Eq.(2.28) arises from the uncertainty on the initial conditions (due to classical thermal fluctuations). In other words, as long as we are not able to reconstruct the

path in phase space due to an intrinsic source of uncertainty on the system (and on its dynamics), the visibility is lowered also in a classical experiment. More precisely, we could then define the classical visibility as

$$\nu_c(t) = e^{-\frac{\chi^2}{\beta}(1-\cos\omega t)} \ . \tag{2.29}$$

This expression leads to a full recovery of visibility after every mechanical period, when all paths in phase space yield the same contribution to the phase shift. Such full revivals are also possible since from a classical perspective the initial mechanical thermal distribution is the only source of uncertainty and the light field is treated as a perfectly monochromatic planar wave.

To look deeper into the comparison, we substitute the optomechanical parameters ($k = \chi\sqrt{\hbar\omega/2}$) and write the classical visibility as $\nu_c(t) = e^{-\frac{2k^2}{\beta\hbar\omega}(1-\cos\omega t)}$, which approaches $\nu_q^{cor}(t)$ in the limit $k_B T_e \gg \hbar\omega$. Actually, the discrepancy between the two pictures is negligible also at very low temperatures, as long as $\bar{n} \gtrsim 1$ (for $T_e = 10^{-6}K$ and $\omega = 2\pi \times 10^5$ Hz we have $|\nu_q^{cor} - \nu_c| \leq |e^{-2k^2} - 1| \sim 0.01$ even pushing the coupling to $k = 0.5$).

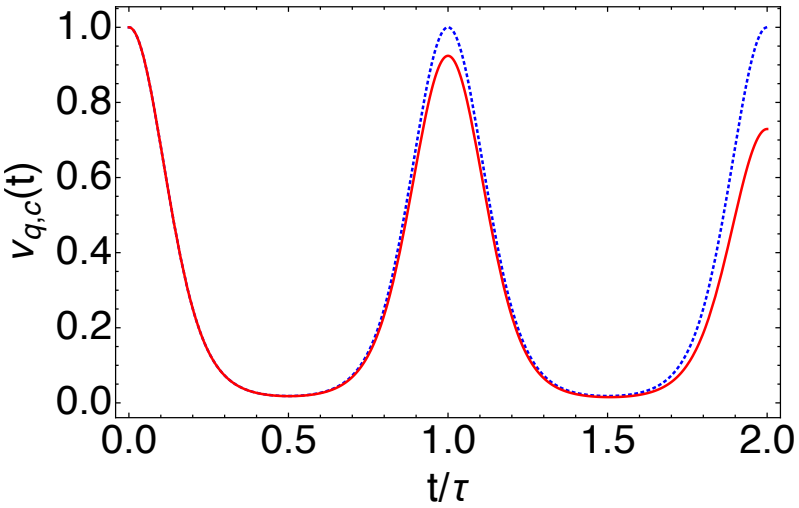


Figure 2.7: Quantum (red continuous line) and classical (blue dotted line) visibilities in Eqs. (2.23) and (2.29) for temperature $T_e = 5 \times 10^{-2}$K. Other parameters are: optomechanical coupling $k = 10^{-2}$, number of photons $N_p = 10^5$ and period $T = 10^{-5}s$. (The figure has been taken from Ref.[23].)

This result confirms that the loss of visibility related to the light-matter correlations $\nu_q^{cor}(t)$ has to be attributed to the random thermal phase arising because of the uncertainty associated to the statistical initial thermal fluctuations of the mirror. The correspondence of the interference patterns and the revivals is then a direct consequence of the equality of the phase shift in the two pictures as well as its independence from the initial state of the mirror after an integer number of mechanical periods.

Moreover, we identify the component $\nu_q^{Kerr}(t)$ as the quantum effect due to the non-linear Kerr interaction that can not be recovered in a classical picture. Indeed, if we model coherent states as perfectly monochromatic waves, the field is classically unaffected by interaction (a part from a vary small frequency contraction that conserves the energy). We show in Fig.2.7 that while the classical result displays a complete revival after every mechanical period, the Kerr nonlinearity lowers the visibility and gives rise to a partial revival in a quantum picture. This effect is however very small and in order to observe significant deviations ($|\nu_q - \nu_c| \geq 10^{-4}$ within a mechanical period) we need to push the coupling constant and the number of photons to $k \geq 10^{-3}$ and $N_p \geq 10^6$, independently of the temperature.

The analysis presented in this section clearly entails that, from a rigorous point of view and in a large range of experimental conditions, the visibility pattern alone is not sufficient to infer non-classicality of the system dynamics, nor to study the correlation between field and mirror (as it was proposed in Refs.[5, 55, 56, 57]). Besides, it is worth noticing that Eq.(2.23) and Eq.(2.29) are independent of the number of photons in the limit $k^2 N_p \ll \bar{n}$ and $k_B T_e \gg \hbar\omega$. In particular, in the same limit, the classical visibility, the quantum visibility in the case of a coherent state and the one found in [5, 55] with single a photon Fock state in input have the same qualitative behaviour.

### 2.5.1 A magic effect: noise

The energy distribution that characterises a coherent state has an intrinsic quantum origin. From a classical perspective the energy quanta cannot be resolved and the light field is described as a monochromatic wave. However, in light of our

findings that link the visibility loss to any uncertainty of the state of the system, we can push forward the similarities between the classical model and the quantum picture, looking at the conditions at which a classical suppression of the visibility analogous to $\nu_q^{Kerr}(t)$ is experienced.

Let us start by the (unavoidable) experimental assumption that the coherent light field has some intrinsic noise. In the most naive hypothesis of Gaussian noise [58], the field energy in the classical Hamiltonian $H_c$ could be written as $E(\epsilon) = E_0(1-\epsilon)$, where the dimensionless parameter $\epsilon$ is described by the distribution $\mathcal{P}(\epsilon) = 1/(\sqrt{2\pi}\Delta)e^{-\frac{\epsilon^2}{2\Delta^2}}$, with $\Delta^2$ the dimensionless variance (that is equivalent to assuming a photon distribution $N(\epsilon) = N_p(1-\epsilon)$ with variance $N_p^2\Delta^2$). The classical phase in Eq. (2.27) and the intensities in Eq. (2.28) will now depend on the noise $\epsilon$: defining $CP(t) = \frac{\omega}{\omega_c}E_0\chi^2(\omega t - \sin\omega t)$ and further averaging Eq.(2.28) over the Gaussian distribution we get the intensities

$$\begin{aligned}\langle (I_C - I_D)(t)\rangle =& I_0 e^{-\frac{\chi^2}{\beta}(1-\cos\omega t)} e^{-(CP(t)\Delta)^2} \\ & \times \left\{\cos\left[CP(t)-\phi\right] - CP(t)\Delta^2 \sin\left[CP(t)-\phi\right]\right\}.\end{aligned} \tag{2.30}$$

The trigonometric function is maximised when $\phi = CP(t)$, thus leading to the visibility

$$\tilde{\nu}_c(t) = \nu_c(t) e^{-2k^4 N_p(\omega t - \sin\omega t)^2}\ , \tag{2.31}$$

where we used $E_0 = \hbar\omega_c N_p$ and $\Delta^2 = 1/N_p$ to compare the Gaussian noise with the Poissonian energy distribution of a coherent state. Because of the classical Kerr-nonlinearity of the phase, which depends on the energy of the driving field rather than on the amplitude (see Eq. (2.18)), any statistical noise causes a further loss in the classical visibility. In particular, in the limit of small coupling $k^2\omega t \ll 1$ and large intensities $N_p \gg 1$, the figure of merit $\tilde{\nu}_c(t)$ approaches over several time periods the quantum prediction $\nu_q^{Kerr}(t)$ in Eq. (2.23). Still, there is deep difference between the two pictures. While from a quantum perspective the well defined Poissonian energy distribution makes $\nu_q^{Kerr}$ periodic, so that to cause revivals, the classical Gaussian noise acts *Markovianly* and only lowers the visibility.

Interestingly, one could push the similarity even further and verify what happens if the

incoming *classical* field has a Poissonian distribution of the energy $P(\epsilon) = \epsilon^n e^{-\epsilon}/n!$. This assumption would imply a classical resolution of the quantisation of the energies through photon counting detectors and therefore goes far beyond a purely classical model. However, it is of didactic benefit in order to understand the nature of the visibility pattern and its relation with the initial state of the system. Hence, following the standard *classical* approach we find the expected phase shift for an initial mixed state of the field with Poissonian distribution of the energy

$$\tilde{\tilde{\phi}}_c(t) = \bar{N}_p \sin(2k^2(\omega t - \sin\omega t)) \ , \tag{2.32}$$

where for the sake of readability we have omitted the dependance on the initial conditions of the mirror that we have already discussed (see Eq.(2.18)). Interestingly, this phase coincides to the one obtained in a quantum picture in Eq.(1.24), within the additional $k^2$ term, which derives exclusively from the commutation relations of the field. This is an additional proof that measuring the $k^2$ term is the only reliable witness of the quantumness of the system. This argument holds both with respect to the phase shift (as in Eq.(1.24)) and to the visibility term $\nu_q^{cor}(t)$ (see Eq.(2.23)). Meanwhile, the visibility associated with the interference measurement of the phase $\tilde{\tilde{\phi}}_c(t)$ reads

$$\tilde{\tilde{\nu}}_c(t) = \nu_c(t) e^{-\bar{N}_p[1-\cos(2k^2(\omega t - \sin\omega t))]} \ , \tag{2.33}$$

which corresponds to the average value of Eq.(2.23), thus perfectly reproducing the curve trend of $\nu_q^{Kerr}(t)$.

## 2.6 Berry phase and Hannay angle

By this point it should be clear that the cyclic nature of the dynamics plays a key role in the evolution of our system, being responsible for the periodic creation and disappearance of light-matter correlations (or entaglement). It is worth now furthering the discussion in more general terms to frame it in a broader context, as well as to better understand the quantum-classical correspondence.

Let us start by observing that when a system undergoes a cyclic evolution in

quantum mechanics, the initial and final state vectors may differ by a phase factor, *i.e.* $|\Psi(T)\rangle = e^{i\phi}|\Psi(0)\rangle$, which can have observable consequences. This extra phase $\phi$ exclusively depends on the structure of the Hilbert space $\mathcal{H}$ and the geometry drawn in phase space. This peculiarity makes it resilient to noise perturbations alongside the evolution and promotes it as an optimal candidate to study, for example, quantum features of massive objects.
The importance of such phase was firstly recognised only towards the end of the last century by Michael Berry [35] for Hamiltonians depending on a set of parameters slowly varying in time, when the adiabatic theorem [59] ensures that the initial state remains in an instantaneous eigenstate during the variation of the parameters.

While the proper assessment of the geometric phase is relatively recent, its classical counterpart, the *holonomic angle*, was firstly introduced in 1900 by Tullio Levi Civita, who formulated the concept of the *parallel transport* of vectors on a surface. This consists in translating a vector alongside a closed path $C$, always keeping it tangent to the surface $\Omega$ which contains $C$. After a closed loop the vector is rotated with respect to its original orientation by an angle whose amplitude and sign respectively depend on the geometry of the loop and on the direction along which it was displaced. Foucault pendulum is probably the most popular device used to provide physical evidence of this mathematical peculiarity that has a more general interpretation. We could state that identical paths in Hilbert space yielding to non equivalent transformations when travelled in different directions witness the non-abelian character of holonomic operations.

The first rigorous analysis of these properties is due to John Hannay [60], who found an algebraic relation between the quantum geometric Berry phase and the classical Hannay angle [60, 61]. Thereafter, the connection between the two pictures has been proven for a wide set of quadratic Hamiltonians and in a range of different contexts [62, 63]. Hence, the aim of this section is precisely to contextualise Berry phase and Hannay angle within the optomechanical framework to provide a complete understanding of the theoretical structure underlying the dynamics. Since the light-matter interaction is regulated by a non-linear cubic term, *i.e.* $ga^\dagger a(b^\dagger + b)$, the retrieved quantum-classical correspondence will be of great interest.

### 2.6.1 Berry phase

We start by looking at the system in a quantum picture to evaluate the geometrical and dynamical contributions to the quantum phase [35]. To this end, we follow the approach in [64] where phase changes in cyclic evolutions are considered without any further theoretical restriction such as adiabaticity.

Given a Hilbert space $\mathcal{H}$ where a state vector that undergoes a closed loop acquires a phase factor $\phi$, *i.e.* $|\psi(T)\rangle = e^{i\phi(T)}\,|\psi(0)\rangle$, we consider the map $\Pi(|\psi\rangle) = \{|\psi'\rangle : |\psi'\rangle = c\,|\psi\rangle$, with $c$ a complex number$\}$ that projects the states on a new Hilbert space $\mathcal{H}'$, $\Pi : \mathcal{H} \to \mathcal{H}'$, where after one period the evolution is actually closed: $|\psi'(T)\rangle = |\psi'(0)\rangle$, being $|\psi(t)\rangle = e^{if(t)}\,|\psi'(t)\rangle$, with $f(t) - f(0) = \phi$. Explicitly writing the Schrödinger equation for $|\psi(t)\rangle$ we have

$$\begin{aligned} & i\frac{d}{dt}\,|\psi'(t)\rangle = (H + \dot{f})\,|\psi'(t)\rangle\,, \text{ and} \\ & \dot{f} = i\frac{\partial}{\partial t}\,|\psi'(t)\rangle - H\,|\psi'(t)\rangle\ . \end{aligned} \tag{2.34}$$

Integrating the last equation over a path $C$ in phase space one obtains

$$\begin{aligned} & \int_0^t \dot{f} d\tau = \phi = \theta_d + \theta_g\ \text{, with} \\ & \theta_d(t) = -\int_0^t d\tau\,\langle\psi(\tau)|\,H\,|\psi(\tau)\rangle \text{ and} \\ & \theta_g(t) = i\int_C \langle\psi'(\tau)|\,\frac{\partial}{\partial\tau}\,|\psi'(\tau)\rangle\ , \end{aligned} \tag{2.35}$$

where $\theta_d(t)$ and $\theta_g(t)$ are defined as the dynamic and geometric phase respectively. Relevantly, $\theta_d$ does not depend on the map $\Pi$ and can be calculated easily in our case since the pulsed Hamiltonian $H$ is time independent: substituting from Eq.(1.21) the state $|\Psi(t)\rangle$ in Eq.(2.35) we get for a generic time $t$

$$\theta_d(t) = (2\gamma_R k N_p - |\gamma|^2)\omega t. \tag{2.36}$$

The calculation for $\theta_g$ is a bit more laborious since it specifically requires the map $\Pi$. In this direction, it is helpful for our purpose to reconsider the evolution operator in

Eq.(1.20) and observe that it is diagonal in the cavity Fock state basis. Thanks to this property, the state

$$|\Psi(t)\rangle = e^{-\frac{|\alpha|^2}{2}} \sum_{n=0}^{\infty} \frac{\alpha^n}{\sqrt{n!}} e^{ik^2n^2(\omega t - \sin\omega t)} e^{ikn[\gamma_R \sin\omega t + \gamma_I(1-\cos\omega t)]} |n\rangle_c \otimes |\Gamma_n(t)\rangle_m \ , \quad (2.37)$$

which was introduced in Eq.(1.21), offers a decomposition that automatically satisfies

$$|\Psi(t)\rangle = \sum_{j=0}^{\infty} e^{if_n(t)} \, |\Psi'(t)\rangle_n \, , \quad (2.38)$$

with $|\Psi'(t)\rangle_n = |n\rangle_c \otimes |\Gamma_n(t)\rangle_m$ and $|\Gamma_n(t)\rangle_m = |\gamma e^{-i\omega t} + kn(1 - e^{-i\omega t})\rangle_m$. Substituting this decomposition in Eq.(2.35) and remembering that the derivative of a coherent state $\frac{\partial}{\partial t}|\Gamma\rangle$ gives $\langle\Gamma|\frac{\partial}{\partial t}|\Gamma\rangle = \frac{\partial}{\partial t}\frac{|\Gamma|^2}{2} + \Gamma^* \frac{\partial \Gamma}{\partial t}$, we obtain the *Berry phase*

$$\theta_g(t) = (|\gamma|^2 - 2\gamma_R k N_p)\omega t + kN_p[\gamma_I(1-\cos\omega t) + \gamma_R \sin\omega t] + k^2(N_p^2 + N_p)(\omega t - \sin\omega t). \quad (2.39)$$

The reason of the name "geometric phase" can be inferred from this last equation, which also suggests an important generalisation of the analysis to the case of open paths in phase space. Indeed, in the calculations so far we have not assumed the state to describe a closed loop, but rather we referred to a generic evolution time. Eq.(2.39) suggests that we could actually imagine to artificially close a loop by virtually connecting with a single displacement the generic point reached in phase space at time $t \in [0, T]$ with the starting point of the motion at time $t = 0$. $\theta_g$ will then correspond to the convex area spanned in phase space by the line segment that joins the instantaneous position to the starting point of the dynamics (see Fig.2.8 for a graphical representation).

Even if each component $\theta_g(t)$, $\theta_d(t)$ depends on the initial conditions, after a mechanical period $T = 2\pi/\omega$ their sum $\phi(T) = \theta_g(T) + \theta_d(T) = 2\pi k^2 N_p^2$ solely depends on the geometry of the evolution in space. More specifically, it is instructive to consider the limit of small coupling $k \ll 1$, which we could identify with the adiabatic regime. In this limit, indeed, the initial coherent state $|\alpha\rangle$ (and the state vector $|\Psi(t)\rangle$ in Eq.(2.37)) is approximately an eigenstate of the Hamiltonian: the phase $\phi(t)$ thus

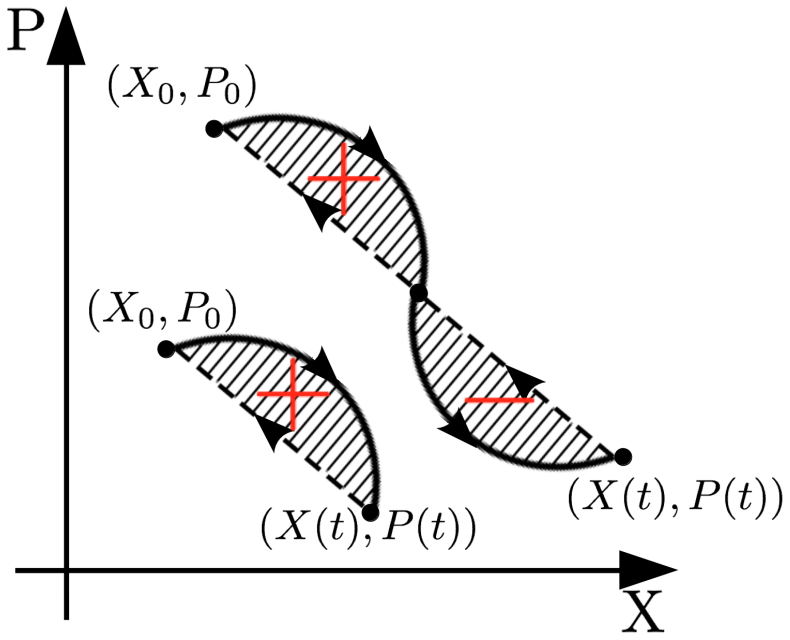


Figure 2.8: Representation of the geometric phase in phase space. The trajectory (of the mirror) is depicted with a continuum line and the geometric phase corresponds to the shaded region delimited by the trajectory and by the dashed line that connects $(X(t), P(t))$ to $(X_0, P_0)$. As a convention, areas enclosed clockwise are positive, those travelled anti-clockwise negative.

coincides with the global phase we could attribute to the quantum superposition state of the system $|\Psi(t)\rangle$.

### 2.6.2 Hannay angle

Non-dissipative models are usually associated with a conserved quantity, namely the total energy (or the number of photons in our case). Within this class of models, periodic motions deserve special attention, as many peculiarities can be sorted out by simply applying a canonical transformation of second type. To this end, it is convenient to switch from the Hamiltonian classical variables $(q, p)$ to the so-called *action-angle* coordinate system $(\phi, I)$, which is characterised by a conserved quantity $I$ (usually representing the total energy), that unambiguously identifies the *orbit* in phase space, and a periodic variable $\phi$, that univocally determines the position of the system on the orbit at any given time. A possible candidate as *generating*

function to provide the desired transformation is

$$S(q, I) = \int_{q_0}^{q} p(q', I) dq' \ , \tag{2.40}$$

where the integral is performed along the orbit defined by $I$, *e.g.* with fixed and constant energy. The canonically conjugate variables can then be derived from $S(q, I)$ as $p = \frac{\partial S}{\partial q}$, which follows straightforwardly by simple substitution in Eq.(2.40), and $\phi = \frac{\partial S}{\partial I}$.

Let us then calculate the phase $\phi$ related to our case of interest, generalising the procedure rigorously addressed in Refs.[60, 61] to non-closed loops in phase space by applying the same technique we presented in the last section to artificially close the path at each time $t$.

We know that a second type generating function (as the one in Eq.(2.40)) transforms the Hamiltonian as $H' = H + \partial S/\partial t$: we can thus derive the phase change rate from Hamilton equation as

$$\dot{\phi} = \frac{\partial H'}{\partial I} = \frac{\partial H}{\partial I} + \frac{\partial^2 \tilde{S}}{\partial t \partial I} - \frac{\partial}{\partial I}\frac{\partial}{\partial t} p dq \ , \tag{2.41}$$

where we have expressed $\partial S/\partial I$ in terms of the new angle-action variables: $d\tilde{S}(\phi, I) = dS(q, I) + \frac{\partial S}{\partial q} dq$.

The classical phase associated with a (closed) path $C$ in phase space is then obtained by integrating

$$\phi(t) = \int_0^t \frac{\partial H}{\partial I} d\tau - \frac{\partial}{\partial I} \int_C p dq \ , \tag{2.42}$$

where we have exploited that $\frac{\partial \tilde{S}}{\partial I} = 0$, *i.e.* $I$ is constant alongside $C$.

At this point we need to choose a conserved quantity to be associate to $I$, of which we will compute the related conjugate angle variable with Eq.(2.42). We choose $I = E_0/\omega_c$, which corresponds to $I = \hbar N_p$ in a quantum framework.

Interestingly, we further notice that Eq.(2.42) consists of two parts that are related

with the dynamical and geometric phase state components introduced in Eq.(2.35)

$$\begin{aligned}\phi_d(t) &= \int_0^t \frac{\partial H}{\partial I} d\tau = \frac{\omega_c x(0) t}{L} \ , \\ \phi_g(t) &= -\frac{\partial}{\partial I}\int_C p dq = -\frac{\omega_c x(0) t}{L} + \frac{\omega_c}{\omega^3 m L^2} E_0(\omega t - \sin\omega t) \\ &\quad + \frac{\omega_c}{2L\omega}\left[x(0)\sin\omega t + \frac{p(0)}{m\omega}(1-\cos\omega t)\right].\end{aligned} \tag{2.43}$$

When the loop is (artificially) closed in phase space, then for Stokes theorem $\phi_g(t)$ corresponds to the area enclosed by the trajectory. It is usually referred to as Hannay angle, named after the physicist John H. Hannay, who first identified the quantity in adiabatic classical systems as the derivative of the Berry phase (see Eq.(2.39)) with respect to the action variable. Replacing the quantum parameters with their classical average expectation values, we verify in our case the relation $\phi_g(t) = \frac{d\theta_g(t)}{dI}$ that was so far proved only for quadratic Hamiltonians.

## 2.7 Conclusions

In this chapter, we have explored the quantum-classical correspondence of the phase acquired by an optical field after its interaction with a movable mirror in an optomechanical cavity. We have seen that both the nonlinear phase shift due to the Kerr effect and the mirror decoupling at certain interaction times are common features of the two descriptions. These findings have further allowed us to challenge the drop of the visibility pattern as a quantum signature. Besides, we inferred that correlations arise because of (classical) statistical uncertainty on the initial state of the system and lead to effects that are qualitatively identical and quantitatively larger than those theoretically observed in a single-photon experiment. Conversely, we were able to isolate genuine quantum features of the interaction that appear on the phase and the visibility, which might be probed in future optomechanical experiments, even in the weak coupling limit. Also, the preparation and assessment of a truly quantum mechanical state would be an essential prerequisite for probing decoherence models, as well as the interface of gravity with quantum mechanics (this

point will be discussed intensively in Chapter4, where we propose a scheme to create non-classical macroscopic quantum states of the harmonic oscillator).

Eventually, we contextualized our discussion in the more general framework of non-abelian transformations in phase space. We successfully verified that also for the cubic non-linear optomechanical interaction the quantal geometric phase causes the state to be displaced along the classical trajectory by an amount equal to the classical geometric phase (Hannay angle) [65].

# Chapter 3

# Probing anharmonicity of a quantum oscillator in an optomechanical cavity

## 3.1 Introduction

*The content of this chapter (with the exception of the last section) is part of a research that I conducted and shared in equal proportions together with a colleague at Imperial College, Federico Armata. More specifically, the topics covered in this chapter were the main object of a paper that has been published in Physical Review A with the title "Probing anharmonicity of a quantum oscillator in an optomechanical cavity" [66].*

Thanks to the possibility to perform very precise position measurements, optomechanical systems have been historically studied in the context of force sensing [67, 19] and were very recently adopted for the ground breaking observation of gravitational waves [68].

However, despite the capability to detect small deviations from standard harmonic dynamics, intrinsic anharmonic contributions to the motion of the quantum mechanical oscillator have been so far neglected in nearly every theoretical proposal and experimental realisation to probe fundamental physics or to measure decoherence [1].

This is surprising if we consider the importance that has been recently recognised to anharmonicity to bring out quantum peculiarities (aside from perturbing the behavior and results that one would obtain in the harmonic case). For instance, Milburn and Holmes studied the quantum and classical dynamics of an anharmonic oscillator in phase space showing that a reduction of coherence results in quantum-to-classical-transition [69]. On the other hand, anharmonicity has proven to be a resource to generate non-classical quantum states [70, 71, 72].
Furthermore, the state-of-the-art in experiments is encouraging since the anharmonic regime has been accessed in a range of different physical platforms, and a measure able to quantify the non-linearity of a quantum oscillator has been recently proposed [73]. To cite a few specific examples, the effects of nonlinearities have been explored (and exploited) in mechanical resonators based on graphene and carbon structures [74, 75], and electrostatic gradient forces produced with NEMS (Nanoelectromechanical Systems) chips are used to enhance the intrinsic quartic anharmonicity of a carbon nanotube [76]. In another framework, the thermal energy of a levitated nanosphere was shown to be sufficient to drive its motion into the nonlinear regime [77].

Given these premises, we would like to dedicate this chapter to propose a protocol able to efficiently measure anharmonicity and analyse its contribution to the dynamics, also in comparison with the harmonic case we have just extensively discussed.
We will present a scheme to estimate the mechanical anharmonicity of a quantum optomechanical resonator, adopting the bad cavity regime introduced in Sec.1.4.1, where a short light pulse is iteratively injected four times into the cavity so that to drive the mirror alongside a closed *deformed* square loop in phase space. The anharmonicity will induce some modifications in the mechanical evolution with respect to the harmonic case that we discussed in Sec.1.4.1, which will be enhanced by the non-abelian character of a loop operation in phase space. We will provide evidence that our protocol allows high precision measurements, only requiring feasible initial cooling of the oscillator via dilution refrigeration techniques. We will also discuss the resilience of the scheme against optical losses. Further to calculating the Quantum Fisher Information (QFI) to obtain the ultimate quantum bound on

anharmonicity estimation that is achievable through an optomechanical setup, we compare it to the Fisher Information (FI) extractable with standard measurements on the optical field, such as homodyne and heterodyne detection, verifying the optimality of the former technique.
In order to investigate the connection between non-linearities and the emergence of quantum properties, we integrate the discussion we started in the past chapter analysing anharmonicity in a fully classical picture. The phase shift imparted to light can still be used as a reliable indicator of quantumness in optomechanics, even though the two regimes are much closer than what was previously thought, and the mechanical non-linearity leads to conceptually and quantitatively very similar results in both frameworks (particularly in the limit of large displacements $\lambda N_p \gg 1$).
Eventually, we illustrate how anharmonicity can be traced back to the application of a non canonical transformation. This allows us to relate it to a wider class of systems where the topology of the Hilbert space is deformed, *i.e.* some of the latest proposals to test the interface between quantum mechanics and gravity [3, 31].

## 3.2 The anharmonic evolution

We generalise the quantum pulsed model depicted in Sec.1.4.1 for a harmonic oscillator to the case where a mechanical anharmonicity is included in the Hamiltonian. The procedure to design a closed loop in phase space, calculate the related total unitary operator and finally access the resulting phase shift imparted to the light are the same we have already discussed. However, the additional anharmonicity not only requires further algebraic manipulations to derive the dynamics, but it also induces some fundamental differences in the evolution, creating further correlations between the field and the mirror that should be considered carefully.

Let us start by introducing a standard anharmonic term scaling as the fourth power of the position $\propto X^4$. This is a very common choice due to symmetry-parity reasons and to the great role played by quartic terms in various physical contexts, from classical Duffing equation and the generation of chaotic motion to quantum

field theory[1]. Nonetheless, we will replicate all the results for the case of a cubic anharmonicity in Appendix B to provide an insightful comparison between odd and even contributions.

The effective Hamiltonian describing the system in a frame rotating with the optical cavity frequency reads $H = H_0 + H_{int}$, where $H_{int} = -gn_cX$ and

$$H_0 = \frac{1}{2}\hbar\omega\left(X^2 + P^2\right) + \frac{\gamma}{4}\hbar\omega X^4 \ , \tag{3.1}$$

with $\gamma \ll 1$ the amplitude of the quartic anharmonicity.

We propose to operate in a bad cavity regime where we inject a light pulse in the cavity that interacts with the mirror for a short time $\tau = 1/\kappa$ and then escapes out. Our aim is to reproduce the protocol presented in Sec.1.4.1 where the phase space trajectory of the mirror performed a square. We demand to arrange a very strong (with a large number of photons) and short interaction, so that the mechanical motion can be neglected within the interval $\tau$. The pulse is then delayed in an engineered loop for a quarter of mechanical anharmonic period before being re-injected: the cycle is iterated four times after which the pulse is eventually measured interferometrically with respect to a reference field. The total unitary operator that characterises the process can be recovered (up to a final rotation of $3\pi/2$ on the mechanical oscillator) following the steps in Eq.(1.12) and reads

$$U = e^{i\lambda n_c X(\frac{3\pi}{2\omega'})}e^{i\lambda n_c X(\frac{\pi}{\omega'})}e^{i\lambda n_c X(\frac{\pi}{2\omega'})}e^{i\lambda n_c X} \ , \tag{3.2}$$

where $X(t)$ is the trajectory in real space of the anharmonic oscillator and $\omega'$ its frequency. Hence, we first need to solve the anharmonic dynamics to explicitly compute Eq.(3.2). To this end, it is convenient to derive the evolution of annihilation and creation operators induced by $H_0$ in Heisenberg picture. This has already been obtained in Refs.[78, 79] with a perturbative approach in $\gamma$ via a multiscale technique: in the following we will capitalise that result. Although a detailed discussion on the derivation is out of the present purposes, we should remind the reader that a

[1]The simplest type of self-interaction in scalar field theory is given by the quartic interaction $\frac{\lambda}{4!}\varphi^4$.

multiscale approach is adopted when the perturbative expansion of the solution contains diverging time dependent terms that violate the expansion itself. As an example, consider the expansion $x(t) = x_0(t) + x_1(t) + x_2(t) + \ldots$, where each term $x_j$ is supposed to be of the order $\gamma^j$, *i.e.* $x_j \sim O(\gamma^j)$. However, if $x_1$ happens to be time divergent (as it is in this case), the range of applicability of the solution will be constrained to those times satisfying $x_1(t) \ll x_0(t)$. Alternatively, to obtain a result that is applicable for a longer time window, one needs to compensate for this divergence by adding another time scale, *e.g.* $t_1 = \gamma t$, and accordingly adapt the zeroth order. In general, the divergences at a given order are counterbalanced and canceled by rescaling the time dependence at previous orders (further details are provided in Sec.3.5 where we solve the dynamics in the classical picture).
Let us then write the evolution induced by Eq.(3.1) at the leading order in $\gamma$ (for times $t$ such that $(\omega t)\gamma|A|^2 \ll 1$)

$$\begin{aligned} b(t) \simeq & e^{-i\omega' t}\left\{ b_0 + \frac{\gamma}{4}\left[ \left(1 - e^{+4i\omega' t}\right)\frac{b_0^{\dagger 3}}{4} + \left(e^{-2i\omega' t} - 1\right)\frac{b_0^3}{2} \right.\right. \\ & \left.\left. + \left(1 - e^{2i\omega' t}\right)\frac{3}{2} b_0^\dagger \left(1 + b_0^\dagger b_0\right) \right] \right\} , \\ \omega' = & \omega + \frac{3}{8}\gamma\omega\left(2 + |A|^2\right) , \end{aligned} \tag{3.3}$$

where $|A|$ is the oscillation amplitude for the unperturbed harmonic oscillator. The frequency shift in Eq.(3.3) implicitly provides a condition on the viability of the perturbative approach, *i.e.* $\gamma|A|^2 = \gamma(\lambda N_p)^2 \ll 1$, which actually corresponds to requiring small deviations from the harmonic displacement. Defining the anharmonic period as $T' = 2\pi/\omega'$, it is straightforward to find quadrature operators

$$\begin{aligned} X(0) &= X , \\ X\left(\frac{T'}{4}\right) &\simeq P + i\frac{\gamma}{4}\Delta , \\ X\left(\frac{T'}{2}\right) &\simeq -X , \\ X\left(\frac{3T'}{4}\right) &\simeq -P - i\frac{\gamma}{4}\Delta , \end{aligned} \tag{3.4}$$

at times $t = 0, T'/4, T'/2, 3T'/4$, by simple substitution in Eq.(3.3) and with the deformation $\Delta = b_0^3 - b_0^{\dagger 3} - 3b_0^\dagger + 3b_0 - 3b_0^{\dagger 2} b_0 + 3b_0^\dagger b_0^2$ due to the anharmonic evolution. We remark that at time $t = T'$, when the final measurement is performed, the oscillator returns to its initial position ($X(T') = X$). As we have already discussed, this is a necessary requirement – though not sufficient – to perform the experiment. Indeed, only with closed loops field and oscillator can be uncorrelated at the end of the evolution, provided that they were initially prepared in a product state [22, 2][2]. In particular, to close the loop we need to estimate in advance the anharmonic frequency, which turns out to be itself a function of the anharmonicity we want to estimate (see Eq.(3.3)). This is a common situation in local quantum estimation theory and can be worked out through subsequent adaptive measurements [80, 81, 82]. To this end, since the final goal is to measure $\gamma$ via an interferometric scheme, an experimentalist could start with a rough prediction on the anharmonicity to perform the first measurement and subsequently ensure the closure of the loop by tuning the waiting time between two pulses so that the visibility of the interference fringes is maximised.

It is worth mentioning in this context that other sources of anhamonicity, *e.g.* the cubic case $\propto X^3$ discussed in Appendix B, do not alter the mechanical frequency. This peculiarity can be exploited to distinguish among different anharmonicities by only looking at the interferometric pattern.

The unitary operator describing the evolution corresponding to the whole square loop is obtained by substituting the mirror dynamics in Eqs.(3.4) into Eq.(3.2) and reads

$$U = e^{i\lambda n_c(-P - i\frac{\gamma}{4}\Delta)} e^{-i\lambda n_c X} e^{i\lambda n_c(P + i\frac{\gamma}{4}\Delta)} e^{i\lambda n_c X} \ . \tag{3.5}$$

We now aim to rewrite this expression in a more compact form, as the product of the harmonic square displacement in Eq.(1.13) and a perturbative anharmonic correction. To this end, we apply BCH at the first order in $\gamma$ to Eq.(3.5) and rephrase the first

[2] An open loop would imply the application of a displacement operator on the mirror, conditioned by the cavity photon number.

and third term respectively as [3]

$$\begin{aligned} e^{-i\lambda n_c(P+i\frac{\gamma}{4}\Delta)} \simeq & e^{-i\lambda n_c P} e^{\frac{\gamma}{4} f_1(b_0, b_0^\dagger)} \ , \\ e^{i\lambda n_c(P+i\frac{\gamma}{4}\Delta)} \simeq & e^{i\lambda n_c P} e^{\frac{\gamma}{4} f_2(b_0, b_0^\dagger)} \ , \end{aligned} \tag{3.6}$$

where

$$\begin{aligned} f_1(b_0, b_0^\dagger) &= \lambda n_c \Delta - 3\lambda^2 n_c^2 (b^{\dagger 2} - b^2) + 2i\lambda^3 n_c^3 P \ , \\ f_2(b_0, b_0^\dagger) &= -\lambda n_c \Delta - 3\lambda^2 n_c^2 (b^{\dagger 2} - b^2) - 2i\lambda^3 n_c^3 P \ . \end{aligned} \tag{3.7}$$

Further proceeding with the BCH expansion to move $f_1$ and $f_2$ to the right in Eq.(3.5) we obtain the evolution operator

$$U = e^{i\lambda^2 n_c^2 + \frac{\gamma}{4} F(b_0, b_0^\dagger)} \ , \tag{3.8}$$

where $F(b_0, b_0^\dagger)$ corresponds to the sum of $f_1$ and $f_2$, after the swap at the sides of Eq.(3.5). Even though the explicit form of $F(b_0, b_0^\dagger)$ is a very bulky expression, it is not of any particular interest, since we already know that we are going to read out the mirror dynamics from interference measurements of the light. We are thus interested in the reduced dynamics of the field, which is given by the completely positive map $\mathcal{E}$ defined as

$$\mathcal{E}(\varrho_c) = \mathrm{Tr}_m[U \varrho_c \otimes \nu U^\dagger] \ , \tag{3.9}$$

where $\mathrm{Tr}_m[\bullet]$ denotes the partial trace on the mechanical oscillator, while $\varrho_c$ and $\nu$ are the initial states of cavity and mirror respectively.

We will focus on the relatively general case where the oscillator is prepared in a state diagonal in the Fock basis, i.e. $\nu = \sum_n \nu_n |n\rangle\langle n|$, that includes the case of a Gibbs thermal state, which is a good approximation of the most common experimental conditions. Performing the trace in Eq.(3.9) we recover the effective unitary operator

[3] If the chained commutator $[A,[A,[A,B]]]$ is a number, then $e^{A+\gamma B}$ can be rewritten at the first order in $\gamma$ as $\exp[A+\gamma B] = \exp[A]\exp[\gamma\,(B - [A,B]/2 + [A,[A,B]]/6 - [A,[A,[A,B]]]/24)]$.

$\xi_{\mathsf{eff}}$ such that $\mathcal{E}(\varrho_c) = \xi_{\mathsf{eff}}\varrho_c\xi_{\mathsf{eff}}^\dagger$, with

$$\xi_{\mathsf{eff}} = \exp\left\{i[\lambda^2 n_c^2 - \frac{\gamma}{2}(\lambda^4 n_c^4 + 3\lambda^2 n_c^2\bar{n})]\right\} \ , \tag{3.10}$$

where $\bar{n}$ is the average initial thermal phonon number. $\xi_{\mathsf{eff}}$ acts on the cavity field and retains all the information on the dynamics, and in particular on the effects induced by anharmonicity. It is worth noticing that in addition to the well known Kerr-nonlinearity scaling as $n_c^2$, the effective anharmonicity is highly enhanced by our protocol, depending on the fourth power of the photon number $n_c^4$. This is due to the high degree of non-commutativity of the cubic operator $\Delta$, with respect to the linear operators $X$ and $P$, whose effects become measurable when performing a loop in phase space. Provided that a strong optical field is used, this indicates the optimality of our scheme to boost the effect of very small anharmonicities.
Importantly, we notice that Eq.(3.10) witnesses the creation of correlations between the field and the mirror which might affect a deterministic parameter measurement, as well as the visibility of the interference fringes when reading out the optical phase. Still, the mild condition on the average number of thermal phonons $\lambda^2\langle n_c\rangle^2 \gg \bar{n}$, which can be satisfied with doable initial mechanical cooling, guarantees that within a range of experimental parameters the oscillator is approximately uncorrelated to the field when the final measurement is performed.

Provided the conditions $\gamma\lambda^4 N_P^3 \ll 1$ and $(\lambda N_P)^2 \gg \bar{n}$ are satisfied (at the end of our analysis we will suggest a possible set of experimental parameters), we calculate the mean value of the optical field after a four-pulse interaction. If the cavity is initialised with a coherent state $\varrho_0 = |\alpha\rangle\langle\alpha|$, it reads

$$\begin{aligned}\langle a\rangle &= \langle\alpha|\xi_{\mathsf{eff}}^\dagger a \xi_{\mathsf{eff}}|\alpha\rangle \\ &= \alpha e^{-(|\alpha|^2+i\lambda^2)}\sum_{n=0}^{\infty}\frac{|\alpha|^{2n}}{n!}e^{-2i\lambda^2 n}e^{-i\frac{\gamma}{2}\lambda^4(4n^3+6n^2+4n+1)} \\ &\simeq \alpha\langle a\rangle_0 e^{-i\frac{\gamma}{2}\lambda^4(4N_p^3+18N_p^2+14N_p+1)},\end{aligned} \tag{3.11}$$

with $\langle a\rangle_0 = e^{-i\lambda^2 - N_p(1-e^{-i2\lambda^2})}$ the phase acquired by the field in the harmonic case.

### 3.2.1 Effect of losses

Since we aim at measuring a very small parameter $\gamma$, and Eq.(3.10) already includes the disturbance due to thermal noise, it is worth making a short digression on the estimation of photon losses that might occur in the delaying fiber loops. While our protocol theoretically relies on having the same light pulse for each interaction, we could naively model the ratio between the number of photons in two consecutive pulses as $N_{p_{i+1}}/N_{p_i} = 1-\epsilon$, with $i \in [1,4]$. This scheme will provide an estimate on the impact of optical losses on the dynamics, as well as on the amount of losses that can be tolerated.

To begin with, we point out that the lossy scheme is equivalent to a system with decreasing coupling strengths, *i.e.* with constant photons but where the couplings satisfy $\lambda_{i+1}/\lambda_i = 1-\epsilon$. The corresponding evolution operator reads

$$U \simeq e^{-i\lambda_4 n_c P} e^{\frac{\gamma}{4} f_1(b_0,b_0^\dagger)} e^{i\lambda_4 n_c P} \xi_h e^{-i\lambda_1 n_c X} e^{\frac{\gamma}{4} f_2(b_0,b_0^\dagger)} e^{i\lambda_1 n_c X} \ , \tag{3.12}$$

where $\xi_h$ is the new lossy harmonic displacement given by

$$\xi_h = D(n_c\mu) e^{i n_c^2 [\lambda_3\lambda_2 + \frac{1}{2}(\lambda_2-\lambda_4)(\lambda_1-\lambda_3)]} \ , \tag{3.13}$$

with $D(n_c\mu) = e^{n_c(\mu b^\dagger - \mu^* b)}$ and $\mu = (1/\sqrt{2})[(\lambda_4-\lambda_2) + i(\lambda_1-\lambda_3)]$. $D(n_c\mu)$ is a displacement operator, conditioned by the number of photons, which acts on the resonator and prevents light and mirror to be disentangled after a closed loop. The functions $f_1(b_0,b_0^\dagger)$ and $f_2(b_0,b_0^\dagger)$ have the same formal definitions as in (3.7) with $\lambda \to \lambda_4$ and $\lambda \to \lambda_1$, respectively. Calculating the exponentials in (3.12) and expanding at the first order in $\gamma$ we get the propagator

$$U \simeq \xi_h + \frac{\gamma}{4} \xi_h F(b_0, b_0^\dagger) \ . \tag{3.14}$$

Performing the partial trace over the mechanical degrees of freedom of Eq.(3.14) and comparing the order of magnitude of each term separately provides an estimate of

the contribution of losses. We obtain

$$\begin{aligned} \langle \xi_h \rangle &= e^{-\frac{|\mu|^2}{2} n_c^2 (1+2\bar{n})} e^{i n_c^2 [\lambda_3 \lambda_2 + \frac{1}{2}(\lambda_2 - \lambda_4)(\lambda_1 - \lambda_3)]} \ , \\ \frac{\gamma}{4} \langle F(b_0, b_0^\dagger) \rangle &\simeq -\frac{\gamma}{4} \lambda^4 n_c^4 + O(\epsilon \lambda^4 n_c^3 \bar{n}) \ . \end{aligned} \tag{3.15}$$

From this result we infer that losses affect the evolution operator, and in particular the separability of mirror and field at the end of the period. The expectation value of $\langle \xi_h \rangle$ reveals that not only we will experience a smaller phase shift of the field, but also a reduction in the visibility that could be estimated by $\exp(-|\mu|^2 n_c(1+2\bar{n}))$. Luckily, since $\mu \sim O(\epsilon\lambda)$ this term is expected to be relatively small, scaling as $\exp(-|\mu|^2 n_c(1+2\bar{n})) \sim 1 - O(\epsilon^2 \lambda^2 N_p \bar{n})$ and could be easily neglected.
Finally, Eq.(3.15) provides a bound on the disturbance that optical losses induce on the estimate of mechanical anharmonicity. We conclude that for our purposes we should require $\epsilon \bar{n} \ll N_p$, which is feasibly satisfied in todays experiments with $N_p \sim 10^8$ and $\bar{n} \sim 10^6$ (corresponding to a few kelvin).

## 3.3 QFI and FI in anharmonicity estimation

Now that we have studied how mechanical anharmonicity affects the evolution and how this is reflected on the expectation value of the measured light phase shift (and visibility), we discuss the effectiveness of such interference measurements at estimating the parameter $\gamma$. Exploiting the tools from local quantum estimation theory [83], we derive the ultimate bounds on the estimation precision and compare them with widely used measurement schemes. We start by calculating the QFI associated to $\gamma$ for the output state generated by the propagator in Eq.(3.10). As the effective dynamics is unitary, an initial pure coherent state $|\alpha\rangle$, will result in another pure state, *i.e.* $|\psi_\gamma\rangle = \xi_{\mathsf{eff}}|\alpha\rangle$, and the QFI can be evaluated as follows

$$\begin{aligned} Q_\gamma &= 4\left(\langle \psi'_\gamma | \psi'_\gamma \rangle - |\langle \psi'_\gamma | \psi_\gamma \rangle|^2\right) = \lambda^8 \left(\langle \psi_\gamma | n_c^8 | \psi_\gamma \rangle - \langle \psi_\gamma | n_c^4 | \psi_\gamma \rangle^2\right) \\ &= \lambda^8 (16 N_p^7 + 216 N_p^6 + 964 N_p^5 + 1640 N_p^4 + 952 N_p^3 + 126 N_p^2 + N_p) \ , \end{aligned} \tag{3.16}$$

where $|\psi'_\gamma\rangle$ is the derivative of the state with respect to $\gamma$. $Q_\gamma$ sets the ultimate lower bound on the estimation precision for the parameter $\gamma$, quantified by the variance of an unbiased estimator through the so-called quantum Cramér-Rao theorem that reads (in the limit $N_p \gg 1$)

$$\mathrm{Var}(\gamma) \geq \frac{1}{MQ_\gamma} \gtrsim \frac{1}{16M\lambda^8 N_p^7} \ , \tag{3.17}$$

where $M$ denotes the number of measurements performed. This last relation implies that the estimation is highly enhanced by the Kerr-nonlinearity in Eq.(3.10), where the anharmonic contribution scales as $\sim \gamma\lambda^4 n_c^4$. This is what makes the optomechanical framework particularly appropriate for this kind of measurement.
The quantum bound for a single parameter in Eq.(3.17) is in principle always achievable, in the sense that there exists a POVM whose (classical) FI is equal to the QFI. To evaluate if feasible measurements are optimal we proceed by calculating the FI, which in general reads

$$F_\gamma = \int d\bullet \, \frac{(\partial_\gamma p(\bullet|\gamma))^2}{p(\bullet|\gamma)} \ , \tag{3.18}$$

where $p(\bullet|\gamma)$ is a generic conditional probability to obtain the measurement outcome $\bullet$, given the value of the parameter $\gamma$. We will specifically refer to the two most common strategies when dealing with phase measurements: *homodyne* and *heterodyne* detection.
We have already mentioned that *homodyne* detection corresponds to a projection on quadrature operators eigenstates, $X_\phi|x\rangle_\phi = x|x\rangle_\phi$, where $X_\phi = x_c\cos\phi + p_c\sin\phi$, and the pair of operators $(x_c, p_c)$ denote respectively the *position* and *momentum* operators for the cavity field. Since the evolution operator in Eq.(3.10) is diagonal in the Fock basis, as suggested in Ref.[84], it is convenient to write also the quadrature operator eigenstates as

$$|x\rangle_\phi = e^{-x^2/2}\left(\frac{1}{\pi}\right)^{1/4}\sum_{m=0}^{\infty}\frac{H_m(x)}{2^{m/2}\sqrt{m!}}e^{-im\phi}|m\rangle \ , \tag{3.19}$$

where $H_m(x)$ is the $m$-th Hermite polynomial. Given a certain anharmoniciy $\gamma$, we then find the conditional probability of obtaining the outcome $x$

$$p(x|\gamma) = |_\phi\langle x|\psi_\gamma\rangle|^2 = \frac{e^{-(|\alpha|^2+x)}}{\sqrt{\pi}} \left| \sum_{m=0}^{\infty} \frac{\alpha^m H_m(x)}{2^{\frac{m}{2}} m!} e^{im\left[\phi - \lambda^2 m(1+\frac{\gamma}{2}\lambda^2 m^2)\right]} \right|^2 . \tag{3.20}$$

Unfortunately, there is no analytical way to compute this series in a more compact expression. However, by fixing all the parameters $\{\alpha,\ \phi,\ \lambda,\ \gamma\}$ and by varying the measurement outcome $x$, we can numerically evaluate the integral and find the FI as in Eq. (3.18). The phase dependence is optimised by the choice $\phi = \pi/2$, independently of the set of experimental parameters. We can then adopt a reasonable value for the rescaled coupling, *e.g.* $\lambda \sim 1.5 \times 10^{-5}$, to compute the ratio between homodyne FI and the corresponding QFI as a function of the number of photons in the cavity (see Fig.3.1). We infer that the larger $N_p$ is, the more the ratio $F_\gamma^{\mathsf{hom}}/Q_\gamma$ approaches one: we already reach a very good agreement with 30 photons, though

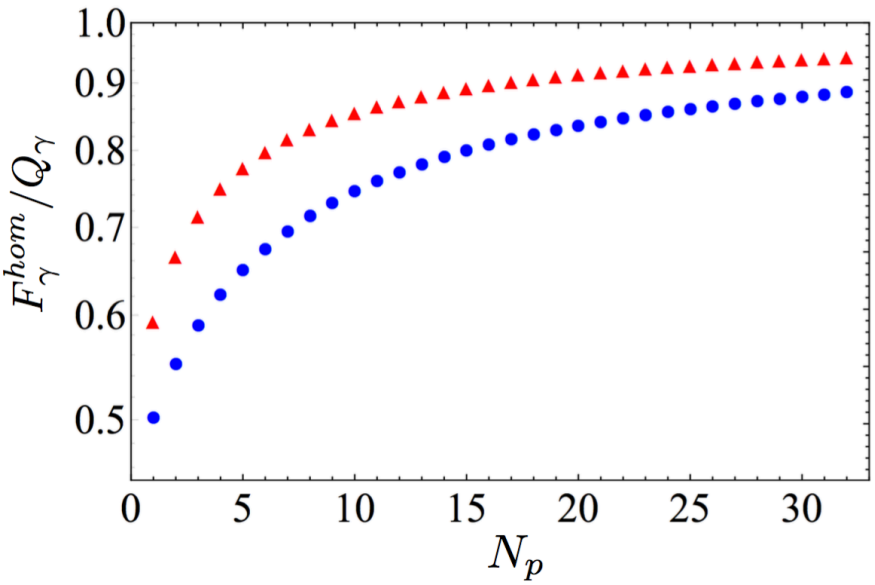


Figure 3.1: Ratio $F_\gamma^{\mathsf{hom}}/Q_\gamma$ for cubic (red triangles) and quartic (blue dots) anharmonicities as functions of the average number of photons $N_p$. Experimental parameters are set as $\lambda \sim 1.5 \times 10^{-5}$, $\gamma = 10^{-25}$ and the phase $\phi$ is optimized to $\phi = \pi/2$. (The figure has been extracted from Ref.[66].)

this is still very low compared to the number of photons in a standard optomechanical cavity setup (where $N_p \sim 10^{8(9)}$). This clearly shows that homodyne detection is an advantageous method to probe anharmonicity with arbitrarily high precision, and we could conjecture its optimality in the limit of large number of photons.

On the other hand, *heterodyne* detection consists in projecting on a coherent state $|\eta\rangle$ and is usually performed through a double-homodyne detection scheme [85]. The corresponding conditional probability is given by

$$\begin{aligned} p(\eta|\gamma) &= |\langle\eta|\psi_\gamma\rangle|^2 \\ &= e^{-(|\alpha|^2+|\eta|^2)} \left| \sum_{m=0}^{\infty} \frac{\alpha^m \eta^{*m}}{m!} e^{-i\lambda^2 m^2 (1+\frac{\gamma}{2}\lambda^2 m^2)} \right|^2 , \end{aligned} \tag{3.21}$$

and the related FI can be computed by integrating over the whole complex plane spanned by coherent states

$$F_\gamma^{\mathsf{het}} = \frac{1}{\pi} \int d^2\eta \ \frac{(\partial_\gamma p(\eta|\gamma))^2}{p(\eta|\gamma)} , \tag{3.22}$$

where the dependence on the phase parameter has dropped out, as opposed to the case of homodyne detection. We evaluated the FI also in this case, for an initial coherent state with up to 35 photons, and numerical results displayed a fixed, constant ratio between FI and QFI, *i.e.* $F_\gamma^{\mathsf{het}}/Q_\gamma = 0.5$, independently of the experimental parameters.
We conclude that homodyne measurements on the cavity field are the most effective for precise anharmonicity estimation, being nearly quantum limited.

## 3.4 Signal-to-noise ratio

While the fact that homodyne FI saturates the QFI witnesses the optimality of such interference measurements at extracting information on mechanical anharmonicity, FI alone is not sufficient to guarantee the accuracy of the scheme. We should consider indeed that we are dealing with phase measurements, where the

power to discriminate between very small phase shifts is required: to perform efficient metrology it is essential to take into account the *signal-to-noise ratio*. This important figure of merit quantifies how the genuine contribution of the desired signal compares to the intrinsic noise typical of the quantum measurement under consideration. In particular, bearing in mind the Cramér-Rao bound theorem, we can define for any parameter $\zeta$ its signal-to-noise ratio $R_\zeta$ and derive the upper bound:

$$R_\zeta = \frac{\zeta^2}{\mathrm{Var}(\zeta)} \leq \zeta^2 M Q_\zeta \,, \tag{3.23}$$

where $Q_\zeta$ denotes the QFI, or the FI in case of non-optimal measurements, for the parameter of interest. A key condition for accurate metrology is to achieve a significant value of the signal to noise ratio $R_\zeta > 1$ with a reasonable number of experimental runs. In our specific case, in the limit of large number of photons we get

$$1 < R_\gamma^{(4)} \lesssim 16\gamma^2\lambda^8 N_p^7 M \,, \tag{3.24}$$

which could be easily satisfied with homodyne detection in the limit of large number of phonons.

Substituting common up-to-date values of cavity parameters in Eq.(3.24), e.g. $N_p \sim 10^9$ and $\lambda \sim 10^{-4}$, and considering $M \sim 10^4$ experimental runs (which still allows us to use optimal asymptotic estimators, such as the Bayesian or the MaxLik estimator), one could in principle probe anharmonicities as low as $\gamma \sim 10^{-20}$ for the quartic case (and $\delta \sim 10^{-15}$ for the cubic case, as shown in Appendix B).

Eventually, we observe that for these values of the parameters all the assumptions that we have made (i.e. $\gamma\lambda^4 N_p^3 \ll 1$, $\lambda^2 N_p^2 \gg \bar{n}$, $\epsilon\bar{n} \ll N_p$) are satisfied for temperatures of a few kelvin, which can be easily achieved through dilution refrigeration techniques, without requiring sideband cooling [1].

## 3.5 Classical anharmonicity

Since non-linearities are believed to play a key role in the generation of non-classical states [70, 71, 72], we dedicate this section to the study of mechanical

anharmonicity in optomechanics. Similarly to Chap.2, where we discussed the harmonic case, we will approach the problem from a classical picture, which will also help us to get a complete understanding of the dynamics. Besides, the interest in the quantum-to-classical transition goes beyond a didactic purpose and lies in the need to properly assess which features of motion can be attributed a quantum nature. This is a prerequisite that one has to address prior to proposing optomechanical resonators for future investigations on more exotic topics such as, for example, quantum gravity and decoherence models [28, 86, 29, 57]. In this direction, we will discuss in Sec.3.6 the connection between anharmonic dynamics and the one induced by deformed commutation relations predicted by quantum gravity theories [87, 88].

Let us then start by writing the classical Hamiltonian of an anharmonic oscillator, corresponding to taking the expectation values of the operators in Eq.(3.1):

$$H_{class} = \frac{p^2}{2m} + \frac{1}{2}m\omega^2 x^2 + \frac{\tilde{\gamma}}{4}m\omega^2 x^4 \ , \tag{3.25}$$

where $\tilde{\gamma} = (m\omega/\hbar)\gamma$ has dimensions $[\tilde{\gamma}] = [\mathrm{L}^{-2}]$. Through Hamilton's equations we obtain the differential equation of motion

$$\ddot{x} + \omega^2 x + \omega^2 \tilde{\gamma} x^3 = 0 \ , \tag{3.26}$$

which is the well known Duffing equation, whose general solution to first order in $\tilde{\gamma}$ has been derived through various methods (e.g. multiscale and renormalisation approaches, see Ref.[78]) and reads, for times $t$ such that $(\omega t)\tilde{\gamma}R_0^2 \ll 1$,

$$x(t) = R_0 \cos\left[\omega' t + \theta_0\right] + \frac{\tilde{\gamma}}{32} R_0^3 \cos\left[3(\omega' t + \theta_0)\right] \ , \tag{3.27}$$

with $R_0$ the unperturbed amplitude and $\omega' = \omega(1 + \frac{3}{8}\tilde{\gamma}R_0^2)$ the anharmonic frequency. The constraint on the integration time and the frequency shift are the same as in Eq.(3.3), being typical of the multi-scale approach, whose accuracy in time increases at the $j^{th}$ order as $\omega t \ll (\tilde{\gamma}R_0^2)^{-j}$. This is a common feature of all differential equations that contain secular terms, *i.e.* terms whose amplitude grows without boundaries in time. The validity of the perturbative expansion of the solution is

preserved adapting the result at any given order by imposing the suppression of the divergences that arises at the following ones.

With the solution of the anharmonic motion at hand in Eq.(3.27), we reconstruct the classical dynamics of the system through the same scheme we applied for the harmonic case (that was depicted in Fig.2.1). Imposing the appropriate initial conditions for $x$ and $\dot{x}$ after each of the four kicks, we let the oscillator freely evolve anharmonically for a quarter of period: the phase shift imparted to the light will depend on the sum of the mirror positions at each reflection time. This approach leads to the classical equivalent of the quantum-mechanical evolution defined in Eqs.(3.4)-(3.10). Considering the mirror initially at rest in its equilibrium position[4] and defining $\bar{R} = I/(m\omega)$, we get for the first three kicks

$$
\begin{aligned}
&1^{\text{st}} \begin{cases} x(0) = 0, \quad \dot{x}(0) = \frac{I}{m} \\ x(t) = \left(\bar{R} - \frac{9}{32}\tilde{\gamma}\bar{R}^3\right)\sin(\omega' t) - \frac{\tilde{\gamma}}{32}\bar{R}^3\sin(3\omega' t) \end{cases} , \\
&2^{\text{nd}} \begin{cases} x(0) = \bar{R} - \frac{\tilde{\gamma}}{4}\bar{R}^3, \quad \dot{x}(0) = \frac{I}{m} \\ x(t) = \sqrt{2}\left(\bar{R} - \frac{9}{16}\tilde{\gamma}\bar{R}^3\right)\cos\left(\omega' t - \frac{\pi}{4} + \frac{3\tilde{\gamma}}{8}\bar{R}\right)^2 + \frac{\tilde{\gamma}\sqrt{2}}{16}\bar{R}^3\cos(3(\omega' t - \frac{\pi}{4})) \end{cases} , \\
&3^{\text{rd}} \begin{cases} x(0) = \bar{R} - \tilde{\gamma}\bar{R}^3, \quad \dot{x}(0) = -\frac{3}{4}\tilde{\gamma}\omega\bar{R}^3 \\ x(t) = \left(\bar{R} - \frac{33}{32}\tilde{\gamma}\bar{R}^3\right)\cos\left(\omega' t + \frac{3\tilde{\gamma}}{4}\bar{R}\right)^2 + \frac{\tilde{\gamma}}{32}\bar{R}^3\cos(3\omega' t) \end{cases} .
\end{aligned}
\tag{3.28}
$$

The dynamics after the fourth kick can be neglected as we have $x(\frac{3\pi}{2\omega'}) = 0 + O(\tilde{\gamma}^2)$ and $\dot{x}(\frac{3\pi}{2\omega'}) = 0 + O(\tilde{\gamma}^2)$.

The first order in $\tilde{\gamma}$ in Eqs. (3.28) corresponds to the classical deviations $\Delta x(t_i)$ from the harmonic dynamics where $x(t_i)$ are the positions of the oscillator at different times $t_i$. Following Eq.(2.3) and summing all these contributions we obtain the

[4]We have widely discussed in Chap.2 how this can be generalised to any initial condition, among which an initial thermal state.

anharmonic correction to the phase shift

$$\Delta\varphi_{class} = 2k_f N_{\rm rt} \sum_{i=1}^{4} \Delta x(t_i) = -2^2 \tilde{\gamma} k_f N_{\rm rt} \left(\frac{I}{m\omega}\right)^3 \hbar^2 \frac{N_p^3 \mathcal{F}'^4}{\lambda_L^4 (m\omega)^2} \ , \tag{3.29}$$

which is acquired by the field after a square-loop pulsed interaction.
Similarly to the harmonic case in Chap.2, we verify that in the limit of large photon number and small coupling the classical additional phase shift reproduces the quantum result in Eq.(3.11) (for the comparison we recall the relations $I/(m\omega) = \sqrt{\hbar/(m\omega)}\lambda N_p$, $N_{\rm rt} = \mathcal{F}'/\pi$ and $\lambda = 4\mathcal{F}'/\lambda_L \sqrt{\hbar/(m\omega')}$). This equivalence can be explained by considering that in the same limit the dynamics of the mirror coincides in the two pictures, *i.e.* the mean value of the position operator on the oscillator state using Eq.(3.3) tends to Eq.(3.28). For example, after the first interaction with the field, the oscillator is displaced in a coherent state of amplitude $\lambda N_p/\sqrt{2}$, whose subsequent anharmonic evolution is described by

$$\langle X(t)\rangle = \left[\lambda N_p \sin(\omega' t) - \frac{\gamma}{4}\left(3\lambda N_p \sin(\omega' t) + \frac{9}{8}\lambda^3 N_p^3 \sin(\omega' t) + \frac{\lambda^3 N_p^3}{8}\sin(3\omega' t)\right)\right], \tag{3.30}$$

which tends to the first line in Eq.(3.28) at the leading order in $(\lambda N_p)$. This implies that in the limit of large displacements $\lambda N_p \gg 1$ the quantumness of the anharmonic oscillator is lost and the dynamics approaches the classical prediction. On the other hand, in a strong coupling and single photon regime we should be able to measure different phase shifts, due to significant deviations between classical and quantum descriptions. This happens not only because of the quantisation of the field (as discussed for the harmonic case), but also since the dynamics of the quantum anharmonic oscillator differs from the classical one.

## 3.6 Generalization to non canonical transformations

We devote this section to a very specific, though enlightening, occurrence: we show how anharmonicity can derive from a deformation of the Hilbert space like the application of a non canonical transformation. As a consequence, any deformation in

commutation relations between $x$ and $p$, *e.g.* those predicted by almost all quantum gravity theories [89, 87, 88], can be translated in a form of anharmonicity and vice-versa. This imposes severe restrictions to the attribution of observable deviations from the harmonic dynamics to either of the two scenarios. Besides, it certifies that the phase shift found in Eq.(3.11) coincides with the one in Refs.[3, 31] that was ascribed to gravity deformations of Heisenberg commutator.

Let us then start the demonstration with a harmonic oscillator, $H = (x^2 + p^2)/2$, embedded in an environment where $x$ and $p$ satisfy the general commutation rule $[x, p] = i[1 + \lambda S(x, p)]$, where $\lambda$ is a small parameter and $S(x, p)$ is a generic function of $x$ and $p$. We thus apply the non-canonical transformation

$$\begin{aligned} x' &= x + \lambda f(x, p) \ , \\ p' &= p + \lambda g(x, p) \ , \end{aligned} \tag{3.31}$$

with $x'$ and $p'$ verifying

$$[x', p'] = i + i\lambda \left( S(x, p) + \frac{\partial f}{\partial x} + \frac{\partial g}{\partial p} \right) . \tag{3.32}$$

It is then sufficient to choose $f$ and $g$ such that $S(x, p) + f_x + g_p = 0$ in order to impose the canonical commutation relations on $x'$ and $p'$. Interestingly, we discover that in principle one only needs to transform one coordinate to fulfill this condition, leaving the other unchanged.

The transformed Hamiltonian will read (at the first order in $\lambda$)

$$H' = \frac{x^{2'} + p^{2'}}{2} - \lambda [x' f(x', p') + p' g(x', p')] \ , \tag{3.33}$$

from which we derive the equations of motion in the transformed frame (i.e. where $x'$ and $p'$ satisfy the standard commutation relations)

$$\begin{aligned} \dot{x}' &= \frac{\partial H'}{\partial p'} = p' - \lambda \left[ x \frac{\partial f}{\partial p} + g + p \frac{\partial g}{\partial p} \right] \ , \\ \dot{p}' &= -\frac{\partial H'}{\partial x'} = -x' + \lambda \left[ x \frac{\partial f}{\partial x} + f + p \frac{\partial g}{\partial x} \right] \ . \end{aligned} \tag{3.34}$$

It is now easy to verify that this dynamics is indistinguishable from the one arising in the original frame with deformed commutators. Such a reference frame would be the result of a non-canonical transformation on a Hamiltonian system, which implies that it will not be Hamiltonian. This means that we will need the "classical" generalised Poisson brackets to derive the equations of motions. As described in Ref.[90], these read

$$\begin{aligned} \dot{x} &= \frac{\partial H}{\partial p}\{x,p\} = p - \lambda\left[p\frac{\partial f}{\partial x} + p\frac{\partial g}{\partial p}\right] , \\ \dot{p} &= -\frac{\partial H}{\partial x}\{x,p\} = -x + \lambda\left[x\frac{\partial f}{\partial x} + x\frac{\partial g}{\partial p}\right] . \end{aligned} \tag{3.35}$$

Substituting the relation $\dot{f} = \dot{x}f_x + \dot{p}f_p = pf_x - xf_p$ (and its analogous for $g$) it is eventually straightforward to verify that Eqs.(3.34) and (3.35) describe the same dynamics. Without knowing a priori whether canonical or deformed commutation rules apply in a certain environment, it is thus impossible to distinguish between an anharmonic motion occurring in the former frame and a harmonic motion in the latter.

As a practical example, we calculate the deformed commutators that would lead to the same dynamics induced by the anharmonicity we have been studying in this chapter. We have

$$\frac{\gamma}{4}X^4 = -\lambda[Xf(X,P) + Pg(X,P)] , \tag{3.36}$$

from which we easily derive $g \equiv 0$, $\lambda \equiv \gamma$ and $f \equiv -X^3/4$, which implies that the associated deformed commutators would read $[X'', P''] = i(1 + 3/4\ \gamma X''^2)$.
Conversely, gravity modification of canonical commutation relations is expected to scale as $\sim \gamma P''^2$, thus implying a more unusual kind of anharmonicity related to the momentum, which might be excluded in experiments from other physical considerations.

## 3.7 Conclusions

In this chapter we have manipulated the results presented in Chap.1-2, such as the exploitation of the bad cavity regime, to engineer closed loops in the mechanical phase space in order to estimate the anharmonicity of a macroscopic oscillator. Relying on a four-pulse interaction with a coherent optical field in input, under an experimentally achievable initial cooling of the mirror, the system ends up in a separable state. Specifically, the oscillator returns to its initial position, while the cavity field undergoes an effective unitary operator which retains information on the anharmonicity of the mechanics. By using tools from local quantum estimation theory, we have derived the ultimate bounds on the estimation precision, showing how this can be arbitrarily high by increasing the number of photons of the initial coherent state. This has allowed us to prove the optimality of homodyne detection in the limit of large number of photons, and the efficiency of our method at estimating small anharmonicities by considering state-of-the-art values of the optomechanical parameters. Also, since different anharmonicities have different impacts on the shift of both mechanical frequency and light phase, the joint measurement of these observables could make the scheme able to discriminate multiple non-linearities.
In addition, to provide a deeper understanding of such mechanical anharmonicities, we have presented a full description of the model in a classical picture, being able to identify the true signatures of quantumness in the dynamics. Besides, we have shown the close relationship that mechanical non-linearities share with more fundamental modifications of the Hilbert space topology, *e.g.* the supposed deformation of commutation relations predicted by quantum gravity.

# Chapter 4

# Preparation of Macroscopic Quantum States

## 4.1 Introduction

*The content of this chapter is the result of the research that I conducted under the supervision of Dr Florian Mintert at Imperial College. The work that is presented here is currently under revision at Physical Review Letters and is available on the arXiv with the title "Deterministic preparation of highly non-classical quantum states of massive oscillators" [91].*

After having discussed the role of Kerr and mechanical non-linearities, also in context of the quantum-to-classical correspondence, we devote this chapter to propose a scheme to deterministically prepare a range of quantum superposition states of the mirror. While literature has been historically focused on the quantumness of microscopic objects, it is a challenge to deterministically isolate genuine quantum features in the macroscopic world that can be accessed in experiments. Few attempts have reported coherent superpositions of quantum objects with large mass [92, 93]. Still, the preparation of a massive system in a quantum state is a matter of great interest both theoretically and experimentally, as it is expected to shed new light on a variety of topics ranging from quantum-to-classical transitions [25, 26, 27] and collapse models [28, 29, 30] to the interface between quantum mechanics and

gravity [3, 31]. In particular, we have seen in previous chapters how optomechanical cavities offer a practical table-top scenario to investigate the dynamics of massive mechanical oscillators [49, 94, 95, 1]. These were proven to exhibit a large degree of macroscopicity, reaching $\mu = 19$ on a scale where the Mach-Zender interference of Cs [96] and the Schrödinger gedanken experiment reach values of $\mu = 10.6$ and $\mu \sim 55$ respectively [97].

While the light-matter interaction in cavity optomechanics has been already proposed as a resource to prepare non-classical states of the mechanical motion, such as squeezed states [98, 99, 100], single phonon excitations [101, 102, 103] and Schrödinger cat states [2, 5, 104, 105], none of these proposals has come up with the deterministic creation of a macroscopic state, relying instead on a probabilistic approach [106, 107] or on a transient regime [108, 109].

In this chapter we will present a protocol to prepare the optomechanical system in a product state of the cavity field and the mirror by driving the latter with appropriately chosen pump profiles with external lasers. As we have already discussed, separability is an essential prerequisite to achieve deterministic preparation of quantum mechanical states of the mirror, which in our case will consist in squeezed states and non-Gaussian coherent superpositions exhibiting sizeable negativity of the Wigner function.

Special attention will be devoted to the latter case where non-classical states are achieved. Besides, we will employ a quantitative measure able to evaluate the *degree* of non-classicality of a given state. Not only this will allow us to certify the creation of maximally non-classical states of the mirror, but it will also make our proposal optimal for accurate tests of decoherence models and of potential limitations on coherent superpositions of a massive object.

We will begin the discussion assuming the ideal initial situation when the system is initially cooled down to the ground state and undergoes a unitary evolution, and we will later analyse the resilience of our scheme to various possible sources of experimental error, from mechanical and optical damping, to thermal mechanical noise and imperfections in the driving pattern.

For ease of reading, we detail hereafter a summary of the content of the chapter.

– In Sec.4.2 we recapitulate the model of a driven optomechanical cavity and formalise

the scope of our investigation. We also introduce the Magnus expansion technique to perturbatively solve a non-linear time dependent Schrödinger equation.

– Sec.4.3 is devoted to the derivation of the driving profiles that have to be applied to obtain the desired quantum states of the mirror, *i.e.* squeezed states (4.3.1) and highly non-classical coherent superpositions (4.3.2). In subsection (4.3.3) we discuss the effectiveness of the perturbative approach, while (4.3.4) reviews standard measurement techniques to experimentally readout such non-trivial mechanical states.

– In Sec.4.4, we analyse and characterise the state of the mirror in terms of the negativity of its Wigner function and of a rigorous *measure of non-classicality*.

– Sec.4.5 is dedicated to the resilience of the control scheme to a range of experimental imperfections, looking at the effects of optical and mechanical decoherence, initial mechanical thermal noise and imperfect optical driving.

## 4.2 The Model

Unlike the pulsed regime that we have adopted in the previous chapters, we will now contemplate a general multi-chromatic external continuous driving of the cavity $\xi(t)$. We will refer to the optomechanical scheme depicted in Fig.1.1 and described by the Hamiltonian in Eq.(1.4), though we will consider the possibility to have more than one external laser source. The complete Hamiltonian of the system reads (see Sec.1.2)

$$\begin{aligned} H &= H_0 + H_{int} \ , \quad \text{with} \\ H_0 &= \omega_c a^\dagger a + \omega b^\dagger b + i\left(\xi(t)a^\dagger - \xi^*(t)a\right) \ \text{and} \\ H_{int} &= -g_0 a^\dagger a(b + b^\dagger) \ , \end{aligned} \tag{4.1}$$

and thanks to the cubic optomechanical interaction, $H_{int}$, it is expected to induce non-Gaussian states of the system. However, as we have already discussed in Chap.1-2, where the driving was turned off during the interaction, the evolution will generally result in a correlated state of the field and the mirror, such that only a mixed

quantum state could to be attributed to each subsystem alone.
Conversely, we will now design *ad hoc* driving patterns $\xi(t)$ to leave the system in a separable state at the end of the preparation time. In other words, if $U(t)$ is the solution of Schrödinger equation at time $t$ relative to the whole system, *i.e.* it satisfies $i\dot{U}(t) = H(t)U(t)$, the functions $\xi(t)$ will be engineered such that, at a predetermined time $t'$, $U(t')$ factorises in the product of two separable propagators $U(t') = U_c(t') \otimes U_m(t')$, acting on the cavity and on the mirror respectively. In particular, we will ensure that the former ends up in its initial state, $U_c(t') = \mathbb{1}$, in order to significantly ease the readout subsequent to the state preparation. As we will discuss in Sec.4.3.4, this is required because most of current state reconstruction techniques of mechanical motional states are achieved through homodyne tomography of a probe light field, via the so called *back-action-evading interaction* [11, 100, 110].

### 4.2.1 The time evolution

A convenient approach to express the time evolution resorts to factorising the propagator $U(t) = U_0(t)V(t)$ in the product of the harmonically driven dynamics ($U_0(t)$), originated by the non-interacting Hamiltonian $H_0(t)$, and the one induced by the non-linear interaction in $H_{int}(t)$ ($V(t)$). The Schrödinger equation can then be split in a system of coupled equations

$$\begin{aligned} i\dot{U}_0(t) &= H_0(t)U_0(t) \ , \text{ and} \\ i\dot{V}(t) &= H_I(t)V(t) \ , \end{aligned} \tag{4.2}$$

where $H_I(t) = U_0^\dagger(t)H_{int}(t)U_0(t)$ is the interaction Hamiltonian in the interaction picture defined by $U_0(t)$. Since $H_0(t)$ is harmonic, and actually refers to two uncoupled harmonic oscillators, one of which being forced by the time dependent driving $\xi(t)$,

its explicit solution can be constructed exactly and reads

$$\begin{aligned} U_0(t) &= e^{-i\omega_c n_c t} e^{-i\omega n_m t} e^{\left(f_1(t)a^\dagger - f_1^*(t)a\right) + f_2(t)\mathbb{1}} \ , \text{ with} \\ f_1(t) &= \int_0^t dt_1 \xi(t_1) e^{i\omega_c(t_1)} \ , \text{ and} \\ f_2(t) &= \frac{1}{2}\int_0^t dt_1 \xi(t_1) e^{i\omega_c(t_1)} f_1^*(t_1) - \text{h.c.} \ . \end{aligned} \tag{4.3}$$

With this at hand, one extracts the interaction Hamiltonian in the frame defined by the harmonic motion as

$$H_I(t) = -g_0\Big(n_c - (f_1 a^\dagger + f_1^* a) + |f_1|^2\Big)X(t) \ . \tag{4.4}$$

Because of the cubic nature and the time-dependence, there is no known exact analytical solution for the dynamics induced by $H_I(t)$. Still, in the limit of weak coupling, $k = g_0/\omega \ll 1$, which is in agreement with state-of-the-art experiments operating at $k \lesssim 10^{-2}$ [49, 1], we can construct the time-evolution operator $V(t, t_0)$ in a perturbative expansion in powers of $k$ through the Magnus series [111]

$$V(t, t_0) = \exp\Big(-i\sum_j \mathcal{M}_j(t, t_0)\Big) \ , \tag{4.5}$$

where the individual terms

$$\begin{aligned} \mathcal{M}_1(t, t_0) &= \int_{t_0}^t dt_1 H_I(t_1) \ , \\ \mathcal{M}_2(t, t_0) &= -\frac{i}{2}\int_{t_0}^t dt_1 \left[H_I(t_1), \mathcal{M}_1(t_1, t_0)\right] \ , \\ \mathcal{M}_3(t, t_0) &= -\frac{i}{3}\int_{t_0}^t dt_1 \left[H_I(t_1), \mathcal{M}_2(t_1, t_0)\right] - \frac{1}{6}\int d^3\tau \ \left[H_I(t_3), [H_I(t_2), H_I(t_1)]\right] \ , \end{aligned} \tag{4.6}$$

(the last integration with $d^3\tau = dt_1 dt_2 dt_3$ is taken over $t \geq t_1 \geq t_2 \geq t_3 \geq t_0$) and similar higher order terms satisfy the proportionality $\mathcal{M}_j(t, t_0) \sim k^j$ for any given driving profile $\xi(t)$.

In the first two chapters of this thesis we showed how light-matter correlations

arosed alongside the evolution when no continuous driving was applied. From the expression for $H_I(t)$ in Eq. (4.4), it emerges that the lowest order term $\mathcal{M}_1(t,t_0)$ will already contain such correlating terms. Besides, the adoption of the external drivings will also induce single-particle terms of the mirror and the cavity alone, which will appear at higher order expansions $\mathcal{M}_j(t,t_0)$ $(j>1)$. In order to achieve deterministic state preparation, we will need that all interaction terms and all single-particle terms of the cavity vanish at $t'$, while the single-particle terms of the mirror induce highly non-classical states.

For this purpose, it will prove useful to consider the case when $t'$ corresponds to an integer number $N$ of periods of the mechanical motion, *i.e.* $t'=NT$ with $T=2\pi/\omega$. We shall then express the propagator $V(TN,0)$ over $N$ periods as

$$V(TN,0)=\prod_{s=1}^{N}V(Ts,T(s-1))=\prod_{s=1}^{N}\exp(-i\mathcal{M}^{(s)})\ , \tag{4.7}$$

where $V(Ts,T(s-1))$ is the propagator of the system for the $s^{\text{th}}$ driving period, *i.e.* the time window where $t\in[(s-1)T,sT]$. It is also implied in Eq.(4.7) that terms are ordered with decreasing value of $s$ in the product. The $\mathcal{M}^{(s)}$ are defined via the relation $\exp(-i\mathcal{M}^{(s)})=V(Ts,T(s-1))$, and can be expanded in the series

$$\mathcal{M}^{(s)}=\sum_j \mathcal{M}_j^{(s)}\ , \tag{4.8}$$

analogously to Eq. (4.6). The Baker-Campbell-Hausdorff relation yields

$$\begin{aligned}
\mathcal{M}_1(TN,0)&=\sum_{s=1}^{N}\mathcal{M}_1^{(s)},\\
\mathcal{M}_2(TN,0)&=\sum_{s=1}^{N}\mathcal{M}_2^{(s)}-\frac{i}{2}\sum_{s>l=1}^{N}[\mathcal{M}_1^{(s)},\mathcal{M}_1^{(l)}]\ ,\\
\mathcal{M}_3(TN,0)&=\sum_{s=1}^{N}\mathcal{M}_3^{(s)}-\frac{i}{2}\sum_{s>l=1}^{N}\Big([\mathcal{M}_1^{(s)},\mathcal{M}_2^{(l)}]+[\mathcal{M}_2^{(s)},\mathcal{M}_1^{(l)}]\Big)\\
&\quad-\frac{1}{6}\sum_{j\geq s\geq l}^{N}\Big([\mathcal{M}_1^{(j)},[\mathcal{M}_1^{(s)},\mathcal{M}_1^{(l)}]]+[\mathcal{M}_1^{(l)},[\mathcal{M}_1^{(s)},\mathcal{M}_1^{(j)}]]\Big)\ ,
\end{aligned} \tag{4.9}$$

and similar contributions for higher order terms. Now that we have decomposed the evolution operator into the sum of $N$ time windows, we can consider the situation where we adopt simple, though different, driving profiles for each period. More specifically, we will consider the set of time dependent functions $\xi_s(t)$, with $s \in [1, N]$, resulting in different interaction Hamiltonians $H_I^{(s)}(t)$ in each interval. The adoption of different drivings in the various intervals algebraically corresponds to applying a set of operators $\{W_s\}$ such that, with the specific choice $H_I^{(s)}(t) = W_s^\dagger H_I^{(1)}(t) W_s$ (with $W_1 = \mathbb{1}$), one obtains

$$V(TN, 0) = \prod_{s=1}^{N} W_s^\dagger V(T, 0) W_s = \prod_{s=1}^{N} \exp(-i\mathcal{M}^{(s)}) \ , \tag{4.10}$$

with $\mathcal{M}^{(s)} = W_s^\dagger \mathcal{M}^{(1)} W_s$. We have thus brought the problem back to reconstructing the dynamics over the first mechanical period. Once this is done, we have to engineer the set $\{W_s\}$, and the corresponding driving pattern, such that any undesired term in $\mathcal{M}_j$ vanishes or is modified as desired.
Eq.(4.10) provides a convenient expression to understand how to design the control scheme and in the next section we will propose physically motivated choices for the $W_s$ that achieve the aim and that translate into rather simple driving profiles.

## 4.3 State preparation

Now that we have laid out the algebraic framework, we have all the tools to find explicit driving profiles $\xi(t)$ that result in desired dynamics. First of all we notice that due to the large separation of the resonance frequencies of cavity and mirror, it is recommended to drive the former close to the sidebands with frequencies $\omega_c \pm \omega$ to enable the exchange of excitations between the two subsystems. In the next two sections, (4.3.1 and 4.3.2), we will derive suitable control patterns to lead the mirror into a strongly squeezed state and a state with pronounced non-Gaussian and non-classical features respectively. Apart from an interest in its own, the discussion on strongly squeezed states in Sec.4.3.1 shall help to exemplify the framework developed above, with simpler algebra than found in the preparation of non-classical states.

### 4.3.1 Preparation of macroscopic squeezed states

The first order expansion of $V(T,0)$, *i.e.* $\mathcal{M}_1^{(1)}$, both with a blue or a red detuned driving alone (respectively $\omega_c+\omega$ and $\omega_c-\omega$) leads to well known propagators that respectively create or exchange excitations between the cavity field and the mirror. However, not only do they both induce light-matter correlations, but they both also induce a displacement of the mirror. Since this effect would outshine the mechanical squeezing, which, as we will see, is a second order effect in $k$, we adopt a bi-chromatic driving with both the detuned lasers $\pm\omega$. The corresponding driving profile

$$\xi(t) = \mathcal{E}e^{-i\omega_c t}(e^{i\omega t} + e^{-i\omega t}) \ , \tag{4.11}$$

with amplitude $\mathcal{E}$ results in the lowest order contribution to the Magnus expansion

$$\mathcal{M}_1^{(1)} = -2\pi k\eta X_c P \ , \tag{4.12}$$

with the cavity quadrature $X_c = a + a^\dagger$ and the unitless amplitude constant $\eta = \mathcal{E}/\omega$. Since the mechanical frequency provides the characteristic time-scale of an optomechanical experiment, it is a common custom to use $\omega$ as a term of reference for all other experimental parameters (drivings, coupling, mechanical and optical damping). In the following, the introduction of $\eta$ will also help to provide more compact analytical expressions.

As we anticipated, we notice that after the first driving period correlations between cavity position quadrature and mirror momentum – $\propto X_c P$ – are created at the first order in the coupling. Let us then consider the particularly simple choice $W_s = \exp(-in_c\varphi_s)$, that rotates cavity operators in phase space as

$$\begin{aligned} e^{in_c\varphi_s} X_c e^{-in_c\varphi_s} &= X_c\cos\varphi_s + P_c\sin\varphi_s \ , \\ e^{in_c\varphi_s} P_c e^{-in_c\varphi_s} &= P_c\cos\varphi_s - X_c\sin\varphi_s \ , \end{aligned} \tag{4.13}$$

with $P_c = i(a^\dagger - a)$. The set of transformations $\{W_s\}$ is obtained by reverse-engineering the derivation of the interaction Hamiltonian (see Eq. (4.4)), and corre-

sponds to the modified driving profiles

$$\xi_s(t) = \mathcal{E} e^{i\varphi_s} e^{-i\omega_c t}(e^{i\omega t} + e^{-i\omega t}) \ . \tag{4.14}$$

These are rather elementary to implement, as different driving periods differ from each other merely by the phase shift $\varphi_s$, and a simple bi-chromatic driving with a step-like phase variation realises the desired dynamics.
Substituting Eqs. (4.12) and (4.13) inside Eq.(4.9) we get

$$\begin{aligned}\sum_{s=1}^{N} \mathcal{M}_1^{(s)} &= \sum_{s=1}^{N} \exp(in_c\varphi_s)\mathcal{M}_1^{(1)} \exp(-in_c\varphi_k) \\ &= -2\pi\ k\eta \left( \sum_{s=1}^{N} X_c \cos\varphi_s + P_c \sin\varphi_s \right) P \,,\end{aligned}$$

such that any undesired interaction term proportional to $\propto kX_c(P_c)P$ cancels for any choice satisfying $\sum_s e^{i\varphi_s} = 0$.
We should now repeat the same reasoning with the second order expansion in Eq.(4.9). Making explicit the quadratic terms in the Magnus expansion over the first period one obtains

$$\begin{aligned}\mathcal{M}_2^{(1)} &= -\pi k^2 \left( m_2^c + m_2^I + \frac{20}{3}\eta^4 \right) \ , \quad \text{with} \\ m_2^c &= 3\eta^2 X_c^2 + 8\eta^2 n_c + 2n_c^2 \ \text{ and} \\ m_2^I &= 2\eta P_c P^2 \ ,\end{aligned} \tag{4.15}$$

together with contributions arising from the commutators

$$\frac{i}{2}[\mathcal{M}_1^{(s)}, \mathcal{M}_1^{(l)}] = 4\pi^2 k^2 \eta^2 \sin(\varphi_s - \varphi_l) P^2 \ . \tag{4.16}$$

As for the first order case, the choice $\sum_s \varphi_s = 2\pi$ guarantees $\sum_s W_s^\dagger P_c W_s = 0$, so that the interaction terms $m_2^{I,s}$ add up to 0 as desired.
Moreover, given the relation

$$\exp(in_c\varphi_s) X_c^2 \exp(-in_c\varphi_s) = a^2 e^{-i2\varphi_s} + {a^\dagger}^2 e^{i2\varphi_s} + 2n_c + 1/2 \ ,$$

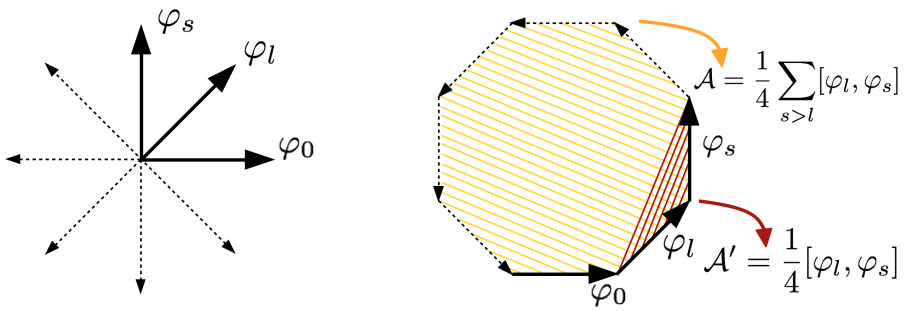


Figure 4.1: Phase space schematic representation of the algebra that lies under the sum of exponential operators that are rotated by angles $\varphi_s$. As illustrated on the left, we consider the case where the set of phases satisfies $\sum_{s=1}^{N} e^{i\varphi_s} = 0$. On the right we show that the total area spanned by the representation of such phases in phase space is related to the sum over all the combinations of commutators: $A = \sum_{s>l}[\varphi_l, \varphi_s]/4 = N\cot[\pi/N]/4$.

it is desirable to achieve also $\sum_s e^{i2\varphi_s} = \sum_s e^{-i2\varphi_s} = 0$, which eventually motivates the selection $\varphi_s = 2\pi(s-1)/N$ (assuming $N > 2$, see Fig.4.1).
The remaining terms in $m_2^{c,s}$ depending on $n_c$ are independent of the choice of $\varphi_s$ and can not be modified. The last, and most important, contribution to $\mathcal{M}_2$ is given by Eq. (4.16). With the choice $\varphi_s = 2\pi(s-1)/N$, the sum over the sin-terms results in

$$\sum_{l<s} \sin\left(2\pi\frac{(s-l)}{N}\right) = \frac{N}{2}\cot\left(\frac{\pi}{N}\right) \ , \tag{4.17}$$

which scales quadratically in the driving time $\sim N^2/(2\pi)$, as illustrated in Fig. 4.1.

Eventually, we have thus arrived at dynamics, such that no results of an interaction appear at the final instance in time and no excitations in the cavity have been created. Up to a global phase factor, which we will henceforth always neglect, the full propagator reads $V(TN,0) = V_c(N) \otimes V_m^{(2)}(N)$ with

$$\begin{aligned} V_c(N) &= \exp\left(2\pi i\ Nk^2\ (n_c^2 + 7\eta^2 n_c)\right) \ , \quad \text{and} \\ V_m^{(2)}(N) &= \exp\left(2i\,(\pi k\eta)^2\, N\cot\left(\frac{\pi}{N}\right) P_m^2\right) \ , \end{aligned} \tag{4.18}$$

where $V_m^{(2)}(N)$ is a unitary operator acting on the mirror and corresponding to a squeezing operation. Indeed, we should recall to the reader that a single mode

quadrature squeezing $S(\beta)$ is defined by the Gaussian unitary operator [112]

$$S(\beta) = e^{\frac{1}{2}(\beta^* b^2 - \beta b^{\dagger 2})} \ . \tag{4.19}$$

The state obtained by applying $S(\beta)$ to the vacuum is called a *squeezed-vacuum* state and is characterized by having, for some values of $\beta$, one of its quadrature variances, *i.e.* $\Delta X^2$ or $\Delta P^2$, below the zero-point level of 1/2.
Let us then show how to recast Eq.(4.18) in the form $V_m^{(2)}(N) = e^{i\delta b^\dagger b} e^{\frac{1}{2}(\zeta^* b^2 - \zeta b^{\dagger 2})}$, with the squeezing parameter

$$\zeta = i\,(2\pi k\eta)^2\, N \cot\left(\frac{\pi}{N}\right) e^{i\delta} \ ,$$

that scales as $|\zeta| \sim N^2$. This transformation can be obtained by considering the action of $V_m^{(2)}(N)$ on the annihilation operator $b$ in Heisenberg picture

$$V_m^{(2)\dagger}(N) b V_m^{(2)}(N) = (1 + i|\zeta|)b - i|\zeta| b^\dagger \ , \tag{4.20}$$

and looking for the application of a vacuum squeezing operation $S(\beta)$ followed by a rotation $R(\phi)$ that corresponds to it

$$R(\phi)^\dagger S(\beta)^\dagger b S(\beta) R(\phi) = b e^{i\phi} \cosh r - b^\dagger e^{i(\theta - \phi)} \sinh r \ , \tag{4.21}$$

where $\beta = r\ e^{i\theta}$. By matching Eqs.(4.20) and (4.21) we obtain $\beta = \zeta$ and $\theta = \delta$.

As we show in Fig.4.2, up to a rotation $\delta = \arctan(|\zeta|)$, the quadratic dependence on time allows substantial squeezing already after a few intervals. Besides, we should keep in mind that the perturbative regime requires reasonably short propagation times, *i.e.* small values of $N$, and the present analysis is valid in the limit $k \ll 1$, as the neglected third order term scales as $\mathcal{M}_3 \sim k^3 \eta^2 N$. For a relatively weak interaction, $k = 1/400$, and sufficiently strong driving, $\eta = 10$, one achieves a squeezing of the position quadrature resulting, after $N = 11$ periods, in $\Delta P_m^2 = 1.57$ and $\Delta X_m^2 \simeq 0.16$ (see Fig.4.2).

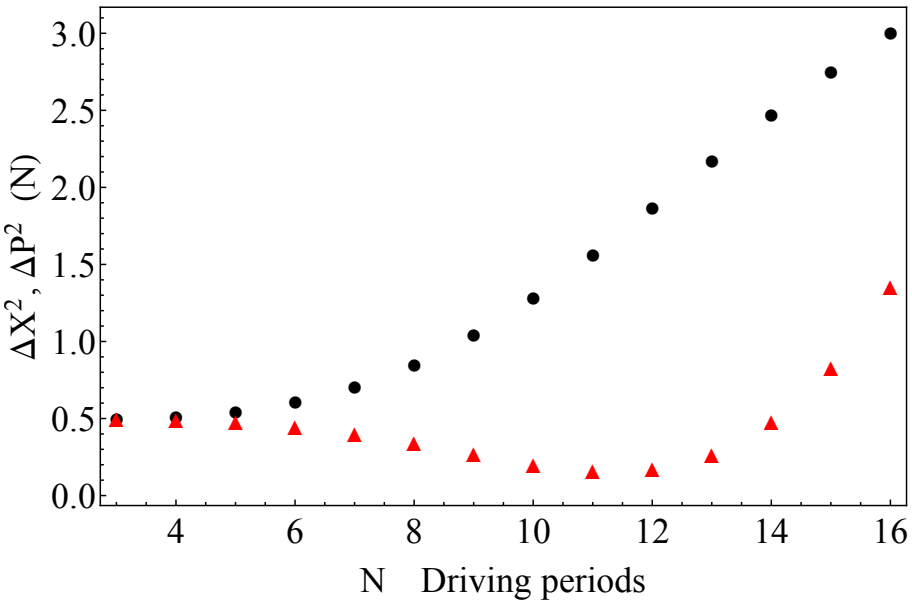


Figure 4.2: Expected values for the quadratures of the mirror as a function of the total driving time expressed in terms of driving periods. Black circles represent $\Delta P^2$ and red triangles $\Delta X^2$, which is squeezed by the evolution operator up to $\Delta X^2 = 0.16$. Experimental parameters are set as: $\eta = 10$, $k = 1/400$.

### 4.3.2 Non-classical Quantum States

The creation of non-classical states relies on third order contributions to the dynamics and thus requires the suppression not only of interaction effects, but also of second order Gaussian terms, since these will outshine the non-linearity and lead the system towards classical states. It is therefore advisable to double the detuning as compared to Sec. 4.3.1, but employ qualitatively similar driving profiles

$$\xi_s(t) = \mathcal{E} e^{i\varphi_s} e^{-i\omega_c t}(e^{i2\omega t} + e^{-i2\omega t}) \ , \tag{4.22}$$

with a new set of phase shifts $\varphi_s$.

Thanks to the chosen double side-band detuning, the first order Magnus $\mathcal{M}_1$ vanishes regardless of the choice for the $\varphi_s$. The second and third order expansions of the

propagator for the first driving period are instead

$$\begin{aligned}\mathcal{M}_2^{(1)} &= \pi k^2 \left( m_2^c + m_2^I - \frac{29}{60}\eta^4 \right) \ , \quad \text{with} \\ m_2^c &= -2n_c^2 + \frac{1}{3}\eta^2(X_c^2 - 6n_c) \quad \text{and} \\ m_2^I &= \eta P_c(b^2 + b^{\dagger 2}) \ ;\end{aligned} \tag{4.23}$$

as well as $\mathcal{M}_3^{(1)} = \frac{\pi}{3}k^3\eta \left(m_3^m + m_3^I\right)$ with

$$\begin{aligned}m_3^I = &\left[14i(a^\dagger n_c - n_c a) - \left(\frac{36}{5}\eta^2 + 4\right) P_c\right] X \\ &+ \left[3X_c + 6i\eta(a^2 - a^{\dagger 2})\right] P - \frac{3}{4}P_c Q_m \ ,\end{aligned} \tag{4.24}$$

and $m_3^m = \eta \ Q_m$ with

$$Q_m = \left[\left(X + i\frac{P}{\sqrt{3}}\right)^3 + \left(X - i\frac{P}{\sqrt{3}}\right)^3 + \frac{3}{2}X\right] \ .$$

Thanks to the fact that $\mathcal{M}_1^{(s)}$ vanishes, all terms at the second and third order in the coupling resulting from non-commutativity of $\mathcal{M}_{1/2}^{(s)}$ and $\mathcal{M}_1^{(l)}$ vanish as well. Following Eq. (4.9), we can thus reconstruct the generator of the dynamics over $N$ periods by considering $\mathcal{M}_2 = \sum_{s=1}^N \mathcal{M}_2^{(s)}$ and $\mathcal{M}_3 = \sum_{s=1}^N \mathcal{M}_3^{(s)}$, where the terms $\mathcal{M}_{2/3}^{(s)}$ are obtained from Eqs. (4.23) and (4.24) by applying the transformation in Eq.(4.10).

Let us then discuss how the new set of phase shifts $\{\varphi_s\}$ should be designed to achieve the desired goals of a product state with an empty cavity and a non-classical state of the mirror. From the past section, we have learned that a bichromatic driving as the one in Eq.(4.22) induces a different rotation at each period of the field operators $a$ and $a^\dagger$ by an amount $-\varphi_s$ and $\varphi_s$ respectively. Since every element of the interaction terms $m_2^I$ and $m_3^I$ at each period, $W_s^\dagger m_j^I W_s$ $(j = 2, 3)$, is proportional to $\exp(\pm i\varphi_s)$ or $\exp(\pm i2\varphi_s)$, then the choice $\varphi_s = 2\pi(s-1)/N$ ensures that they all cancel each other via the same mechanism we showed for the creation of squeezed states in Sec.4.3.1.

Making use of all the cancellations when summing over the $N$ periods of driving, we arrive at a separable propagator $V(TN,0) = V_c(N) \otimes V_m^{(3)}(N)$ with

$$\begin{aligned} V_m^{(3)}(N) &= \exp\left(-\frac{\pi}{3} i \; N k^3 \eta^2 \; Q_m\right) \;, \text{ and} \\ V_c(N) &= \exp\left(2\pi i \; k^2 \left(n_c^2 + \frac{2}{3}\eta^2 n_c\right) N\right) \;. \end{aligned} \tag{4.25}$$

As expected, since all powers of $a^\dagger$ and $a$ average to zero (with the only exception of terms proportional to $\propto a^\dagger a$), $V_c$ does not create any excitations in the cavity and the initial optical vacuum state is preserved by the dynamics. Instead, the cubic mirror operator $Q_m$ induces highly non-classical states, which we will examine in detail in Sec.4.4.

**Perturbative correction of the driving profiles**

Prior to an accurate discussion on the mechanical states induced by $Q_m$, however, it is worth taking a critical look at the perturbative expansion. In fact, since the generator $V_m^{(3)}$ in Eq.(4.24) scales as $k^3\eta^2$, the cubic dependence on $k$ requires a fairly strong coupling to yield to sizeable effects on the mirror. This would generally make an experimental realisation more challenging than the one proposed to create squeezed states, which are a second order effect. Still, thanks to the quadratic dependence on $\eta^2$, strong driving can compensate for the weak interaction. Yet, the strong driving regime should be handled with care, as it may compromise the effectiveness of the perturbative Magnus expansion which contains at each order raising powers of $k$ and $\eta$. In this sense, particular attention should be devoted to the product $k\eta$. Let us then start our analysis by looking at $\mathcal{M}_2^{(1)}$ in Eq.(4.23), which contains terms $\sim (k\eta)^2 n_c$ , as well as it generates fourth order contributions $\sim (k\eta)^4 n_c$ resulting from the commutators $[\mathcal{M}_2^{(s)}, \mathcal{M}_2^{(l)}]$. These should not have directly a detrimental impact on the state preparation, since such terms describe neither an interaction between cavity and mirror nor do they create excitations in the system. They do induce, however, a back-action effect on the dynamics, rotating the cavity field at each period and spoiling the effect of the previously engineered set of rotations $W_s = \exp(-i n_c \varphi_s)$. The driving profiles need to be adapted so that to

compensate this extra unwanted rotation, ensuring that at the end of the driving time the propagator factorises into individual propagators of mirror and cavity. To this end, it is instructive to look deeper at the role played by the operators $W_s$ and rewrite the propagator over the first interval, neglecting terms of order $k^4\eta^q$ with $q < 4$ and terms of order $k^j$ with $j > 4$ as

$$\begin{aligned} V(T,0) &\simeq e^{i\frac{4}{3}\pi k^2\eta^2 n_c} e^{-i\tilde{\mathcal{M}}^{(1)}} \ , \text{ with} \\ \tilde{\mathcal{M}}^{(1)} &= \pi k^2(\tilde{m}_2^c + m_2^I) + \mathcal{M}_3^{(1)} \ , \text{ and} \\ \tilde{m}_2^c &= -2n_c^2 + \eta^2(a^{\dagger 2} + a^2 + 1)/3 \ , \end{aligned} \tag{4.26}$$

where the term $\exp(i\frac{4}{3}\pi k^2\eta^2 n_c)$ in the expression for $V(T,0)$ is the undesired extra-rotation (which similarly arises at every period for $V(sT,(s-1)T)$). Recalling Eq. (4.10), the propagator over $N$ periods can be conveniently written as

$$V(TN,0) = W_{N+1}^\dagger \left( \prod_{s=1}^{N} W_{s+1} W_s^\dagger V(T,0) \right) W_1 \ ,$$

from which it is clear that the extra term $e^{i\frac{4}{3}\pi k^2\eta^2 n_c}$ in Eq. (4.26) that arises at each period can be cancelled by appropriately choosing the set of $W_s$, *i.e.* the prefactors $W_{s+1}W_s^\dagger$. This is achieved with the new set of phases

$$\varphi_s = \left( \frac{2\pi}{N} + \frac{4\pi}{3}(k\eta)^2 \right)(s-1) \ , \tag{4.27}$$

which counterbalances exactly the phase shift $\Delta = \frac{4\pi}{3}k^2\eta^2$ that the cavity experiences through the driving over each period as described in Eq.(4.26). Hence, the propagator can be recasted in the form

$$V(TN,0) = \prod_{s=1}^{N} \exp\left( e^{\frac{2\pi i}{N}(s-1)n_c} \tilde{\mathcal{M}}^{(1)} e^{-\frac{2\pi i}{N}(s-1)n_c} \right) \ , \tag{4.28}$$

and the basic principles for the cancellation of field operators within the sum over the $N$ driving periods developed above apply. However, the terms $\sim (k\eta)^2 n_c$ no longer appear, and the only remaining contribution scaling as $\sim (k\eta)^2$ in $m_2^c$ in

Eq. (4.26) is the polynomial $a^{\dagger 2} + a^2 + 1$. Operators $a^{\dagger 2}$ and $a^2$ cancel out exactly in the summation defined in Eq. (4.9) thanks to the specific set of phase shifts, and the '+1' brings an irrelevant global phase. The terms $\sim (k\eta)^4$ arising from the commutators $[\mathcal{M}_2^{(s)}, \mathcal{M}_2^{(l)}]$ (which are of the form $[a^2, a^{\dagger 2}] = 4n_c + 2$) contribute either to the global phase or to a global final rotation in $V_c$. Lastly, we will see that the only term $\sim (k\eta)^4$ in $\mathcal{M}_4^{(1)}$ depends on $P_c$ and averages out in the summation over the $N$ periods.
Overall, the mirror will undergo the same evolution defined by $V_m^{(3)}$ in Eq.(4.25), while the propagator for the field will read

$$V_c(N) = e^{2\pi N i \; k^2 \left[ n_c + \frac{2}{3}\eta^2 + \frac{2\pi k^2 \eta^4}{9} \cot\left(\frac{2\pi}{N}\right) \right] n_c} , \tag{4.29}$$

which corresponds to the one in Eq. (4.25), up to the perturbative modification in the cavity phase shift $\left(\frac{2\pi k^2 \eta^2}{3}\right)^2 N \cot\left(\frac{2\pi}{N}\right)$.

### 4.3.3 Perturbative regime

As is has emerged from the past discussion, it is essential to gauge the range of applicability of the perturbative approximation. To this end, we devote this subsection to the comparison between the dynamics obtained with the Magnus expansion in third and fourth order approximation.
The operator $V_m^{(4)}$ is constructed in the same way as the corresponding second and third order generators $V_m^{(2)}$ and $V_m^{(3)}$, which we dealt with in the past two sections. However, this time we will also need to compute the fourth order Magnus expansion $\mathcal{M}_4(NT, 0)$, which can be rewritten, under the adoption of the usual set of operators $\{W_s\}$, in the form

$$\mathcal{M}_4(NT, 0) = \sum_{s=1}^{N} \mathcal{M}_4^{(s)} - \frac{i}{2} \sum_{s>l=1}^{N} [\mathcal{M}_2^{(s)}, \mathcal{M}_2^{(l)}] , \tag{4.30}$$

where the full expression has been simplified by exploiting the fact that there is no contribution from the first order in Magnus. Choosing the same set of phases $\{\varphi_s\}$ proposed in Eq.(4.27), one takes advantage of the same crossing-out of the field

operators we presented in Sec.4.3.2 and obtains a separable evolution of the system. This results in the fourth-order generator $V_m^{(4)}$ acting on the mirror, which reads

$$\begin{aligned} V_m^{(4)}(N) =& e^{-\frac{\pi}{3}i\ Nk^3\eta^2 Q_m}\ e^{-i\frac{\zeta^{(4)}}{2}(b^{\dagger 2}+b^2)^2} \\ &\times e^{i\pi k^4\eta^2\ N\left[\frac{124\eta-5}{20}(b^2+b^{\dagger 2})+\frac{575+634\eta}{90}b^\dagger b\right]}\ , \end{aligned} \tag{4.31}$$

with $\zeta^{(4)} = (\pi k^2\eta)^2 N\cot(\pi/N)$.

In order to quantitatively evaluate the accuracy of the perturbative approach, we construct $V_m^{(3)}(N)$ and $V_m^{(4)}(N)$ numerically in a truncated Hilbert space including up to $80\times10^3$ excitations. As a prototype also for other future discussions, we choose the specific experimental parameters values $\eta = 20$ and $k = 1/60$, consistently with the perturbative expansion. We will consider the states $|\psi_3(N)\rangle = V_m^{(3)}(N)\,|0\rangle$ and $|\psi_4(N)\rangle = V_m^{(4)}(N)\,|0\rangle$ obtained after $N$ periods of driving with the mirror initially in its ground state.

For a thorough discussion, it proves very useful, here and in the following, to recall an important figure of merit, *i.e.* the state fidelity between two quantum states, which is defined from their density operators $\varrho_A$ and $\varrho_B$ as

$$\mathcal{F}_{A,B} = \left(\mathrm{Tr}\sqrt{\varrho_A^{1/2}\varrho_B\varrho_A^{1/2}}\right)^2 . \tag{4.32}$$

This quantity can be adopted to provide an estimate of the accuracy of the third order Magnus preparation of the mirror by comparing its reduced density matrix $\varrho_3 = |\psi_3(N)\rangle\langle\psi_3(N)|$ with its fourth order correspondent $\varrho_4 = |\psi_4(N)\rangle\langle\psi_4(N)|$, obtained numerically propagating Eq.(4.31). Fig. 4.3 depicts $\mathcal{F}_{3,4}$ as function of the integration time. We infer that the deviations between $\varrho_3$ and $\varrho_4$ are in the permille regime for the first 10 driving periods, and even at $N = 20$, the third order approximation is accurate within $\simeq 1\%$. We deem an error of 1% below the accuracy of what could be achieved experimentally within the next years, and thus feel that the perturbative treatment is highly adequate for the present purpose.

It is also worth remarking that the accuracy of the third order approximation in Magnus should not be considered a limiting factor, as long as one can prove the achievement of a maximally non-classical state (which we will address shortly). In

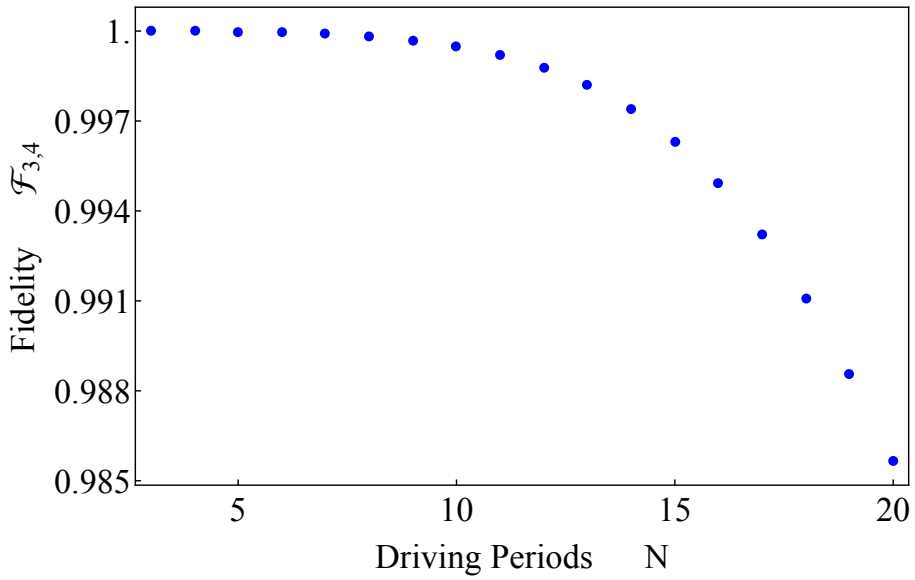


Figure 4.3: Fidelity between the state of the mirror computed via a third and a fourth order Magnus expansion as a function of the integration time, expressed in terms of mechanical driving periods. The experimental parameters are set as $\eta = 20$, $k = 1/60$. The graph indicates that high fidelity is obtained up to $N = 20$ driving periods: $\mathcal{F}_{3,4} \gtrsim 0.985$.

other words, we expect that at higher orders in Magnus similar techniques apply to those we have adopted so far to obtain a separable state for the cavity and the mirror at the end of the interaction. Since non-classicality is induced by non-linear operators, it is reasonable to conjecture that those higher-than-cubic terms arising at the subsequent orders in Magnus would give rise to interesting quantum states of the mirror, and actually also potentially enlarge the experimental domain to larger coupling and/or longer interaction times.

### 4.3.4 Readout

The final readout of the mechanical motion is a matter that has been widely analysed theoretically [11, 16] and implemented experimentally [100, 110] with high precision. We presented in Sec.1.3 (and applied throughout the manuscript) the interference measurement schemes based on homodyne and heterodyne detection to reconstruct the field wavefunction. However, in our specific situation, we end up with a separable state of the system, the cavity being empty at the end of the

interaction. In order to perform quantum state reconstruction we thus need first to induce an exchange of excitations from the mirror to the cavity and then perform a measurement of the field. In this direction, the most promising technique is called *back-action-evading* interaction and is based on state transfer. When bichromatic driving is turned off, the mirror is in the state of interest and the cavity is empty, a red detuned laser with frequency $\omega_d = \omega_c - \omega$ induces a swap between the two subsystems. Hence, tomography of the prepared mechanical state of the mirror can be deterministically carried out through homodyne measurement of the light leaking out of the cavity [17, 18].

A clue to understand how the exchange process works comes from the first order Magnus expansion of the related interaction Hamiltonian: $\mathcal{M}_m^{(1)}(t) = \frac{\mathcal{E}' g t}{\omega}[\frac{\mathcal{E}'}{\omega}(b^\dagger + b) + i(a^\dagger b - a b^\dagger)]$, with $\mathcal{E}'$ the driving amplitude adopted for the measurement. The corresponding propagator induces a quantum state transfer of the mechanical excitations onto the cavity field as the two states interchange themselves at a rate $2k\mathcal{E}'$ [10]. The relation between the expectation values of the operators of the field and the mirror after the measurement time $t_m = (2k\mathcal{E}')^{-1}$ can be derived easily

$$\begin{aligned}
\langle a(a^\dagger)(t_m)\rangle &= \sin(\Theta)\, {}_m\langle\psi(t')|b(b^\dagger)\,|\psi(t')\rangle_m \ , \\
\langle a^\dagger a(t_m)\rangle &= \frac{1-\cos(2\Theta)}{2}\, {}_m\langle\psi(t')|b^\dagger b\,|\psi(t')\rangle_m \ , \\
\langle a^2(a^{\dagger 2})(t_m)\rangle &= \frac{1-\cos(2\Theta)}{2}\, {}_m\langle\psi(t')|b^2(b^{\dagger 2})\,|\psi(t')\rangle_m \ ,
\end{aligned} \tag{4.33}$$

where $\Theta = k\mathcal{E}'T$ and $t' = NT$. As a matter of fact, it is worth mentioning that this measuring scheme is interesting *per se*, having a variety of applications in literature. On the one hand, it was shown in [113] that when a red detuned laser enters the cavity, photons are more likely to increase their frequency to $\omega_c$ because the photon density of states is maximal around resonance. This requires one phonon of energy from the mechanical motion, thus inducing the so-called *sideband cooling* of the mirror [114, 115].

On the other hand, a novel approach to light storage was suggested in Ref.[116], where the authors studied the coupling of an optical waveguide to an optomechanical crystal array. Light in the waveguide is dynamically and coherently transferred

into long-lived mechanical vibrations of the array, which would be theoretically capable of achieving large bandwidths and storage/delay times, paving the way to the implementation of a continuous variable quantum memory.

## 4.4 State Analysis

In contrast to the well characterised squeezed states discussed in Sec. 4.3.1, it is not clearly established what type of states are obtained with the cubic generator

$$V_m^{(3)}(N) = \exp(-\pi/3i\ Nk^3\eta^2\ Q_m) \tag{4.34}$$

at the third order in the coupling (see Eq. (4.25)). We will devote this section to the analysis of such mechanical states via a numerical computation of $V_m^{(3)}$.
For this purpose, it is advantageous to represent the quantum state of the mirror $\rho$ in terms of its Wigner function

$$W(q,p) = \frac{1}{\pi}\int_{-\infty}^{\infty} \langle q+y|\rho|q-y\rangle e^{-2ipy} dy\ , \tag{4.35}$$

which is a quasi-probability distribution in phase space spanned by momentum and displacement variables $p$ and $q$. Fig. 4.4a) depicts the Wigner function for the state

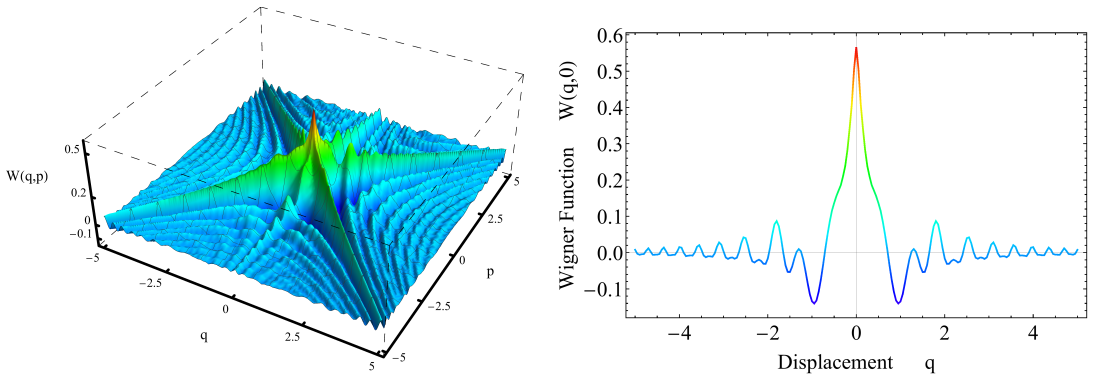


(a) (b)

Figure 4.4: a) 3D Wigner function of the mirror after 20 driving periods and b) its profile when it is cut by the plane $p = 0$. The experimental parameters are set as $\eta = 20$, $k = 1/60$ and the resulting average population is $\langle b^\dagger b\rangle \simeq 20$.

$\rho = |\psi_3(20)\rangle \langle\psi_3(20)|$. The non-classical nature of a given state is well reflected by oscillations of $W(q,p)$ including negative values. The amplitude of these oscillations is linked to the degree of coherence, while their wave-length is inversely related to the macroscopicity of the state. As one can see, the Wigner function of $|\psi_3(20)\rangle$ features short wavelength oscillations with large amplitudes. This is visible on a more quantitative level also in Fig. 4.4b) which shows the cut $W(q,0)$ through the Wigner function.

For a quantitative assessment of the *quantumness* of the state, we resort to the *measure of non-classicality* proposed in Ref.[117]

$$\mathcal{I} = -\frac{\pi}{2} \int dp\ dq\ W(q,p) \left( \frac{\partial^2}{\partial q^2} + \frac{\partial^2}{\partial p^2} + 1 \right) W(q,p)\ . \tag{4.36}$$

While there is no fundamental reason to choose this specific functional among others that have been proposed in literature, this quantity has a convenient feature. Indeed, it lies in the interval $\mathcal{I} \in [0, \langle n \rangle]$, where $\langle n \rangle$ is the average number of excitations in the system. The minimal value $\mathcal{I}_{min} = 0$ is obtained for classical states like Gaussian or thermal states, while purely quantum states, such as for example Fock and cat

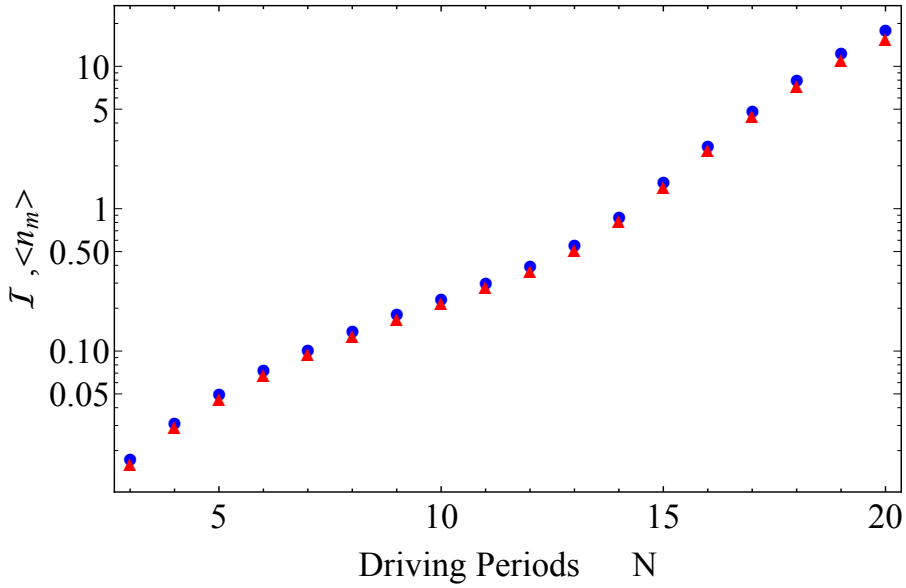


Figure 4.5: Comparative plot of the quantum estimator $\mathcal{I}$ (red triangles) and the average number of mechanical excitations $\langle n_m \rangle$ (blue dots) as functions of the number of driving periods. The experimental parameters are set as $\eta = 20$, $k = 1/60$.

states, yield the maximum value of $\mathcal{I}_{max} = \langle n \rangle$. Fig.4.5 depicts $\mathcal{I}$ (red triangles) and $\mathcal{I}_{max} = \langle n \rangle$ (blue dots) as functions of the total driving time expressed in terms of mechanical periods. As one can see, quantumness and population both increase approximately exponentially in time and the former nearly saturates the bound $\mathcal{I}_{max}$ imposed by the latter. This witnesses the rapid evolution towards states of macroscopic character as well as their close-to-maximal non-classicality.

## 4.5 Experimental imperfections

So far, we have addressed the theoretical principles that allow deterministic state preparation and proposed the adoption of different, easy-to-perform, driving profiles to prepare a set of macroscopic superposition states of the mirror. We would now like to discuss how several possible sources of experimental imperfections could affect the desired process. Going beyond the ideal case of unitary evolution, we will also estimate the effect of noise and dissipation induced by the environment. More specifically, we will look at the impact of optical and mechanical decoherence, initial thermal excitations in the mirror and imperfect phase shifts of the driving fields.

### 4.5.1 Optical decoherence

From an experimental perspective, the most delicate aspect affecting the unitarity of the evolution, and consequently the preparation of the desired mechanical state, is attributable to optical losses. Instead, since it can be safely assumed to arrange a cavity with zero initial thermal population, *i.e.* $\langle n_c^{th} \rangle = 0$, we will henceforth neglect the effect of decoherence arising from a nonzero optical thermal distribution.
A common approach to include the leakage of photons from the cavity in the dynamics is to express the evolution in terms of the Master equation $\dot{\rho} = -i\,[H, \rho] + \kappa \mathcal{L}[\rho]$, where $H$ is the system Hamiltonian, $\rho$ the density matrix, $\mathcal{L}[\rho]$ the Lindblad operator $\mathcal{L}[\rho] = (a\rho a^\dagger - \{a^\dagger a, \rho\}/2)$ and $\kappa$ the cavity decay rate. Moreover, we should consider that many experimental groups have already managed to access the *resolved sideband* regime with $\kappa \ll \omega$ [118, 113, 1, 98]. This allows us to gauge the impact of photon loss in terms of a perturbative solution of the Master equation. For this purpose, it is

convenient to consider the Master equation for $\tilde{\rho} = V(t)\rho V^\dagger(t)$, where $V(t)$ satisfies $i\dot{V} = H_I V$, as detailed in Secs. 4.2.1 - 4.3.

Solving this perturbatively, yields the contribution of photon loss to the dynamics in terms of powers of $\kappa/\omega$. The integration for a generic time $t$ assumes a rather complex form and extra correlations between field and mirror are created because of dissipation. However, thanks to the very specific bi-chromatic driving pattern many terms cancel out at the end of the evolution. Actually, our proposed set of constant phase shifts $\{\varphi_s\}$ is crucial to suppress the majority of these unwanted non-unitary and de-coherent contributions, including all correlation terms proportional to the driving amplitude $\eta$.

More specifically, at leading order in $k$ and $\kappa$, we obtain

$$\begin{aligned} \tilde{\rho}(t) &= \tilde{\rho}(0) + \kappa \int_0^t \left( a(\tau)\tilde{\rho}a^\dagger(\tau) - \{a^\dagger a(\tau), \tilde{\rho}\}/2 \right) d\tau \ , \text{ with} \\ a(\tau) &= e^{-i\int_0^\tau H_I(\tau')d\tau'} a e^{i\int_0^\tau H_I(\tau')d\tau'} \ , \end{aligned} \tag{4.37}$$

which at the end of the preparation time, when $t = \mathrm{NT}$, reduces to an expression that is completely independent of $\eta$ and is thus well suited to describe the strong

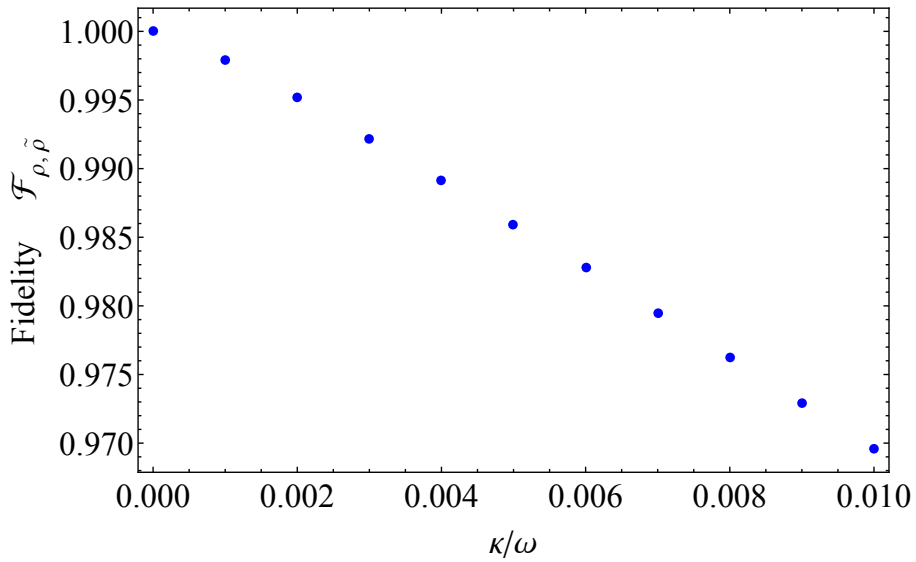


Figure 4.6: Fidelity between the final state of the system (cavity plus mirror) in case of photon losses and the ideal scenario as a function of the cavity decay rate $\kappa$ for an evolution lasting $N = 20$ mechanical periods.

driving regime

$$\begin{aligned}\tilde{\rho}(NT) &= \tilde{\rho}(0) + \kappa NT\left(\tilde{a}\tilde{\rho}\tilde{a}^{\dagger} - \{\tilde{a}^{\dagger}\tilde{a}, \tilde{\rho}\}/2\right) \ , \text{ with} \\ \tilde{a} &= a e^{\frac{g_0}{\omega}(b^{\dagger}-b)} \ .\end{aligned} \tag{4.38}$$

This is a convincing result, as it has a clear physical interpretation. In fact, we know that the light-matter interaction conditionally displaces the mirror by an amount proportional to the number of photons in the cavity times $k = g_0/\omega$. We thus expect each photon that has leaked out of the resonator to induce a *missing* displacement $e^{g_0(b^{\dagger}-b)/\omega}$ of the mirror.

We depict in Fig.4.6 the state fidelity (as it was defined in Eq.(4.32)) as a function of the ratio $\kappa/\omega$ between the full state of the system (cavity plus mirror) obtained in the leaking scenario in Eq.(4.37) and the ideal one predicted by Eq.(4.25). We extrapolate from the plot that a loss rate satisfying $\kappa/\omega < 10^{-2}$ results in a reduction of the fidelity by $\lesssim 3\%$. This condition, together with the adoption of a strong driving regime, is in accordance with Ref.[12], where the resolved sideband regime and the condition $g_0/\kappa > 1$ were theoretically derived as requirements to resolve the *granularity* of the photon stream and fully exploit the non-linearity of the system to observe purely quantum features.

### 4.5.2 Thermal initial state of the mirror

As we have already widely discussed, the evolution operator in Eq.(4.25) factorises into a propagator for the mirror and a propagator for the cavity, so that no light-matter correlations are created at the end of the driving time. This means that there is no fundamental need to require mirror and cavity to be initially cooled exactly to the ground state (as we assumed for ease of calculations in Sec.4.4), and we are in principle allowed to consider a wider range of possible initial conditions, among which the very common case of a Gibbs thermal state. However, as we remarked when we arranged the driving detunings so that to cancel out the second order Gaussian contributions (see Sec.4.3.2), such classical thermal fluctuations could potentially outshine the *quantumness* of the achieved mechanical state. An accurate analysis of

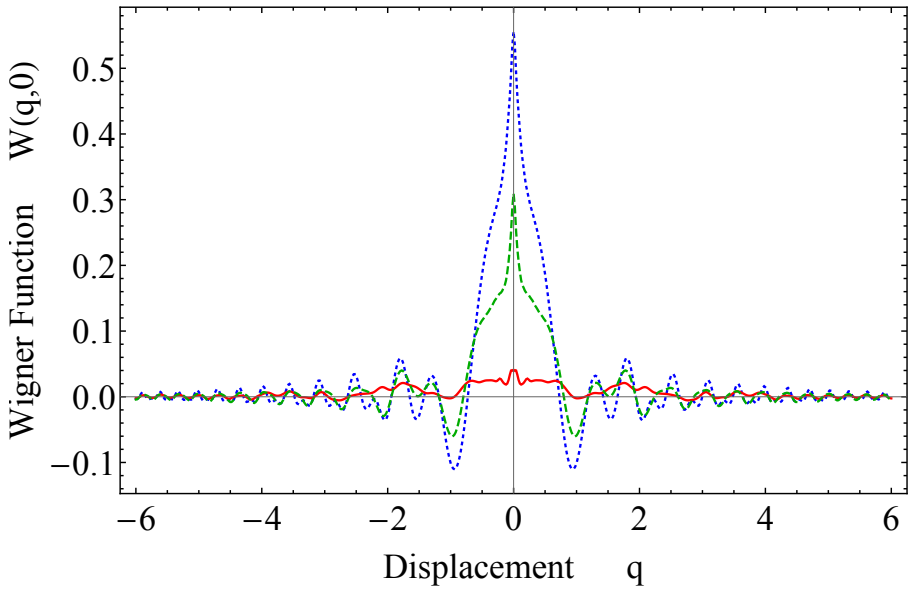


Figure 4.7: Comparison of the cut profiles $p = 0$ of the Wigner function of the state of the mirror after an evolution lasting 20 mechanical periods with the mirror initially in its ground state (blue dotted line) and two thermal states with respectively $\langle n_m^{th} \rangle \sim 1$ (green dashed line) and $\langle n_m^{th} \rangle \sim 10$ (red line). The experimental parameters are set as $\eta = 20$, $k = 1/60$ and $\omega = 2\pi \times 10^7$Hz.

the impact that an initial thermal occupation of the mirror has on the dynamics is thus in order.[1]

In this perspective, we depict in Fig.4.7 cuts through the Wigner function of the mirror at $p = 0$ for different initial thermal populations with $\langle n_m^{th} \rangle = 1$ and $\langle n_m^{th} \rangle = 10$ (the latter can be reached by only using dilution refrigeration techniques). Nevertheless, such states are both above the experimental threshold of $\langle n_m^{th} \rangle \sim 0.2$ achievable with sideband cooling (at a mechanical frequency $\omega = 2\pi \times 10^7$Hz) [113, 110]. The strong oscillatory behaviour with negative values of $W$ is clearly still displayed for an initial state with $\langle n_m^{th} \rangle = 1$. Only for $\langle n_m^{th} \rangle = 10$, which could be considered substantially above what is obtained with sideband cooling, the quantum mechanical features are mostly washed out by the thermal contributions.

Even though the preparation of a non-classical state seems to be undermined at large temperatures, we should consider, as we discussed in Sec.4.3.3, that the

[1]We remark that while it is feasible to assume a cavity with fixed boundaries to be empty when no driving is applied, i.e. $\langle a^\dagger a(0) \rangle = 0$ (as we have already done in the manuscript), cooling a movable mirror close to its ground state is experimentally more challenging.

technique to find optimal driving patterns can be easily extended to higher orders in the Magnus expansion and correspondingly longer propagation times and/or larger coupling $k$. We expect that these conditions would give rise to more highly excited states and hence to measurable quantum effects also in case of higher initial thermal noise. Unfortunately, the simulation of such a regime with higher temperatures and larger populated states is restricted by the limited computational resources on a personal computer.

### 4.5.3 Mechanical decoherence

As every quantum system does, macroscopic states particularly suffer from the effect of decoherence. This is because the larger an object is, the more interactions it establishes with its surrounding environment, and undesired correlations that are at the basis of the decoherence process spontaneously arise [119]. One therefore needs to ensure that noise originated from the environment on the motional state of the mirror remains negligible for the entire duration of the experiment so that to preserve mechanical non-classicality.

Given the damping rate $\gamma_m$, which is defined through Eq.(1.5) as the analogous of field decay rate $\kappa$ for the mirror, Refs.[4, 5] provide an estimate for the mechanical decoherence rate $\Gamma_m$ as $\Gamma_m = \gamma_m k_B T_E \langle n_m \rangle / (\hbar\omega)$, where $k_B$ is the Boltzmann constant, $T_E$ the temperature of the environment and $\langle n_m \rangle$ the average number of phonons. This quantity corresponds to the rate at which the non-diagonal elements of the density matrix that describes the mirror exponentially decay with time, inducing decoherence towards a classical mixed state. The condition $\Gamma_m NT \ll 1$ gives a rough bound on the number of driving periods that can be safely performed $N \ll \hbar\omega Q \langle n_m \rangle / (k_B T_E)$, with $Q = \omega/\gamma_m$ the quality factor of the mechanical oscillator. Assuming a state-of-the-art quality factor $Q \sim 10^5$ [120, 1] and initial mechanical sideband cooling, we obtain $N \gtrsim 10^2$.

From this coarse analysis we infer that with present technology thermal induced mechanical decoherence has a far less detrimental impact than photon leakage from the cavity, which is actually a direct consequence of the experimental relation that is satisfied by most of todays physical implementations $\gamma_m \ll \kappa$.

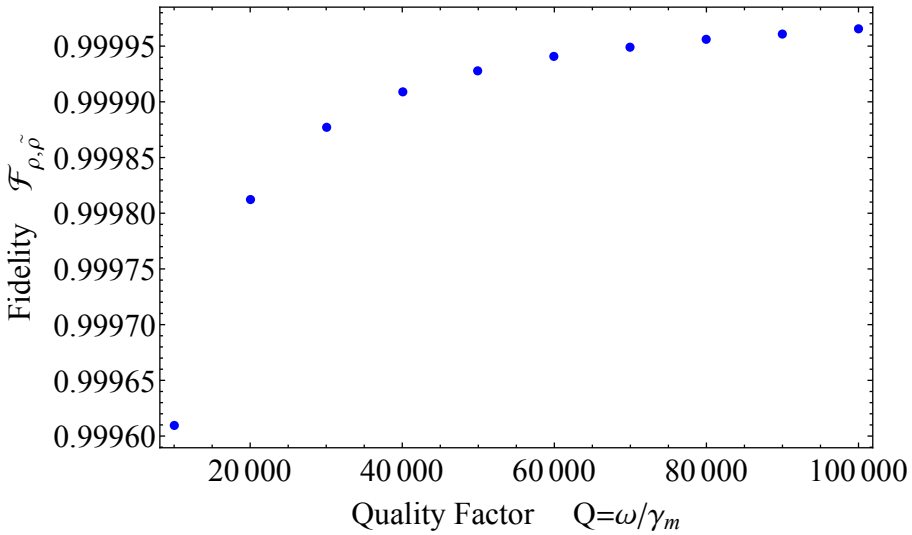


Figure 4.8: Fidelity between the final state of the system (cavity plus mirror) in case of a mechanical damped evolution and the ideal scenario as a function of the mechanical quality factor $Q = \omega/\gamma_m$. The total evolution is supposed to last 20 mechanical periods with the mirror initially in its ground state and the dimensionless driving and coupling respectively set as $\eta = 20$ and $k = 1/60$.

Even though we have just shown that optomechanical resonators provide a framework particularly resilient to mechanical decoherence, since highly non-classical coherent superpositions of macroscopical states are *per se* extremely sensitive to decoherence, a critical assessment of motional decoherence is still in order. To this end, we use a stochastic perturbative model of mechanical damping. We assume coherent dynamics during each period $T$, after which the state vector suffers a phonon loss described by the jump operator $(\mathbb{1} \otimes b_m)\,|\Psi\rangle$ with probability $p = \gamma_m T$. A mixed state of the mirror is obtained by averaging over such processes, and since $p$ is sufficiently small, one can safely restrict the average to processes including at most two phonon losses.

Fig.4.8 depicts the state fidelity after $N = 20$ periods of driving as a function of $Q$. Despite the general sensitivity of non-classical states to decoherence, the impact of mechanical damping on the state fidelity is of the order $O(10^{-4})$, and thus negligible as compared to the other imperfections discussed above.

This high degree of robustness against mechanical damping, which is intrinsic to the optomechanical platform, is a promising feature that appears to be essential

to perform sensitive measurements of other more exotic sources of mechanical decoherence (also through estimators such as the one we proposed in Sec.4.4), *e.g.* from gravitational effects to collapse models.

### 4.5.4 Laser driving

The exchange of excitations from the cavity to the mirror is achieved through the employment of a pair of oppositely detuned lasers with respect to the cavity resonance frequency. In particular, the application of appropriate phase shifts after each period of driving is key for the deterministic state preparation. We trust the experimental implementation of such phase shifts to be feasible, as they are required to operate at the mechanical rate $\omega \sim 10^6 s^{-1}$, which is orders of magnitude smaller than the optical characteristic frequency. Still, we deem it useful to assess the resilience of our proposal to imperfections in the driving profiles by considering the impact of deviations from the ideal control scheme with the step-like phase shifts $\varphi_s$ described in Sec.4.3.

To this end, let us replace the discontinuously evolving phase $\varphi(t) = \frac{2\pi}{N}\sum_s \Theta(t-sT)$[2] with the continuous function

$$\varphi_c^{(d)}(t) = \frac{2\pi}{N}\frac{t}{T} + \sum_{l=1}^{d} \varphi_l(t) \ ,$$

where $\frac{2\pi}{N}\frac{t}{T}$ is a linearly increasing phase factor and each term $\varphi_l(t) = A_l \sin(l\omega t)$ oscillates with frequency $l\omega$ and amplitude $A_l$. The set of amplitudes is chosen such that at any order $d$, $\varphi_c^{(d)}(t)$ is tangent to the step function in the centre of the step, *i.e.* for $t = (2j\pi+1)/\omega$ with $j \in [0, N-1]$ (see Fig.4.9 for a graphical representation). It is possible to verify that $\lim_{d\to\infty} \varphi_c^{(d)}(t) = \varphi(t) = \frac{2\pi}{N}\sum_s \Theta(t-sT)$.

Since $\varphi_c^{(d)}(t)$ is a continuous function of time for every $d$, we can analytically compute the generator $V(t,0)$ with a Magnus expansion for a generic time $t$ (as discussed in Sec.4.2.1), and subsequently numerically integrate the dynamics directly over $N$ mechanical periods (without having to consider the contribution of each single period separately). Interestingly, one obtains a separable propagator for the

[2]The $\Theta$ (theta) function is defined as $\Theta(x<0) = 0$ and $\Theta(x \geq 0) = 1$.

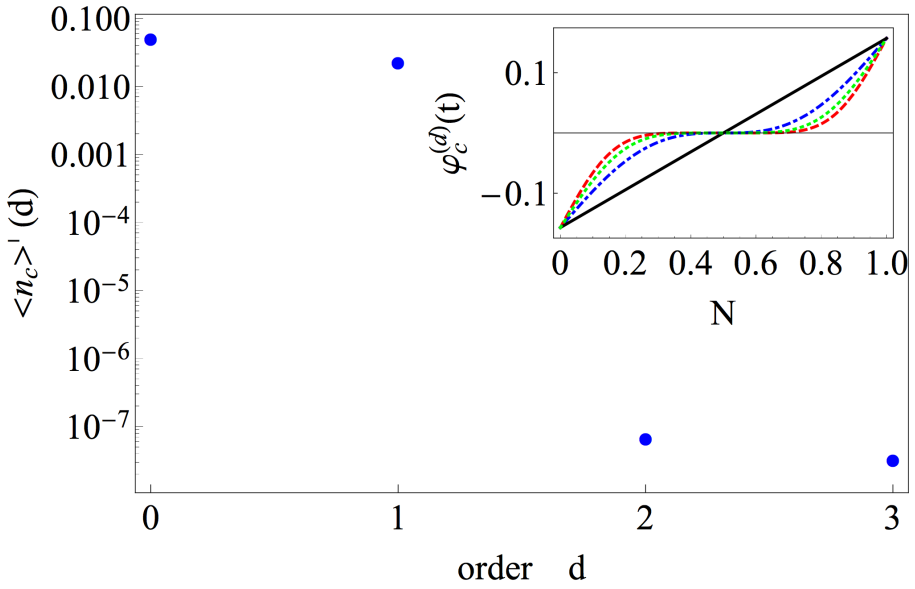


Figure 4.9: Cavity occupation renormalized with respect to the population of the mirror $\langle n_c\rangle' = \langle n_c\rangle/\langle n_m\rangle$ as a function of the order of the decomposition of the step function $d$. In the top-right corner we plot an enlargement of the driving profiles defined by $\varphi_c^{(d)}(t)$ over the first mechanical period: linear approximation with $d = 0$ (black line), $d = 1$ (blue dashed-dotted), $d = 2$ (green dotted) and $d = 3$ (red dashed). The experimental parameters are set as $\eta = 20$, $k = 1/60$, $N = 20$.

cavity and for the mirror at every order $d$, thus naturally resulting in the desired deterministic state preparation.

However, looking closer at the dynamics, we observe that single-particle terms of the cavity do not completely cancel out if we resort to the sole linear function $\frac{2\pi}{N}\frac{t}{T}$, inducing a non-negligible final average population $\langle n_c\rangle \sim 0.2\langle n_m\rangle$. As we show in Fig.4.9, these contributions are efficiently suppressed already at the second order $d = 2$, when $\langle n_c\rangle \sim O(10^{-7})\langle n_m\rangle$, which is an essential requirement to prevent cavity excitations from affecting the final readout through *back-action-evading* interaction.[3] Besides, we also numerically observe that the final non-classical mechanical state of the mirror obtained with these imperfect driving patterns presents high fidelity

[3]It is unclear, at least to the extent of the author, how to justify the significant improvement of several orders of magnitude that takes place from $d = 1$ to $d = 2$, though this has been confirmed by the numerical simulation. Still, we notice that at the first order there is an important improvement of the overall fidelity thanks to cancellation of an unwanted displacement of the mirror that is introduced with the linearly increasing phase shift at the zeroth order. Hence, when considering the whole system, both the first two orders in the expansion contribute significantly to improve the state fidelity (the first having a larger impact on the mirror, the second on the light).

$\mathcal{F} \simeq 0.98$ with the ideal step-like case.

## 4.6 Conclusions

This chapter has addressed the instance of deterministically creating macroscopic massive quantum states. Exploiting the Magnus expansion formalism to deal with the cubic equations of motion induced by the non-linear optomechanical interaction, we were able to perturbatively solve the dynamics without recurring to any linearisation. We have thus derived a control protocol to prepare a range of interesting quantum states of the mirror, obtaining strong squeezing of the mechanical quadrature as well as maximally non-classical quantum superposition states. We have also provided evidence of the resilience of the scheme to various potential sources of experimental imperfections, from mechanical thermal noise to non-optimal implementation of the driving pattern. From an open quantum systems perspective, our proposal has responded positively to optical decoherence, as well as, thanks to the high degree of insulation of optomechanical resonators, it has proved to be robust against mechanical damping.
This last property will turn out to be essential for many future theoretical and practical applications, such as the use of the mirror as a continuous variable quantum memory, which has already been proposed in Ref.[115], or as probe for decoherence. To this end, the measure of non-classicality $\mathcal{I}$ of the mirror is an ideally suited quantitative indicator in the light of the very sensitive measurements of decoherence which are required to probe fundamental physics, such as gravitationally induced effects on the mechanical motion.

As a general comment, we should point out that the approach to find optimal driving patterns can be easily extended to higher orders in the Magnus expansion, allowing longer propagation times and/or larger coupling $k$ to be considered. These would give rise to more highly excited states and hence to measurable quantum effects also in presence of relatively small classical contributions that would otherwise outshine the non-classicality of the state, *e.g.* higher initial thermal noise.

Remarkably, we should eventually stress that the proposed control scheme is not

necessarily restricted to the mirror-cavity setup discussed here, but similar driving patterns can also be applied to a variety of systems that share similar non-linear Hamiltonians such as atomic spin ensembles, trapped atoms or levitated nanoparticles [121, 122, 33, 123].

# Chapter 5

# Conclusions and outlook

In this thesis we have investigated the non-classical features arising within a widely employed optomechanical setup, consisting of a Fabrit-Pérot cavity with a movable boundary. The main results of the present work have been (i) the exploration of the quantum-classical correspondence, (ii) the characterisation of mechanical anharmonicities and (iii) the theoretical proposal to prepare highly non-classical superpositions states of the mirror. Our methods have proved themselves promising to exploit optomechanical resonators for a range of theoretical and practical applications, from the foundations of quantum mechanics and the test of some of the latest studies on decoherence models and quantum gravity, to force sensing and the potential engineering of future quantum technologies. The suggested set of experimental parameters is within reach with up-to-date technologies.

First of all, the identification of classical and quantum features in the dynamics has challenged some of the intakes from past literature, such as adopting the visibility pattern as a signature of the creation of a quantum superposition state. Most importantly, we have shed new light on the topic showing that light-matter correlations can be largely explained by considering the (classical) statistical uncertainty on the initial state of the system. As far as cavity and mirror are defined by a probability distribution exhibiting classical features, it is not trivial to attribute any non-classical behaviour to the dynamics. Many properties of the observables in a classical experiment, instead, are qualitatively very similar, for example, to those that

were theoretically predicted to be observed in experiments relying on single-photon sources. Still, we have been able to isolate genuine quantum peculiarities of the interaction that appear on the optical phase shift and on the visibility pattern, which might be probed in future optomechanical experiments, even in the weak coupling limit. For a deeper understanding of the quantum-classical correspondence, as well as to contextualise our discussion in the more general framework of non-abelian transformations in phase space, we also provided a topological interpretation of the problem. Resorting to the formalism of the geometric phase introduced by Michael Berry and John Hannay we verified that the quantal geometric (Berry) phase causes the state of the system to be displaced along the classical trajectory by an amount equal to the classical geometric phase (Hannay angle).

Secondly, we presented a protocol to estimate the anharmonicity of a macroscopic oscillator up to very small values. Relying on the *so called* bad cavity regime, we adopted a four-pulse interaction with a coherent optical field in input, which, under reasonable initial cooling of the mirror, leaves the system in a product state of the light and the mechanics. Specifically, after the fourth interaction, when the mirror returns back to its original position, the optical field escapes the cavity and retains important information on mechanical anharmonicity, which can thus be optimally estimated via homodyne detection. We have shown how state-of-the-art values of optomechanical parameters are already sufficient to saturate the ultimate bound on the measurable precision given by quantum estimation theory. A parallel analysis has been conducted in a fully classical picture to identify, also in this case, reliable quantum signatures of the dynamics. Always in light of providing a more general interpretation of our results, we have also illustrated the close relationship that mechanical non-linearities share with more fundamental modifications of the Hilbert space topology, *e.g.* the supposed deformation of commutation relations predicted by quantum gravity.

Third, having acquired the tools for assessing non-classical features in optomechanics, we proposed a scheme to deterministically create a range of quantum superposition states of the mirror. Without resorting to any linearisation of the Hamiltonian, we capitalised on the cubic optomechanical interaction and resorted to

the Magnus expansion formalism to perturbatively solve the dynamics. Our control protocol has proved that strong squeezing of the mechanical quadrature as well as maximally non-classical quantum superposition states can be achieved.
We discussed how the robustness of optomechanical resonators against mechanical damping makes them an ideal platform for many future theoretical and practical applications, such as the use of the mirror as a continuous variable quantum memory or as probe for decoherence. In the same direction, the quantitative measure of non-classicality ($\mathcal{I}$) for the mirror that we adopted is a well suited estimator that could be used for very sensitive measurements of decoherence to probe fundamental physics, including gravitationally induced effects on the mechanical motion.

Overall, we hope the results presented in this thesis will be of some inspiration for future works. More specifically we could identify a set of possible upcoming related lines of research:

- The relationship between an initial classical statistical distribution of the system, which we could naively conceive as a "*lack of knowledge*" on the exact initial state, and the correlated state that arises during the evolution could be investigated in more general terms. In particular it would be interesting to understand which non-classical features an initial state should have to give rise to genuinely quantum correlations.

- The pulsed scheme has been shown to be a promising platform to perform very precise measurements. This advantage could be exploited to build compact force sensors, as well as gravimeters and accelerometers, which would find practical application in a series of technological devices.

- The ability to perform holonomic operations on a massive mirror and to subsequently deterministically read out the dynamics could pave the way to design contextuality inequalities with continuous variables to be violated by massive objects. In this direction, it has already been shown that the algebra of displacements in phase space can be adapted to the one obeyed by Pauli operators to construct a Peres-Mermin like inequality in phase space [124].

- The deterministic creation of interesting massive mechanical non-classical states via easy-to-perform control schemes is a breakthrough in terms of quantum state preparation techniques. We expect future works to investigate the range of states that can be achieved, also broadening the attention to a variety of setups that share similar non-linear Hamiltonians with the optomechanical case. Such investigations would trigger novel studies on foundations of quantum mechanics, as well as unprecedented applications to build new enhanced quantum technologies.

# Appendix A

# Semiclassical approach

After having discussed the fully quantum and classical descriptions of the system, it is interesting to see which are the predictions of a semiclassical approach, i.e. when one of either the optical field or the mirror is described classically.
Let us first consider a quantum field and a classical oscillator. The field Hamiltonian in a frame rotating at frequency $\omega_f$ can be written as $\hat{H}_f = \epsilon \hat{a}^\dagger \hat{a} x(t)$ where $x(t)$ is the classical equation of motion of the oscillator and $\epsilon = \hbar\omega_f/L$ is the resulting coupling constant. If the field is initially in the coherent state $|\alpha\rangle_f$ and a continuous interaction with the mirror takes place, the field density matrix will read

$$\hat{\rho}_f(t) = e^{-|\alpha|^2} \sum_{n,m} \frac{\alpha^n \alpha^{*m}}{\sqrt{n!m!}} e^{-\frac{i}{\hbar}\epsilon(n-m)\int_0^t x(\tau)d\tau} |n\rangle_f \langle m| \tag{A.1}$$

and the mean value of the optical field which gives us the acquired optical phase is

$$\langle \hat{a} \rangle = \alpha e^{-\frac{i}{\hbar}\epsilon \int_0^t x(\tau)d\tau}. \tag{A.2}$$

If we model the classical mirror as a harmonic oscillator driven by a constant force $E_0/L$ as in Eq.(2.16) where here $E_0$ is the mean value of the field energy distribution, we can safely substitute the dynamics in Eq.(2.17) into Eq. (A.2) obtaining

$$\langle \hat{a} \rangle = \alpha e^{-i\varphi(t)} \tag{A.3}$$

where the phase $\varphi(t)$ coincides with the classical phase showed in Eq. (2.18). We deduce from Eq.(A.3) that when the field is quantized and the oscillator is classical we regain exactly the classical result for the phase.
We are now going to show that the same happens for the inverse situation, when the field is described classically and the mirror quantum-mechanically. In this case, the phase acquired by the optical field will be given by

$$\varphi(t) = 2\frac{\mathrm{k}_f}{d\tilde{\tau}} \int_0^t \langle \hat{x}(\tau) \rangle d\tau \tag{A.4}$$

i.e. the integral over the interaction time of the mean value of the oscillator position. If we assume the mirror initially in a coherent state $|\tilde{\Psi}(0)\rangle = |\gamma_R + i\gamma_I\rangle$, its evolution under the quantum Hamiltonian $\hat{H}_m = \hbar\omega\hat{b}^\dagger\hat{b} - \frac{E_0}{L}\sqrt{\frac{\hbar}{2m\omega}}(\hat{b}^\dagger + \hat{b})$ reads

$$\begin{aligned} |\tilde{\Psi}(t)\rangle &= e^{ik^2N_p^2(\omega t - \sin\omega t)} \\ &\times e^{i2kN_p[\gamma_I(1-\cos\omega t)+\gamma_R\sin\omega t]}|\gamma e^{-i\omega t} + kN_p(1-e^{-i\omega t})\rangle, \end{aligned} \tag{A.5}$$

where we have used $kN_p = E_0/(L\omega\sqrt{2\hbar m\omega})$ to express the result in terms of the characteristic optomechanical parameters. It can be easily verified that the mean value of the position operator given by Eq.(A.5) coincides with the results found in Eqs.(1.23) and (2.17) within a fully quantum and/or classical description of the interaction. Hence, the phase acquired by the optical field in Eq. (A.4) coincides with the classical result reported in Eq. (2.18). Again, in terms of optical phase shift a semiclassical description provides the same result of the fully classical one. We can then infer, as already highlighted in the main manuscript, that such a semi-classical description is insufficient to describe all features of the full interaction. Similar considerations can be extended to the visibility.

# Appendix B

# Cubic Anharmonicity

In the case of a cubic anharmonicity the correction to the free Hamiltonian reads

$$\mathcal{H}_{an} = \frac{\delta}{3}\hbar\omega_m X_m^3 \,, \tag{B.1}$$

where the parameter $\delta$ quantifies the anharmonicity. Following [79] we get the evolution for annihilation (creation) operator at the first order in $\delta$ and for initial displacements that satisfy $\delta\lambda N_p \ll 1$

$$b(t) \simeq \; e^{-i\omega t}\left\{ b_0 + \frac{\delta}{2^{3/2}}\left[ \left(e^{i\omega t}+1\right)\left(2b_0^\dagger b_0 + 1\right) + \left(e^{-i\omega t}-1\right) b_0^2 + (1-e^{3i\omega t})\frac{b_0^{\dagger 2}}{3}\right]\right\}, \tag{B.2}$$

where in this case $\omega = \omega_m$ since the frequency is unperturbed at the first order in $\delta$. We highlight that we might exploit this feature to distinguish the two anharmonicities by looking at the revival in the visibility interference. The overall evolution operator can thus be evaluated as in Eq.(3.2) by the anharmonic evolution of quadrature

operators, which results in

$$\begin{aligned} X_m(0) &= X_m \\ X_m\left(\frac{T}{4}\right) &\simeq P_m + \delta(\Delta + b_0^{\dagger 2}\nu + b_0^2\nu^*) \\ X_m\left(\frac{T}{2}\right) &\simeq -X_m + \delta(2\Delta + \frac{1}{3}(b_0^{\dagger 2} + b_0^2)) \\ X_m\left(\frac{3T}{4}\right) &\simeq -P_m + \delta(\Delta + b_0^{\dagger 2}\nu^* + b_0^2\nu) \end{aligned} \tag{B.3}$$

being $\Delta = -(b_0^\dagger b_0 + 1/2)$ and $\nu = -(1/6)(2i+1)$. Going through the same procedure we showed in Sec.3.2, we recover the final effective evolution operator for the cavity field only (in the limit $\lambda^2 N_p^2 \gg \bar{n}$)

$$\xi_{\mathsf{eff}} \simeq \exp\{i(\lambda^2 n_c^2 - \frac{2\delta}{9}\lambda^3 n_c^3)\}. \tag{B.4}$$

From which we deduce that the optical field experiences a Kerr nonlinearity $\propto n_c^3$ entering into the cavity. Hence, the mean value of the optical field after four pulses now results (in the limit $\delta\lambda^3 N_p^2 \ll 1$)

$$\langle a\rangle = \langle\alpha|\xi_{\mathsf{eff}}^\dagger a \xi_{\mathsf{eff}}|\alpha\rangle \simeq \alpha\langle a\rangle_0 e^{-i\frac{2}{9}\delta\lambda^3(3N_p^2+3N_p+1)}. \tag{B.5}$$

Given an initial coherent state $|\alpha\rangle$, the corresponding extractable QFI for a cubic anharmonicity $\delta$ reads

$$\begin{aligned} Q_\gamma &= 4\left(\langle\psi_\gamma'|\psi_\gamma'\rangle - |\langle\psi_\gamma'|\psi_\gamma\rangle|^2\right) \\ &\simeq \lambda^6\left(\langle\psi_\gamma|n_c^6|\psi_\gamma\rangle - \langle\psi_\gamma|n_c^3|\psi_\gamma\rangle^2\right) \\ &\simeq \frac{16}{81}\lambda^6(9N_p^5 + 54N_p^4 + 84N_p^3 + 30N_p^2 + N_p) \end{aligned} \tag{B.6}$$

which leads to the Cramér-Rao bound,

$$\mathrm{Var}(\delta) \geq \frac{1}{MQ_\gamma} \gtrsim \frac{9}{16M\lambda^6 N_p^5}\ , \tag{B.7}$$

and to the corresponding signal-to-noise ratio

$$R_\gamma^{(3)} \lesssim \frac{16}{9}\delta^2\lambda^6 N_p^5 M \ . \tag{B.8}$$

# Bibliography


[1] Aspelmeyer, M., Kippenberg, T. J. & Marquardt, F. Cavity optomechanics. *Rev. Mod. Phys.* **86**, 1391 (2014).

[2] Bose, S., Jacobs, K. & Knight, P. L. Preparation of nonclassical states in cavities with a moving mirror. *Phys. Rev. A* **56**, 4175 (1997).

[3] Pikovski, I., Vanner, M. R., Aspelmeyer, M., Kim, M. S. & Brukner, Č. Probing planck-scale physics with quantum optics. *Nature Physics* **8**, 393–397 (2012).

[4] Bose, S., Jacobs, K. & Knight, P. L. Scheme to probe the decoherence of a macroscopic object. *Phys. Rev. A* **59**, 3204 (1999).

[5] Marshall, W., Simon, C., Penrose, R. & Bouwmeester, D. Towards quantum superpositions of a mirror. *Phys. Rev. Lett.* **91**, 130401 (2003).

[6] Dorsel, A., McCullen, J. D., Meystre, P., Vignes, E. & Walther, H. Optical bistability and mirror confinement induced by radiation pressure. *Phys. Rev. Lett.* **51**, 1550 (1983).

[7] C. K. Law. Interaction between a moving mirror and radiation pressure: a hamiltonian formulation. *Phys. Rev. A* **51**, 2537 (1995).

[8] Collett, M. J. & Gardiner, C. W. Squeezing of intracavity and traveling-wave light fields produced in parametric amplification. *Phys. Rev. A* **30**, 1386 (1984).

[9] Gardiner, C. W. & Collett, M. J. Input and output in damped quantum systems: Quantum stochastic differential equations and the master equation. *Phys. Rev. A* **31**, 3761 (1985).

[10] Parkins, A. S. & Kimble, H. J. Quantum state transfer between motion and light. *J. Opt. B* **1**, 496 (1999).

[11] Zhang, J., Peng, K. & Braunstein, S. L. Quantum-state transfer from light to macroscopic oscillators. *Phys. Rev. A* **68**, 013808 (2003).

[12] Miao, H., Danilishin, S., Corbitt, T. & Chen, Y. Standard quantum limit for probing mechanical energy quantization. *Phys. Rev. Lett.* **103**, 100402 (2009).

[13] Szorkovszky, A., Brawley, G. A., Doherty, A. C. & Bowen, W. P. Strong thermomechanical squeezing via weak measurement. *Phys. Rev. Lett.* **110**, 184301 (2013).

[14] Brawley, G. A. *et al.* Nonlinear optomechanical measurement of mechanical motion. *Nature Commun.* **7**, 10988 (2016).

[15] Vanner, M. R., Hofer, J., Cole, G. D. & Aspelmeyer, M. Cooling by measurement and mechanical state tomography via pulsed optomechanics. *Nature Commun.* **4**, 2295 (2013).

[16] Vanner, M. R., Pikovski, I. & Kim, M. S. Towards optomechanical quantum state reconstruction of mechanical motion. *Ann. Phys.* **527**, 15 (2015).

[17] Smithey, D. T., Beck, M. & Raymer, M. G. Measurement of the wigner distribution and the density matrix of a light mode using optical homodyne tomography: Application to squeezed states and the vacuum. *Phys. Rev. Lett.* **70**, 1244 (1993).

[18] D'ariano, G. M., Macchiavello, C. & Paris, M. G. A. Detection of the density matrix through optical homodyne tomography without filtered back projection. *Phys. Rev. A* **50**, 4298 (1994).

[19] Braginsky, V. & Khalili, F. *QUantum measurement* (Cambridge University Press, 1995).

[20] Vanner, M. R. *et al.* Pulsed quantum optomechanics. *PNAS* **108**, 16182–16187 (2011).

[21] Aldana, S., Bruder, C. & Nunnenkamp, A. Equivalence between an optomechanical system and a kerr medium. *Phys. Rev. A* **88**, 043826 (2013).

[22] Mancini, S., Man'ko, V. I. & Tombesi, P. Ponderomotive control of quantum macroscopic coherence. *Phys. Rev. A* **55**, 3042 (1997).

[23] Armata, F. *et al.* Quantum and classical phases in optomechanics. *Phys. Rev. A* **93**, 063862 (2016).

[24] Meystre, P., Wright, E., McCullen, J. & Vignes, E. Theory of radiation-pressure-driven interferometers. *J. Opt. Soc. Am. B* **2**, 1830 (1985).

[25] Penrose, R. Quantum computation, entanglement and state reduction. *Phil. Trans. R. Soc. Lond. A* **356**, 1927 (1998).

[26] Bekenstein, J. D. Is a tabletop search for planck scale signals feasible? *Phys. Rev. D* **86**, 124040 (2012).

[27] Arndt, M. & Horneberger, K. Testing the limits of quantum mechanical superpositions. *Nature Physics* **10**, 271 (2014).

[28] Ghirardi, G. C., Pearle, P. & Rimini, A. Markov processes in hilbert space and continuous spontaneous localization of systems of identical particles. *Phys. Rev. A* **42**, 78 (1990).

[29] Romero-Isart, O. Quantum superposition of massive objects and collapse models. *Phys. Rev. A* **84**, 052121 (2011).

[30] Bahrami, M., Paternostro, M., Bassi, A. & Ulbricht, H. Proposal for a noninterferometric test of collapse models in optomechanical systems. *Phys. Rev. Lett.* **112**, 210404 (2014).

[31] Bawaj, M. *et al.* Probing deformed commutators with macroscopic harmonic oscillators. *Nature Commun.* **6**, 7503 (2015).

[32] Vacanti, G. *et al.* Geometric-phase backaction in a mesoscopic qubit-oscillator system. *Phys. Rev. A* **85**, 022129 (2012).

[33] Scala, M., Kim, M. S., Morley, G. W., Barker, P. F. & Bose, S. Matter-wave interferometry of a levitated thermal nano-oscillator induced and probed by a spin. *Phys. Rev. Lett.* **111**, 180403 (2013).

[34] Asadian, A., Brukner, C., & Rabl, P. Probing macroscopic realism via ramsey correlation measurements. *Phys. Rev. Lett.* **112**, 190402 (2014).

[35] Berry, M. V. Quantal phase factors accompanying adiabatic changes. *Proc. R. Soc. Lond. A* **392**, 45 (1984).

[36] Bohm, A., Mostafazadeh, A., Koizumi, H., Niu, Q. & Zwanziger, J. *The geometric phase in quantum systems* (Springer, 2003).

[37] Schneider, S., James, D. F. V. & Milburn, G. J. Method of quantum computation with hot trapped ions. *arXiv 9808012* (1998).

[38] Sørensen, A. & Mølmer, K. Entanglement and quantum computation with ions in thermal motion. *Phys. Rev. A* **62**, 022311 (2000).

[39] Milburn, G. J., Schneider, S. & James, D. F. V. Ion trap quantum computing with warm ions. *Fortschr. Phys.* **48**, 801 (2000).

[40] Leibfried, D. *et al.* Toward heisenberg-limited spectroscopy with multiparticle entangled states. *Science* **304**, 1476 (2004).

[41] Roos, C. F. *et al.* Control and measurement of three-qubit entangled states. *Science* **304**, 1478 (2004).

[42] Pechal, M. *et al.* Geometric phase and nonadiabatic effects in an electronic harmonic oscillator. *Phys. Rev. Lett.* **108**, 170401 (2012).

[43] Asjad, M., Tombesi, P. & Vitali, D. Quantum phase gate for optical qubits with cavity quantum optomechanics. *Opt. Express* **23**, 7786 (2015).

[44] Bocchieri, P. & Loinger, A. Quantum recurrence theorem. *Phys. Rev.* **107**, 337 (1957).

[45] Penrose, O. Foundations of statistical mechanics. *Rep. Prog. Phys.* **42**, 129 (1979).

[46] Tipler, F. J. General relativity, thermodynamics, and the poincarè cycle. *Nature* **280**, 203 (1979).

[47] Rakhmanov, M. Doppler-induced dynamics of fields in fabry-perot cavities with suspended mirrors. *Applied Optics* **40**, 1942 (2001).

[48] Rakhmanov, M., Savage, R., Reitze, D. & Tanner, D. Dynamic resonance of light in fabry–perot cavities. *Phys. Lett. A* **305**, 239 (2002).

[49] Kippenberg, T. J. & Vahala, K. J. Cavity optomechanics: Back-action at the mesoscale. *Science* **321**, 1172 (2008).

[50] Rabl, P. Photon blockade effect in optomechanical systems. *Phys. Rev. Lett.* **107**, 063601 (2011).

[51] Nunnenkamp, A., Børkje, K. & Girvin, S. M. Single-photon optomechanics. *Phys. Rev. Lett.* **107**, 063602 (2011).

[52] Nunnenkamp, A., Børkje, K. & Girvin, S. M. Cooling in the single-photon strong-coupling regime of cavity optomechanics. *Phys. Rev. A* **85**, 051803(R) (2012).

[53] Brennecke, F., Ritter, S., Donner, T. & Esslinger, T. Cavity optomechanics with a bose-einstein condensate. *Science* **322**, 235 (2008).

[54] Leijssen, R. & Verhagen, E. Strong optomechanical interactions in a sliced photonic crystal nanobeam. *Sci. Rep.* **5**, 15974 (2015).

[55] Kleckner, D. *et al.* Creating and verifying a quantum superposition in a micro-optomechanical system. *New J. Phys* **10**, 095020 (2008).

[56] Yang, R., Gong, X., Pei, S., Luo, Z. & Lau, Y. K. Sagnac interferometry as a probe to the commutation relation of a macroscopic quantum mirror. *Phys. Rev. A* **82**, 032120 (2010).

[57] Bassi, A., Lochan, K., Satin, S., Singh, T. & Ulbricht, H. Models of wave-function collapse, underlying theories, and experimental tests. *Rev. Mod. Phys.* **85**, 471 (2013).

[58] Sanders, B. C. & Milburn, G. J. Quantum limits to all-optical phase shifts in a kerr nonlinear medium. *Phys. Rev. A* **45**, 1919 (1992).

[59] Kato, T. On the adiabatic theorem of quantum mechanics. *J. Phys. Soc. Jap.* **5**, 435 (1950).

[60] Hannay, J. H. Angle variable holonomy in adiabatic excursion of an integrable hamiltonian. *J. Phys. A* **18**, 221 (1985).

[61] Berry, M. V. & Hannay, J. H. Classical non-adiabatic angles. *J. Phys. A* **21**, L325 (1988).

[62] Ge, Y. C. & Child, M. S. Nonadiabatic geometrical phase during cyclic evolution of a gaussian wave packet. *Phys. Rev. Lett.* **78**, 2507 (1997).

[63] Ge, Y. C. & Child, M. S. Nonadiabatic geometric phase in periodic linear systems. *Phys. Rev. A* **58**, 872 (1998).

[64] Aharonov, Y. & Anandan, J. Phase change during a cyclic quantum evolution. *Phys. Rev. Lett.* **58**, 1593 (1987).

[65] Jarzynski, C. Geometric phase effects for wave-packet revivals. *Phys. Rev. Lett.* **74**, 1264 (1995).

[66] Latmiral, L., Armata, F., Genoni, M. G., Pikovski, I. & Kim, M. S. Probing anharmonicity of a quantum oscillator in an optomechanical cavity. *Phys. Rev. A* **93**, 052306 (2016).

[67] Caves, C. M., Thorne, K. S., Drever, R. W. P., Sandberg, V. D. & Zimmermann, M. On the measurement of a weak classical force coupled to a quantum-mechanical oscillator. i. issues of principle. *Rev. Mod. Phys.* **52**, 341 (1980).

[68] B. P. Abbott er al. Observation of gravitational waves from a binary black hole merger. *Phys. Rev. Lett.* **116**, 061102 (2016).

[69] G. J. Milburn and C. A. Holmes. Dissipative quantum and classical liouville mechanics of the anharmonic oscillator. *Phys. Rev. Lett.* **56**, 2237 (1986).

[70] Joshi, C., Jonson, M., Andersson, E. & Ohberg, P. Quantum entanglement of anharmonic oscillators. *J. Phys. B* **44**, 245503 (2011).

[71] L$'$u, X.-Y., Liao, J.-Q., Tian, L. & Nori, F. Steady-state mechanical squeezing in an optomechanical system via duffing nonlinearity. *Phys. Rev. A* **91**, 013834 (2015).

[72] B. Teklu, A. Ferraro, M. Paternostro and M. A. Paris. Nonlinearity and nonclassicality in a nanomechanical resonator (2015). ArXiv: 1501.03767.

[73] Paris, M., Genoni, M. G., Shammah, N. & Teklu, B. Quantifying the nonlinearity of a quantum oscillator. *Phys. Rev. A* **90**, 012104 (2014).

[74] Dykman, M. *Fluctuating nonlinear oscillators: from nanomechanics to quantum superconducting circuits* (Oxford University Press, 2012).

[75] Eichler, A. *et al.* Nonlinear damping in mechanical resonators made from carbon nanotubes and graphene. *Nature Nanotech.* **6**, 339 (2011).

[76] Rips, S., Wilson-Rae, I. & Hartmann, M. J. Nonlinear nanomechanical resonators for quantum optoelectromechanics. *Phys. Rev. A* **89**, 013854 (2014).

[77] Gieseler, J., Novotny, L. & Quidant, R. Thermal nonlinearities in a nanomechanical oscillator. *Nature Physics* **9**, 806 (2013).

[78] Landau, L. D. & Lifshitz, E. M. *Mechanics* (Butterworth-Heinemann, 1976).

[79] Krivoshlykov, S., Man'ko, V. & Sissakian, I. Coherent state evolution for the quantum anharmonic oscillator. *Phys. Lett. A* **90**, 165 (1982).

[80] Higgins, B. L., Berry, D. W., Bartlett, S. D., Wiseman, H. M. & Pryde, G. J. Entanglement-free heisenberg-limited phase estimation. *Nature* **450**, 393 (2007).

[81] Brivio, D. *et al.* Experimental estimation of one-parameter qubit gates in the presence of phase diffusion. *Phys. Rev. A* **81**, 012305 (2010).

[82] Berni, A. A. *et al.* Ab initio quantum-enhanced optical phase estimation using real-time feedback control. *Nature Photonics* **9**, 577 (2015).

[83] M. G. A. Paris. Quantum estimation for quantum technology. *Int. J. Quantum Information* **7**, 125 (2009).

[84] A. Ferraro, S. Olivares and M. G. A. Paris. *Gaussian States in Quantum Information* (Bibliopolis, 2005).

[85] M. G. Genoni, S. Mancini and A. Serafini. General-dyne unravelling of a thermal master equation. *Russian Journal of Mathematical Physics* **21**, 329–336 (2014).

[86] Bernstein, E. & U.Vazirani. Quantum complexity theory. *SIAM J. Comput.* **26(5)**, 1411–1473 (1997).

[87] Garay, L. G. Quantum gravity and minimum length. *Int. J. Mod. Phys.* **A10**, 145 (1995).

[88] Kempf, A., Mangano, G. & Mann, R. B. Hilbert space representation of the minimal length uncertainty relation. *Phys. Rev. D* **52**, 1108 (1995).

[89] Maggiore, M. Quantum groups, gravity, and the generalizes uncertainty principle. *Phys. Rev. D* **49**, 5182 (1994).

[90] Benczik, S. *et al.* Short distance versus long distance physics: The classical limit of the minimal length uncertainty relation. *Phys. Rev. D* **66**, 026003 (2002).

[91] Latmiral, L. & Mintert, F. Deterministic preparation of highly non-classical quantum states of massive oscillators. *arXiv:1705.10334* (2017).

[92] Hackermüller, L. *et al.* Wave nature of biomolecules and fluorofullerenes. *Phys. Rev. Lett.* **91**, 090408 (2003).

[93] Hackermüller, L., Hornberger, K., Brezger, B., Zeilinger, A. & Arndt, M. Decoherence of matter waves by thermal emission of radiation. *Nature* **427**, 711 (2004).

[94] Marquardt, F. & Girvin, S. M. Trend: Optomechanics. *Physics* **2**, 40 (2009).

[95] Yang, H., Miao, H., Lee, D. S., Helou, B. & Chen, Y. Macroscopic quantum mechanics in classical spacetime. *Phys. Rev. Lett.* **110**, 170401 (2013).

[96] Isenhower, L., Williams, W., Dally, A. & Saffman, M. Atom trapping in an interferometrically generated bottle beam trap. *Optics Letters* **34**, 1159 (2009).

[97] Nimmrichter, S. & Hornberger, K. Macroscopicity of mechanical quantum superposition states. *Phys. Rev. Lett.* **110**, 160403 (2013).

[98] Wollman, E. E. *et al.* Quantum squeezing of motion in a mechanical resonator. *Science* **349**, 952 (2015).

[99] Pirkkalainen, J.-M., Damskägg, E., Brandt, M., Massel, F. & Sillanpää, M. Squeezing of quantum noise of motion in a micromechanical resonator. *Phys. Rev. Lett.* **115**, 243601 (2015).

[100] Lei, C. U. *et al.* Quantum nondemolition measurement of a quantum squeezed state beyond the 3 db limit. *Phys. Rev. Lett.* **117**, 100801 (2016).

[101] Rips, S., Kiffner, M., Wilson-Rae, I. & Hartmann, M. J. Steady-state negative wigner functions of nonlinear nanomechanical oscillators. *New J. Phys* **14**, 023042 (2012).

[102] Qian, J., Clerk, A. A., Hammerer, K. & Marquardt, F. Quantum signatures of the optomechanical instability. *Phys. Rev. Lett.* **109**, 253601 (2012).

[103] Børkje, K. Scheme for steady-state preparation of a harmonic oscillator in the first excited state. *Phys. Rev. A* **90**, 023806 (2014).

[104] Asjad, M. & Vitali, D. Reservoir engineering of a mechanical resonator: generating a macroscopic superposition state and monitoring its decoherence. *J. Phys. B: At. Mol. Opt. Phys.* **47**, 045502 (2014).

[105] Lombardo, D. & Twampley, J. Deterministic creation of macroscopic cat states. *Sci. Rep.* **5**, 13884 (2015).

[106] Romero-Isart, O. *et al.* Large quantum superpositions and interference of massive nanometer-sized objects. *Phys. Rev. Lett.* **107**, 020405 (2011).

[107] Abdi, M., Degenfeld-Schonburg, P., Sameti, M., Navarrete-Benlloch, C. & Hartmann, M. J. Dissipative optomechanical preparation of macroscopic quantum superposition states. *Phys. Rev. Lett.* **116**, 233604 (2016).

[108] Abdi, M., Pernpeintner, M., Gross, R., Huebl, H. & Hartmann, M. J. Quantum state engineering with circuit electromechanical three-body interactions. *Phys. Rev. Lett.* **114**, 173602 (2015).

[109] Liao, J.-Q. & Tian, L. Macroscopic quantum superposition in cavity optomechanics. *Phys. Rev. Lett.* **116**, 163602 (2016).

[110] Clark, J. B., Lecocq, F., Simmonds, R. W., Aumentado, J. & Teufel, J. D. Sideband cooling beyond the quantum backaction limit with squeezed light. *Nature* **541**, 191 (2017).

[111] Blanes, S., Casas, F., Otero, J. A. & Ros, J. The magnus expansion and some of its applications. *Physics Reports* **470**, 151 (2009).

[112] Loudon, R. *The quantum theory of light* (Oxford University Press, 2000).

[113] Teufel, J. D. *et al.* Sideband cooling of micromechanical motion to the quantum ground state. *Nature* **475**, 359 (2011).

[114] Marquardt, F., Chen, J. P., Clerk, A. A. & Girvin, S. M. Quantum theory of cavity-assisted sideband cooling of mechanical motion. *Phys. Rev. Lett.* **99**, 093902 (2007).

[115] Chan, J. *et al.* Laser cooling of a nanomechanical oscillator into its quantum ground state. *Nature* **478**, 89 (2011).

[116] Chang, D. E., Safavi-Naeini, A. H., Hafezi, M. & Painter, O. Slowing and stopping light using an optomechanical crystal array. *New Journal of Physics* **13**, 023003 (2011). URL `http://stacks.iop.org/1367-2630/13/i=2/a=023003`.

[117] Lee, C.-W. & Jeong, H. Quantification of macroscopic quantum superpositions within phase space. *Phys. Rev. Lett.* **106**, 220401 (2011).

[118] Thompson, J. D. *et al.* Strong dispersive coupling of a high-finesse cavity to a micromechanical membrane. *Nature* **452**, 72 (2008).

[119] Zurek, W. H. Decoherence and the transition from quantum to classical. *Phys. Today* **44**, 36 (1991).

[120] Jiang, X., Lin, Q., Rosenberg, J., Vahala, K. & Painter, O. High-q double-disk microcavities for cavity optomechanics. *Opt. Express* **17**, 20911 (2009).

[121] Myatt, C. J., King, B. E., Turchette, Q. A. & Sackett, C. A. Decoherence of quantum superpositions through coupling to engineered reservoirs. *Nature* **493**, 269 (2000).

[122] Julsgaard, B., Kozhekin, A. & Polzik, E. S. Experimental long-lived entanglement of two macroscopic objects. *Nature* **413**, 400 (2001).

[123] Hammerer, K. *et al.* Strong coupling of a mechanical oscillator and a single atom. *Phys. Rev. Lett.* **103**, 063005 (2009).

[124] Asadian, A., Budroni, C., Steinhoff, F. E. S., Rabl, P. & Gühne, O. Contextuality in phase space. *Phys. Rev. Lett.* **114**, 250403 (2015).